AlGaN/GaN High Electron Mobility Transistor for Various Sensing Applications: A Review

Aasif Mohammad Bhat[a], Ritu Poonia[a], Arathy Varghese[b], Nawaz Shafi[c] and C. Periasamy[a*]

[a] Department of Electronics and Communication Engineering, Malaviya National Institute of Technology, Jaipur-302017, India

[b] School of Engineering, Cardiff University, Cardiff CF24 3AA, United Kingdom

[c] School of Electronics Engineering, Vellore institute of technology, Vellore Tamil Nadu, India-632014

Abstract

AlGaN/GaN high electron mobility transistors (HEMTs) demonstrate exceptional properties desired for sensing regime applications due to their extraordinary chemical stability, non-toxicity, surface amenable to functionalization, high surface charge sensitivity and high temperature endurance. This report provides a comprehensive review on the AlGaN/GaN HEMT based solid-state microsensors used for detection of gases, biomarkers, ions and high energy radiation which has application in environmental, clinical and water quality monitoring besides medical research. The material properties and fabrication aspects are highlighted first and then sensing mechanisms for different applications and various device design advancements during past decades in literature are discussed along with the modelling and simulation perspectives. There are some reports which discuss AlGaN/GaN HEMT for a particular application only and thus there was a need for a review which discusses various aspects and applications in one study to render an overall bird's eye view of potential of this material system.

Keywords: AlGaN/GaN HEMT, Gas sensor, Biosensor, pH sensor, Heavy metal ion sensor, Radiation sensor

*Corresponding author

Email address: cpsamy.ece@mnit.ac.in (C. Periasamy[a*])

1 Introduction

AlGaN/GaN high electron mobility transistors (HEMTs) have already made a mark in optoelectronics, high power and next generation radio frequency (RF) domains by the virtue of superior material properties and are currently under huge focus of research in harnessing its sensing capabilities. In the modern days of Internet of things (IOT) technology there is a general urge to make processes automatic, the sensors form the eyes and ears of the systems through which detection and monitoring is performed. There is a plethora of applications where we need sensors such as gases, heavy radiation, biosensors, chemical sensor etc to detect or monitor a specific quantity or any of analyte attributes to consider it for any decision and consequently a reflex action. The interdisciplinary combination of various fields such as medical science, clinical chemistry and nanotechnology has paved the entry of sensors into the medical, health care, food industry, chemical industry, outer space exploration and point of care diagnosis [1], [2]. Given the advancements in the technologies in recent times system monitoring has become decentralized in a way that the data from the site of sensor can be transferred to smart phones or computerized systems for monitoring, evaluation, interpreting and decision making. A sensor system consists of recognition element and a transducing element. The former interacts with the target analyte and the later converts the recognition event into measurable signal. The two key performance parameters of any sensor are sensitivity and selectivity besides repeatability, limit of detection and response times which need to be taken care during design process [3]. There are numerous types of sensors reported in literature however, the semiconductor-based field effect transistor (FET) sensors seem to be the most promising alternate for future applications due to the mature fabrication and bulk production aspects. The silicon-based FETs have been under investigation since 1970s with the inception of ion sensitive field effect transistor (ISFET) by P. Bergveld. Since then, number of variants in terms of design were proposed to improve sensing metrics [4]. However, Si based FETs render satisfactory operation limited up to 200 ^{o}C due to the performance degradation which makes sensor unreliable [5]. Similarly, two dimensional materials like MOS_2 have also been harnessed for sensing applications exhibiting excellent properties such as good conductivity, fast electron transport, tunable band gap, thermal stability, natural abundance as molybdenite along with high surface to volume ratio thereby capturing more analyte species resulting in high sensitivity and thus an outstanding contender for future electronic systems, however its immature fabrication process limits its potential [6].

GaN is III-V compound semiconductor material that is non-toxic to bio systems, radiation hard, high temperature endurance and its high bond strength makes it resistant to corrosion and etching in aqueous environment. The genesis of spontaneous and piezoelectric polarization in AlGaN/GaN material system results in the formation of high mobility, density and saturation velocity two-dimensional electron gas (2DEG) at the heterojunction [7]. The surface states are considered as the source of 2DEG that are very close to the channel making it highly sensitive to the changes in the surface proximity [8]. Also, AlGaN/GaN provides a surface amenable to functionalization and thereby different sensor platforms can be developed for many sensing applications [9]–[12]. These sensors provide better figure of merits (FOMs) like sensitivity, selectivity, linearity, limit of detection, response time besides wide band gap nature leads to low intrinsic concentration which is desired for low noise and better signal to noise ratio (SNR) [13], [14]. The other advantage with AlGaN/GaN HEMT is its compatibility with CMOS fabrication technology processes and allows for on chip integration for remote or wireless monitoring. However, the growth of AlGaN/GaN HEMT stack is still immature and a lot of research focus is on eliminating the issues of dislocation and defects or traps [15].

In this review we are reporting on the sensing capabilities of AlGaN/GaN HEMT based sensors spanning from the macro scale with its applications in environmental monitoring systems to nano scale where it can be used in the detection of proteins and DNA hybridization or DNA sequencing. This review covers many reports on different sensing application domains, different methodologies and designs to sense a specific analyte. The various application domains broadly included in this report are the applications in gas sensing, ionizing radiation, heavy metal ion sensing, biosensing and others. Some reviews are reported earlier on AlGaN/GaN HEMT sensors where they have touched a specific application only. So, there was a need for a comprehensive review where the sensing applications from different domains are discussed at one place to have an overall bird's eye vision and appreciate the advantages of AlGaN/GaN HEMT material system.

2 GaN properties and HEMT basics

GaN is a III-V group compound semiconductor material with a typical hexagonal Bravais lattice Wurtzite structure having four atoms per unit cell and imperfect tetrahedral scheme. The crystal surface can have Gallium or Nitrogen atoms on top and called as a Ga-face or N-face crystal with the crystal directions of [0001] or [0001] respectively [7]. Due to the difference in electronegativities between Ga and N (3.04 and 1.81 Pauling units) the electron cloud is shifted more towards N due to its larger electronegativity and thus each bond has dipole moment and by virtue of imperfect tetrahedral structure it leads to formation of spontaneous polarization field vector which leads to genesis of spontaneous polarization [16]. The prerequisite for the spontaneous polarization is that the c/a ratio must differ from the ideal value of 1.633, the atoms must be different or bonds must be polar, lack of inversion symmetry in crystal and similar atoms must be on same plane. The c/a ratio for Ga-face crystal is 1.6259 and the spontaneous polarization is negative ($P_{sp,GaN} = -0.029\ \mathrm{C}/m^2$) implying directed towards the substrate while the total polarization will be directed towards the surface for N-face crystal [17]. Similarly, the alloy material such as AlGaN has spontaneous polarization though with different lattice constant. As the AlGaN material is grown over GaN there could be a tensile or compressive stress at the heterojunction due to the difference in lattice constants which leads to strained barriers and thus strain-induced or piezoelectric polarization [18]. The spontaneous and piezoelectric polarization vectors are parallel (aiding each other) or anti parallel (opposing each other) for tensile and compressive strain respectively. Due to the discontinuity at the heterojunction the polarization can increase or decrease within the two layers causing an emergence of fixed polarization charge density equal to the gradient of polarization as shown in Figure 1(a) and can be given as in Eq. (**Error! Reference source not found.**)

$$\rho = -\nabla P\ (/cm^3) \tag{1}$$

$$\rho = -\lim_{\Delta x \to 0} \frac{\Delta P}{\Delta x} \Rightarrow \rho \Delta x = \sigma_{int} = -\lim_{\Delta x \to 0} \Delta P$$

$$\sigma_{int} = P_{total,GaN} - P_{total,AlGaN} \tag{5}$$

$$\sigma_{int} = \left[\left(P_{sp} + P_{pz}\right)_{GaN} - \left(P_{sp} + P_{pz}\right)_{AlGaN}\right] /cm^2 \tag{6}$$

$$P_{sp,AlGaN=}\left(-0.052x - 0.029\right)\ C/m^2$$

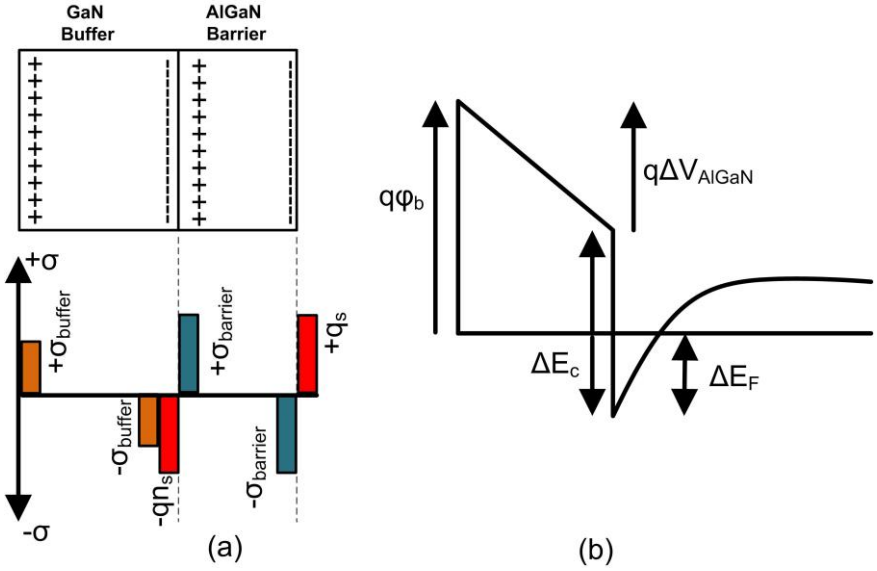

Figure 1 (a) Distribution of polarization charges in various layers of AlGaN/GaN HEMT and (b) Band diagram depiction of AlGaN/GaN HEMT

From Gauss's law, the discontinuity in polarization vector at the hetero junction interface which implies a sheet charge concentration which manifests as the electric field that supports this charge. Due to this charge dipole across AlGaN having negative charge at heterojunction and positive charge at surface sets up electric field. Therefore, we observe a constant slope band bending for AlGaN and a potential well formation at the heterojunction with GaN where the conduction band extent goes below the fermi level [2]. The first observation of 2DEG in AlGaN/GaN hetero junction was reported by pioneering work of Asif Khan [19]. From the band diagram we can write for the potential drop across the AlGaN layer as given in Eq. (7) [20]:

$$\Delta V_{AlGaN} = \varphi_b - \Delta E_c + \Delta E_F \tag{7}$$

Where, ΔE_c is the band offset at heterojunction, φ_b is the barrier height, and ΔE_F is the extent of fermi level below the fermi level as given in Figure 1(b). We can also write for the electric field intensity in the barrier layer as the algebraic sum of associated charges as given in Eq. (8) which can be evaluated to get the 2DEG concentration as given in Eq. (9):

$$\frac{\Delta V_{AlGaN}}{d_{AlGaN}} = \frac{\sigma_{AlGaN}}{\epsilon_{AlGaN}} - \frac{qn_s}{\epsilon_{AlGaN}} \tag{8}$$

$$n_s = \frac{\sigma_p}{q} - \frac{\epsilon_{AlGaN}}{q^2 d_{AlGaN}}(q\varphi_b + \Delta E_F - \Delta E_c) \tag{9}$$

Where, n_s is the 2DEG concentration, σ_p is the polarization charge, ϵ_{AlGaN} is the AlGaN permittivity and d_{AlGaN} is the AlGaN thickness. While applying some negative bias the above equations are modified with this bias term as

$$\Delta V_{AlGaN} = \varphi_b + V_G - \Delta E_c + \Delta E_F$$

$$n_s = \frac{\sigma_p}{q} - \frac{\epsilon_{AlGaN}}{q^2 d_{AlGaN}}(q\varphi_b + V_G + \Delta E_F - \Delta E_c) \tag{10}$$

Assuming completely ionized barrier layer the Schrodinger-Poisson solver self-consistent solution can be written as in Eq. (11)

$$n_s = \frac{\epsilon_{AlGaN}}{q d_{AlGaN}}(V_G - V_{th} - E_F) \tag{11}$$

From the above equations, we have

$$V_{th} = -\left(\varphi_b - \frac{\sigma_{AlGaN}\, d_{AlGaN}}{\epsilon_{AlGaN}} - \frac{\Delta E_c}{q}\right) \tag{12}$$

Where first term signifies contribution of barrier height, second term is that of potential across barrier and third term corresponds to the CB offset at heterojunction. Considering barrier layer is also doped with dopant density (n_D), therefore the threshold voltage equation will be modified as given below:

$$V_{th} = -\left(\varphi_b - \frac{q\sigma_{AlGaN}\, d_{AlGaN}}{\epsilon_{AlGaN}} + \frac{qn_D\, d_{AlGaN}^2}{2\,\epsilon_{AlGaN}} - \frac{\Delta E_c}{q}\right) \tag{13}$$

The surface states are believed to be the source of 2DEG that donate electrons to form donor states, however for surface states to ionize and donate electrons to 2DEG a minimum critical thickness of AlGaN is necessary. The critical AlGaN thickness can be evaluated from Eq. (17) by rearranging Eq. (12) for the thickness of barrier to be critical thickness, For that we use $n_s = 0$, ΔE_F=0 and qφ_b= E_D [8], therefore

$$d_{cr} = \frac{\epsilon_{AlGaN}\,(E_D - E_C)}{q\sigma_p} \tag{17}$$

While the closed form of 2DEG concentration can be given as:

$$n_s = \frac{\sigma_p}{q}\left(1 - \frac{d_{cr}}{d}\right) \tag{18}$$

There is also a higher limit for the distance from 2DEG channel to surface or AlGaN thickness rendered from device design concept known as aspect ratio. The effective gate length and the separation between 2DEG from the gate metal contact are important parameters and their ratio is known as aspect ratio, where for good microwave performance this ratio should not be less than 10. The various physical parameters of various materials like silicon, Gallium arsenide, Gallium nitride, Silicon carbide, Gallium oxide and Diamond are depicted in Table I [21]–[23]. The material properties of GaN are very unique and superior to conventional material systems such as a lower intrinsic concentration and therefore lower leakage and noise related problems ensuring a high temperature operation besides higher critical electric field for high power breakdown applications due to its wide bandgap [24], [25]. The higher saturation velocity manifests into higher current capacity. The other aspect is the formation of heterojunction between AlGaN/GaN which leads to the confinement of higher concentration of 2DEG in the potential well at the heterojunction which has larger mobility due to it being away from parent ionized donor atom and lack of impurity scattering that in turn gives it

Table I Comparison of Physical Parameters of Si, GaAs, 4H-SiC, 6H-SiC, GaN, Ga_2O_3 and Diamond

Parameter	Si	GaAs	4H-SiC	6H-SiC	GaN	Ga_2O_3	Diamond
Band gap energy, E_g (eV)	1.12	1.42	3.27	3.02	3.4	4.85	5.45
Relative dielectric constant, ε_r	11.7	12.9	9.7	9.66	8.9	10	5.5
Electron mobility, μ_e ($cm^2/V \cdot s$)	1400	8500	900	400	1000	300	2200
Electric breakdown field, Ecrit (10^6 V/cm)	0.3	0.4	3	3.2	3.3	8	10
Saturation velocity, v_{sat} (10^7 cm/s)	1	1	2	2	2.5	2	2.7
Thermal conductivity, k (W/K · cm)	1.3	0.55	3.7	4.9	1.3	0.23	22
BFMSi, $\varepsilon_r\mu_e E_{crit}^3$	1	14.7	223	317	850	3214	-
JFMSi, $v_{sat}E_{crit}/2$	1	-	215	-	1090	2844	-
Maximum estimated temperature (°C)	200	-	500	-	700	-	2100
Melting Point K	1415	1238	2827	3376	2791	2173	9000

Table II Comparison of Substrates properties suitable for AlGaN/GaN HEMT Devices

Property	Si	Sapphire	SiC	GaN
Thermal conductivity (W/K・cm)	1.5	0.47	4	2.3
Lattice mismatch (%)	17	16	4	0
Thermal expansion coefficient (10^{-6}/K) at room temperature/1000 K	2.4/4.4 56%		4.5 34%	3.72/5.45 25%
Availability/price	Low	High	High	Very High

a high current carrying capability impurity scattering that in turn gives it a high current carrying capability and low R_{on} that ensures high power/frequency and high efficiency operation. The concurrence of higher 2DEG concentration, mobility and saturation velocity manifests into channel carriers being very sensitive to the surface changes that eventually translate into the higher sensitivity and rapid response sensor platform developed from such a material system [2]. The substrate material that can be used to grow the AlGaN/GaN HEMT epitaxial layer system are silicon, sapphire, silicon carbide and Gallium nitride and their associated properties of interest in terms of being chosen as a substrate material are compared in Table II [26]. Sapphire is semi insulating which can withstand high growth temperatures as required for HEMT epitaxy and relatively cheap but higher lattice mismatch, lower thermal conductivity and large thermal expansion coefficient restrict its use in high power applications. Silicon is the cheapest technology option due to its mature fabrication process, large diameter wafer possibility and ease of integration with silicon electronic systems but it also suffers from higher lattice mismatch, lower thermal conductivity and larger thermal coefficient mismatch. Silicon carbide is better material in terms of the material properties desired from a substrate material but it is very costly. Thus, for high power and RF applications SiC is the material of choice while for sensing purpose, since the operating voltages are relatively very small, the choice of substrate is not a big issue if the growth process yields acceptable epitaxy with lower threading dislocation and trap associated issues. Gallium oxide is an ultra-wide bandgap material depicting huge potential in power electronics (field effect transistors and Schottky barrier diodes), optoelectronics (electroluminescence and solar blind UV detector), memory (random access memory and spintronics) and sensing applications (pH, biosensing and gas). We have included the sensing perspective of gallium oxide while adding some reports on its pH, biosensing, optoelectronic and gas sensing applications [27]–[30] . The best choice for the substrate of GaN epitaxy is GaN itself however, due to material and fabrication constraints besides high cost of free standing GaN substrate the large GaN based wafer are not realized yet and is a matter of ongoing research.

2.1 Working principle of AlGaN/GaN HEMT

AlGaN/GaN HEMT is a type of field effect transistor (FET) where the conduction in channel between ohmic source and drain electrodes is governed by the third usually schottky terminal known as gate. HEMT comprises of two different semiconductor materials forming a heterojunction where the band gap one is greater than other. In case of III-V nitrides AlGaN/GaN HEMT is very popular due to its superior properties and has established its superiority in high power and RF applications. The difference in band gap and polarization effects results into the band bending of the conduction band below fermi level forming a 2DEG channel with high carrier concentration between source and drain that makes it a normally ON device as can be seen from Figure 1. The Normally ON feature enables the device operation even when no gate bias is applied or we can remove gate

from design easing fabrication and measurement in case of biosensors. AlGaN/GaN HEMT is also explored for biosensing applications due to its non-toxicity and better material properties and larger output with high signal to noise ratio (SNR) due to low noise. The silicon counterpart sensors suffer from high temperature limitations (200 ^{o}C), low output, easy corrosion of surface and noise related issues.

The GaN HEMT-based devices have a wide range of applications in sensing due to GaN's high chemical stability, and the ionic bond between Ga and N can easily attract the biomolecule and attach it to the surface . The sensing mechanism depends on the intended application as different analytes can be detected through different procedures. The analyte can be any biomarker, pH, antibody, enzyme, gene, metal ion, gas or radiation. The detection of pH can be understood from the site binding model and Gouy-Chapman-Stern theory which postulates the presence of binding sites over sensing region that will bind to the analyte species and eventually changes the surface charge density or surface potential of the GaN HEMT[4]. To sense a biomolecule or disease-causing biomarker the sensing region is functionalized with a corresponding binding species known as functionalization. There are various methods and procedures of functionalization that can be achieved while functionalizing the GaN surface itself or usually a gold gate [31] . Similarly, various heavy metal ions can be detected by functionalizing the sensing region with an appropriate binding species so as to detect heavy metal ions in water quality measurement applications [32]. The sensing mechanism for the gas sensor is ascribed to the dissociation of the molecular gas atom on a catalytic metal gate, followed by diffusion of the atomic species to the semiconductor interface, which changes the charge in the channel. The gases can be detected by physical or chemical modification of the device such as using a physical barrier membrane that permits only the target gas, using sensor arrays or chemical modification like catalyst decoration or functionalization to provide a specific target recognition [33], [34]. The sensing surface modification is performed in order to make the device selective to the intended analyte in particular and to increase its other figure of merits like sensitivity, limit of detection, linearity and signal-to-noise ratio. The immobilization of the analyte on the sensing surface will lead to a change in surface potential due to the accumulation of positive or negative charges of the analyte on the surface. This accumulated charge will change the charge carriers in the channel, which leads to a change in the drain current and threshold voltage of the sensors and this change in drain current and threshold voltage is considered as performance parameters for the sensor.

The drain current sensitivity can be calculated by normalized current method which is represented by the following formula;

$$S_{I_{DS}} = \frac{I_{DS(Analyte)} - I_{DS(Blank)}}{I_{DS(Blank)}}$$

Where $I_{DS(Analyte)}$ is the current in the presence of analyte and $I_{DS(Blank)}$ is the current for bare device.

The change in threshold voltage can be expressed as;

$$\Delta V_{TH} = V_{TH,\ Analyte} - V_{TH,\ Blank}$$

Where, $V_{TH,\ Analyte}$ and $V_{TH,\ Blank}$ are the threshold voltages in the presence and absence of analyte.

2.2 Fabrication Process of AlGaN/GaN HEMT

2.2.1 Epitaxial layer system

The epitaxial layer system for AlGaN/GaN HEMT is grown over silicon, sapphire or silicon carbide due to difficulty in forming large diameter free standing GaN substrate and its expensiveness. Metal organic chemical vapour deposition (MOCVD) or molecular beam epitaxy (MBE) are usually used to grow GaN epitaxy [15], [35], [36] as shown in Figure 2. The various aspects of different substrates are already mentioned above.

2.2.2 Nucleation layer

This is a sandwiched layer of Aluminium nitride between substrate and GaN buffer layer to reduce lattice mismatch as proposed by Hiroshi Amano [37] (for which he got Nobel prize) or a super lattice of AlGaN system with decreasing mole fraction towards GaN buffer. The insertion of nucleation layer mitigates the threading

dislocation density in GaN buffer and is usually used with low temperature growth process using sapphire or SiC as substrates. The AlGaN super lattice nucleation layer is used with the silicon substrate where the step graded approach ensures smoother transition between different lattice materials resulting in better GaN

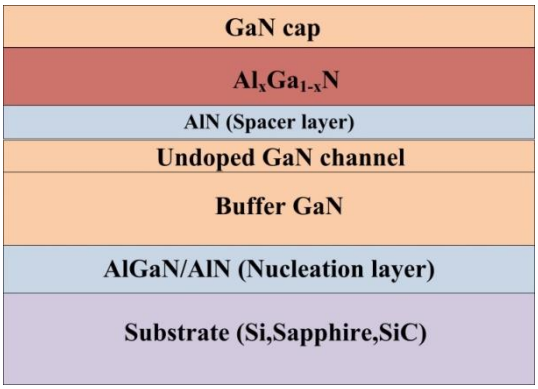

Figure 2 Epitaxial layer structure of AlGaN/GaN HEMT

buffer layer quality with low dislocation density. GaN is grown using trimethyl gallium and ammonia as precursors at 500 ºC.

2.2.3 GaN buffer layer

The GaN buffer layer is an important part of the epitaxial layer system and a very high-quality layer with low defect density, dislocations and high resistivity is desired to get rid of buffer leakage, charge trapping and current collapse. These effects are responsible for pinch off related issues, lowering breakdown voltage and microwave output power. In order to have a good interface with AlGaN to achieve better confinement and reduced interface scattering mobility degradation the buffer GaN surface should be smooth. Larger GaN buffer thickness shows improvements in terms of reducing dislocation density and improving mobility due to the improved interface quality with AlGaN for increased GaN buffer thickness. GaN is grown using trimethyl gallium and ammonia as precursors at 1000-1100 ºC [16].

2.2.4 AlGaN layer

The AlGaN layer is considered as the heart of AlGaN/GaN HEMT and is also known as barrier or supply layer. The composition of AlGaN is a key parameter in determining the concentration of 2DEG formed in the device. An increased amount of Al mole fraction and larger AlGaN thickness renders higher 2DEG concentration, however the effect of mole fraction is dominant. To achieve higher 2DEG density higher Al mole fraction can be used but care should be taken as larger amounts of Al may cause relaxation of AlGaN layer. The higher thickness of barrier layer seems to be obvious choice for high 2DEG density but there is an upper limit on AlGaN thickness imposed by the High aspect ratio requirement as discussed earlier. Similarly, there is a limit in terms of minimum AlGaN thickness known as critical thickness which is the necessary for surface donors to reach fermi level and achieve 2DEG density as already discussed. AlGaN is grown using trimethyl aluminium, trimethyl gallium and ammonia as precursors at 1100 ºC [16], [18], [38]

2.2.5 Spacer layer

This is usually a 1-3 nm layer of AlN or AlGaN grown between GaN buffer and AlGaN layer. It helps to reduce the Coulombic scattering of 2DEG carriers by the ionized parent atoms in the supply layer which enhance the mobility and consequently transconductance of the device. Spacer layer of AlN is grown using trimethyl aluminium and ammonia as precursors at 1000-1100 ºC [17].

2.2.6 Cap layer

GaN or AlGaN thin cap layer is grown on top of epitaxy to reduce gate leakage and increase schottky barrier height. A thicker cap layer reduces the dependence on passivation layer and can also render normally off

operation. Triple-layer such as GaN/AlN/GaN rendered higher breakdown voltage and lower sheet resistance where the lower GaN layer establishes schottky gate contact, AlN layer improves 2DEG and the top GaN layer provides smooth surface morphology [17].

2.2.7 Passivation

The surface passivation is required to prevent the surface states from neutralization due to trapped electrons and maintain a positive surface charge to avoid virtual gate formation. The passivation has yielded better results in terms of device performance and many oxides have been tried such as SiO_2, Sc_2O_3, Si_3N_4, Al_2O_3, HfO_2, among others, however Si_3N_4 is the most commonly used material for passivation [39]–[42]. The passivation should be performed after proper cleaning of device surface otherwise imperfect passivation may lead to charge trapping and deteriorate the device performance.

After the growth of epitaxy, the wafer is cleaned with the solvent cleaning process. The first step of fabricating a device can be either the mesa isolation or the source/drain contact deposition whose patterning can be done using a photoresist through photolithography or e-beam lithography depending on the minimum feature size. Mesa isolation is performed to isolate the devices from adjacent device so as to break the continuity of 2DEG. This is achieved by forming islands of the active material layer so as to provide electrical insulation between adjacent devices. The wet chemical etching is not feasible due to the strong bond energy of GaN besides a very slow etch rate and proper mask. The dry etch processes are widely used like reactive ion etching using inductively coupled plasma (RIE-ICP) with $Ar/CH_4/H_2/Cl_2$ plasma and ion beam etching based on Ar+ ion sputtering [21] . Ion implantation techniques are also harnessed for mesa isolation where the incident ion energy and dosages can be optimized for a damage and disorder-free process schemes utilizing H^+, He^+, N^+, F^+, Mg^+ and Ar^+/Kr^+ ions [43], [44]. Mostly Ti/Al/Ni/Au stack is used for the source/drain metal ohmic contact formation where Ti is deposited first on the wafer surface to provide better mechanical stability and it extracts N atoms from GaN to form a thin TiN layer of lower work function creating N-vacancies forming a heavily n-doped region causing barrier thinning below contact surface for ohmic contact formation. Al has lower melting point and together with its propensity to oxidize at elevated temperatures. To avoid this propensity of oxidation at elevated temperatures, Ni/Au is added on top of this bilayer, Ni acts as a barrier for Au and Al which prevents the formation of highly resistive Al/Au purple plague and Au is used due to its high conductivity and to improve contact quality [45]. Al has high electrical conductivity which lowers the contact resistance of ohmic contact. Also, Al will restrict the aggressive reaction of Ti to avoid TiN aggregate formation while forming intermetal alloy like $TiAl_3$ instead. An important optimized parameter is a ratio for Ti/Al which should be 1/5 for ohmic formation of contacts [46]–[49]. The next step is the annealing of the device and the optimized temperature and time seems to be 850 ^oC and for 30 seconds respectively, in Nitrogen ambient [50]. Annealing is an important step for ohmic contact formation as at this environment the metal stack flows down to the 2DEG while forming alloys like Al_3Ti desired in terms of not letting oxidation of Al and the TiN alloy renders lower work function of 3.7 eV than Ti with 4.1 eV thereby reducing the barrier height for easy transport [46].

In order to operate the device in open gate configuration only step afterwards is the encapsulation of device with the photoresist and opening the sensing region for analyte or functionalization of any biomarker and the source/drain contacts for electrical connections. In some configurations the surface is passivated with some oxide and then a gate metal stack usually Ni/Au is deposited where the analyte or functionalization is performed on the gate metal itself or by extending the gate away from active device area so as to reduce problems associated aqueous environment testing [12], [51], [52]. The fabricated and functionalized devices can then be mounted on PCB to develop a handheld sensor platform for different biosensing applications.

2.3 Sensing scheme

A sensor platform can be considered as comprising of an element which detects the analyte and generates a response signal. This response signal forms the input of the transduction unit comprising of a transducer, which transforms it into a detectable response. The final element is the detector which comprises of a display unit along with the signal processing and conditioning unit which amplifies and denoises the signal for better understanding as depicted in Figure 3. The analyte could be an enzyme, protein, antibody, nucleic acid or whole cell from the biological domain while the sensing entity could be a specific gas, a heavy metal ion, ionizing

radiation, stress/strain and chemical with pH. Thus, sensors can be classified as gas sensors, ion sensors, radiation sensors, mechanical sensors, optical sensors and as biosensors. The sensing or transduction layer is a very important component and different materials are under research for the best response including Pt or Pd gate metal contacts for gas detection, different materials have been used for bio sample and ion detection as per their feasibility in different environments. The transducer can be any active device like schottky diode, FET based devices such as ISFET, JLFET, Nanowire, Graphene, TFET, 2D material-based FET, wide band gap material-based FETs like AlGaAs/GaAs HEMT, AlGaN/GaN HEMT etc, while the detection unit consists of readout circuitry and display unit along with other signal processing modules. The idea of FET based biosensing was propounded by Leland Clark and further championed by the work of P. Bergveld which led to the advent of ion sensitive field effect transistor (ISFET) [4], [53], [54]. Since then, different FET designs have been proposed to have better figure of merits (FOMs) for the sensor. The various FOMs of the sensors include linearity, sensitivity, selectivity, limit of detection (LOD), and signal to noise ratio (SNR) [3]. Linearity is the property of sensor response where the sensors respond linearly to the concentration of analyte, sensitivity refers to the response signal for every unit change in concentration of analyte and a larger value of sensitivity is desired, selectivity implies the property of distinguishing an analyte of interest in presence of many interfering entities or

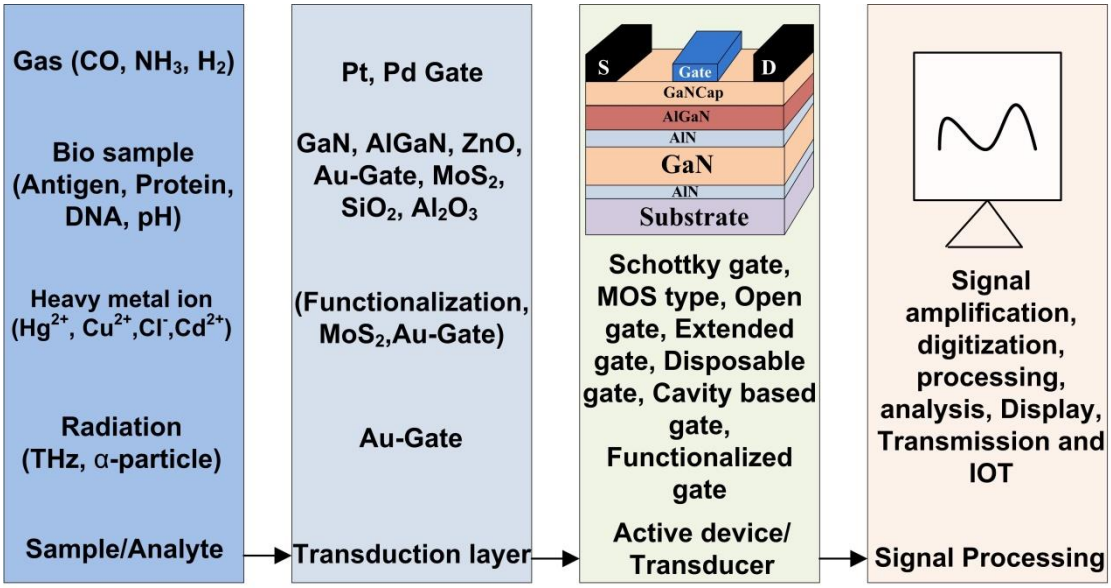

Figure 3 Illustration of sensing scheme of a sensor platform.

in other words, a sensor should be specific, LOD reflects the minimum amount or concentration that can be detected by the sensor with reasonable confidence level where a smaller value is desired and the SNR is the ratio of desired signal level to the unwanted noise and a higher SNR is desired. Besides these the other desirable properties like repeatability, reproducibility, re-usability, drift rate, hysteresis, response and recovery time. The quest is to have a sensor with all FOMs and in such many designs like open gate, extended gate, disposable gate, dual gate, multi-gate designs were proposed. From the FET domain back gate design has become popular due to the feature of separation between back gate biasing and electrolyte and sensitivity beyond Nernst limit of sensitivity, while the FINFETs, gate all around designs also render higher sensitivity and very small amount or concentration detection or in other words better LOD. The 2D materials are also actively being explored for sensing application due to their impressive properties like tunable band gap, better conductivity, high surface to volume ratio, excellent thermal and mechanical characteristics making it superior material for future technologies[1], [55], [56]. With all the better properties of silicon or 2D materials the silicon-based materials cannot be used in harsh environment and high temperature, similarly the 2D materials suffer from problems associated to fabrication. GaAs by virtue of its wurtzite structure has spontaneous polarization and piezoelectric polarization due to mechanical stress which influences the channel 2DEG consequently exhibits potential in pressure, gas and biosensing applications [57], [58]. AlGaAs/GaAs based HEMTs offer highest mobilities and optimal device characteristics, however the toxicity of arsenic hinders its physiological applications in respect to

AlGaN/GaN HEMT while AlGaAs/GaAs HEMT fabrication technology is more mature and various reports are reported for AlGaAs/GaAs HEMT biosensors [59], [60]. AlGaN/GaN HEMT renders superior material properties, non-toxic nature, harsh environment durability, no doping related thermal budget and CMOS compatible fabrication process therefore, making it a promising alternate for future biomedical and biosensing applications.

3 AlGaN/GaN HEMT based sensor applications

3.1 Gas sensors

A gas sensor detects the presence and concentration of a specific target gas and its performance can be accrued from its sensitivity and selectivity besides other figures of merits. Sensitivity is the intensity of response obtained and a higher sensitivity is desired such that its limit of detection decreases so as to be able to detect lesser amounts of target species. Selectivity can be defined as the ability of a sensor to produce an output corresponding to a specific target in the presence of other interfering species. A robust sensor must ensure high selectivity for target recognition such that the information can be trusted about the presence, absence, and concentration of a target gas such as in real-time air pollution, food quality monitoring etc. In order to increase the selectivity of the device the sensing region is usually modified through physical and chemical methods. The physical methods include modifying the physical attributes to enhance the selectivity to a target species such as modifying surface structure, sensor arrays or using membranes that allow only a particular target gas to reach the sensing layer. While, the chemical modifications for selectivity improvement involve modifying sensing surface chemically through catalyst decoration, composite formation or surface functionalization depending upon the target-specific species to be detected. However, selectivity for target gas in the presence of interfering gases needs further enhancement for real-time applications which can be obtained via catalyst decoration with noble metals like Pt and Pd. The oxidizing gases like NO_2 and CO_2 are likely to gain electron while, the reducing gases like SO_2, CO, NH_3 and H_2S are prone to donate electrons from the MOS, respectively which will accordingly change the channel carrier concentration and output drain current. The incorporation of catalytically active materials like platinum, palladium or iridium instils the feature of gas sensing in semiconductor devices such as MOSCAPs, Schottky diodes or field effect transistors [61].

3.1.1 Hydrogen sensing perspectives

We see there is a lot of concern about environmental pollution and global warming in contemporary times due to its impact on our planet. The combustible exhausts from industries and transport are the main sources of adding polluting gases like hydrogen (H_2), ammonia (NH_3), nitrous oxide (NO_2), nitric oxide (NO) and carbon monoxide (CO) to the environment while using the non-renewable carbon-based fossil fuels. The impact is two-fold as we are exhausting our natural resource and at the same time its usage adds harmful exhausts to the surroundings. The continuous increase in population and industries necessitates higher energy resources. In recent times, there is a lot of thrust in replacing the conventional energy resources by a clean renewable energy source like hydrogen due to its excellent properties. The energy density of hydrogen is of the order of 120-142 MJ/Kg which is about 3 times that of gasoline, inherently clean, green, sustainable and being renewable makes it to be the most prospective alternate to replace petroleum based sources as next generation energy driver for reduced carbon footprint and eco-friendly environment [62]–[64]. Therefore, hydrogen is making unprecedented inroads of being the energy driver of the world and a lot of attention has shifted to hydrogen fuel cell for commercial electric vehicles and outer space exploration for becoming interplanetary species. However, hydrogen is colourless, odourless and has lower kindling energy (0.017 mJ) besides tendency to leak and combustibility for more than 4% in air, thus there are some safety concerns on its use. These characteristics of hydrogen necessitate robust sensors which can monitor and detect hydrogen concentration and leaks with very fast response and recovery times to avoid any hazard [65]. Tremendous research focus is in the field of developing low power and miniaturized sensors which can be fitted in field of industrial or consumer applications to continuously monitor and detect gas concentration and leakages for safe operation and safety of the personnel.

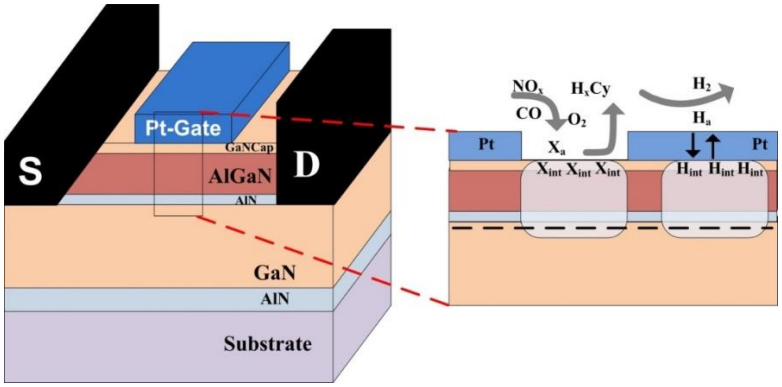

Figure 4 Gas sensing mechanism for the Pt gated AlGaN/GaN HEMT (Ha, Hint: adsorbed and interfacial hydrogen; Xa, Xint: adsorbed and interfacial molecules).

The Pt based gate was proposed to investigate and demonstrate the gas sensitiveness of AlGaN/GaN HEMT. The incorporation of catalytically active materials like platinum, palladium or iridium instils the feature of gas sensing in semiconductor devices such as MOSCAPs, schottky diodes or field effect transistors and some are given in Table III. A commonly understood sensing mechanism of Pt-HEMT is depicted in Figure 4. It was also observed that a porous Pd gate electrode was sensitive to CO. The higher temperature triggers reactions at the Pt gate electrode and depending on the porosity of the gate material caused due to the aggregation of Pt clusters during high temperature annealing device processing. The device can be sensitive to hydrogen or other oxidizing and reducing gas species. Using porous Pt gate electrode at 400ºC makes it sensitive to hydrogen, CO, acetylene and nitrous oxide. The direct adsorption of gas on Pt or porous site may lead to the formation of non-stoichiometric gallium oxynitride which leads to a change in the depletion layer of semiconductor material. This can be attributed to surface dipole creation or removal directly and has likelihood to prevail in CO detection. In case of adsorption of high electronegative gas species, transfer of electron from GaN to the adsorbate leads to the extension of depletion region in GaN. Hydrogen on the other hand is able to diffuse through the thin metal layer forming a hydrogen dipole at the GaN/oxide interface via chemisorption. It is reported that the dipole moment orients out of GaN causing a negative voltage drop which may be balanced by the surface states or in some cases by the depletion layer modulation that leads to SBH reduction [33]. In general modulation of depletion layer due to oxidizing and reducing gases leads to increase and decrease of depletion layer causing a corresponding decrease and increase in 2DEG which in-turn reduces and improves drain current, respectively. However, the limitation of Si MOSFET is that it can't be used continuously above 250 ºC, in such a scenario III-Nitride material like GaN having higher band gap can be used and operated easily at elevated temperatures and harsh conditions. Therefore, many variants of GaN based devices like schottky diodes and HEMTs have been proposed. Figure 5 (a) and (b) depict the output and gate leakage characteristics at different hydrogen concentrations at a temperature of 300 ºC, respectively while Figure 5 (c) renders the relative change in drain current response to various reducing/oxidizing gases besides hydrogen at 400 ºC.

S T Hung et al, [66] studied the sensitive response of the SnO_2 functionalized gate for H2 detection where non-annealed sample was found to be insensitive to H_2. The samples annealed at 200 ºC showed poor SNR, however considerable variation in sensitivity was observed when ON/OFF responses were repeated 2 times. While the samples annealed at 300 ºC showed 3 times increase in sensitivity with respected to sample annealed at 200 ºC because of the increase in contact area due to larger cracks, smaller grain size (6 nm) and porosity after annealing at higher temperature. Sensitivity increased with the increase in operating temperature and it doubled for samples being annealed at 400 ºC in respect to the samples annealed at 300 ºC. The response and recovery times for the samples annealed at 300 ºC were 4 min and 9.5 min and exhibited good repeatability.

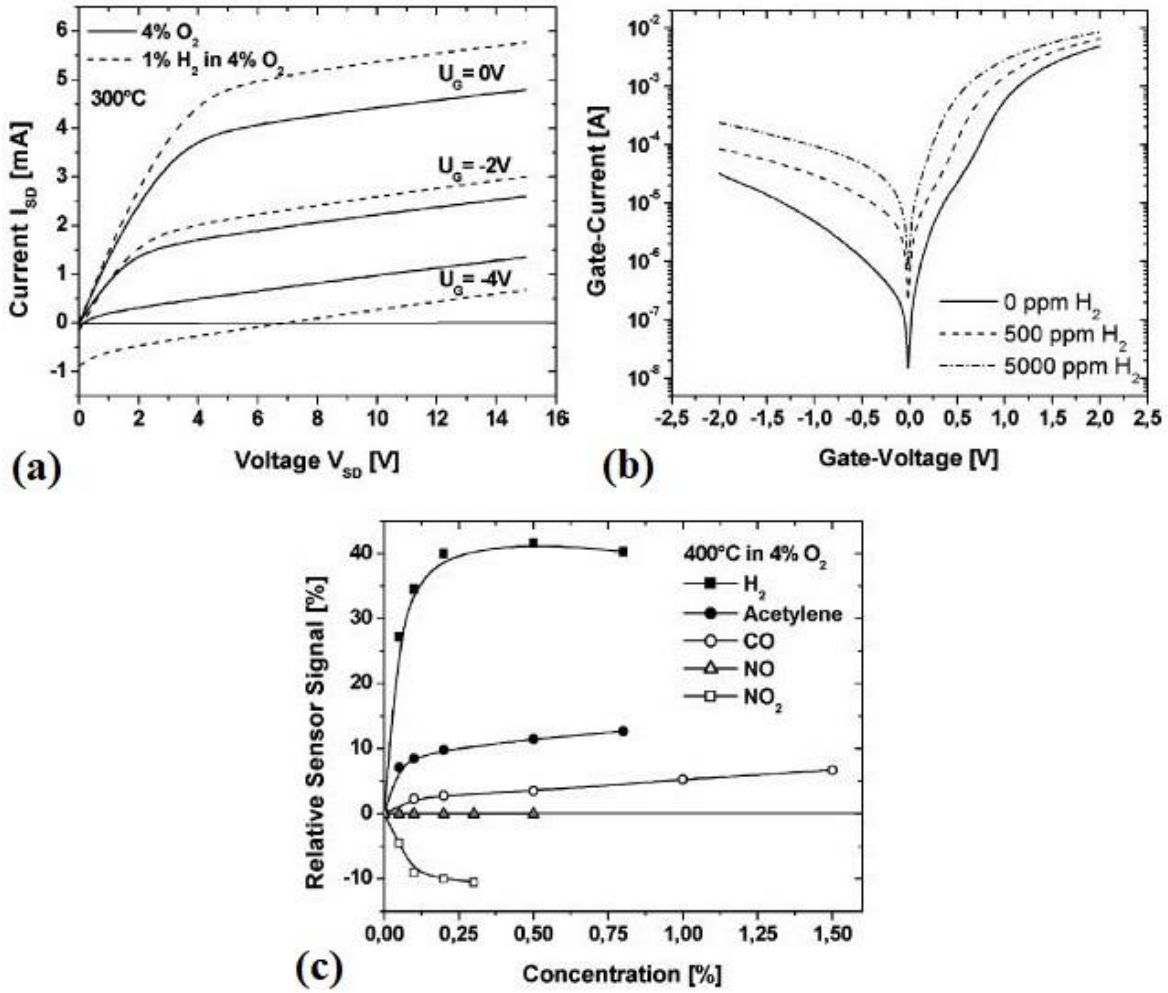

Figure 5 Current-Voltage characteristics of Pt gate AlGaN/GaN HEMT at 300oC (a) Output current characteristics, (b) Logarithmic input characteristics at different concentration of hydrogen and (c) Relative change in output current when exposed to different gases at 400oC. Reprinted from [33], J. Schalwig, G. Müller, M. Eickhoff, O. Ambacher, and M. Stutzmann, "Gas sensitive GaN/AlGaN-heterostructures." Sensors and Actuators B: Chemical. vol. 87, pp. 425-30, (2002). Copyright (2002) with permission from Elsevier.

G H Chung et al [67] demonstrated the detection of hydrogen gas using AlGaN/GaN HEMT based sensor under harsh environment conditions such as high temperature of the order of 200-350 ºC. The sensor was developed with a Pt gate electrode and a floating gate configuration was used for testing purpose. The sensor also showed a stable operation when irradiated with high energy proton with a dosage of 1015 /cm^2 at 5MeV. The HEMT stack was grown on silicon substrate with a gate area of 6x50 µm^2. The sensor depicted a sensitivity of 16, 21, 27 and 33% at a temperature of 200, 250, 300 and 350 ºC respectively, when operated at a drain bias of 10V. The sensor also displayed a stable operation in harsh environment when used at high temperature of 350 ºC along with proton irradiation with a sensitivity of 30% implying it to be a strong candidate for harsh environment conditions. Figure 6 (a), (b) and (c) depict the device schematics, fabricated device and the transfer characteristics of the sensor, respectively. The response of the sensor before and after proton irradiation is depicted in Figure 6 (d) and (e) while the transient response is given in Figure 6 (f).

S Jung et al [68]studied the effect of critical environmental factor humidity on the sensing performance. It was observed that the encapsulated devices don't show any decrease in response in presence of water and detection limits upto 100 ppm were obtained. Due to higher humidity or water molecules, the available sites for hydrogen are reduced as the water molecules will block most of the sites and therefore reduce sensitivity. PMMA encapsulated layer prevented water molecules to reach platinum gate and block adsorbent site while it allowed the permeation of hydrogen molecules without any decrease in sensitivity.

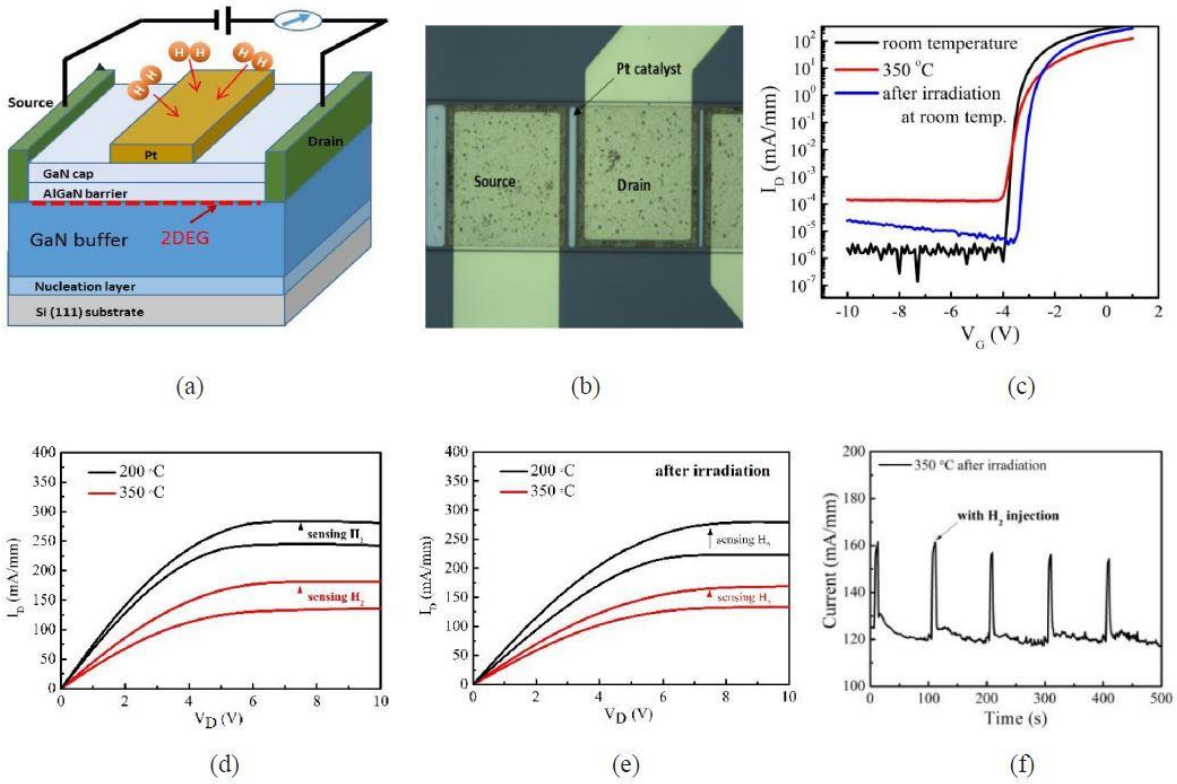

Figure 6 (a) Device structure, (b) Fabricated device micrograph, (c) Transfer characteristics before and after proton irradiation at room temperature and 350oC, Output characteristics at different temperatures (d) With irradiation (e) Without irradiation and (f) Transient response characteristics at drain bias of 10V. Reprinted from [67], G. H. Chung, T. A. Vuong, and H. Kim, "Demonstration of hydrogen sensing operation of AlGaN/GaN HEMT gas sensors in extreme environment," Results Phys, vol. 12, pp. 83–84, Mar. 2019, doi: 10.1016/j.rinp.2018.11.064. Copyright (2019), with permission from Elsevier.

Chen et al [65] studied the MOS schottky diode with sputtered HfO2 oxide to form Pd/HfO_2/GaN stack for hydrogen sensing. The sensor ensures detection of very small concentration of hydrogen with LOD of 5 ppm. The response time decreased from 39 sec to 5.3 sec while recovery time decreased from 42 sec to 2.5 sec when operated at elevated temperature of 383K. The effect of humidity in adsorption mechanism is also studied which showed a decrease in sensitivity with increase in humidity at 300K operation, however the degradation of sensing response was negligible when operated at 383 K which can be attributed to the evaporation of water at higher temperature.

Robert et al [69] investigated the effect of gate recess (5-15 nm) on the hydrogen gas sensing performance of Pt based gate metal contact AlGaN/GaN HEMT which showed a 145% increased response in respect to non-recessed sensor. The gate recess was performed by precision cyclic etching method for 30 nm barrier layer to the depths of 25 nm. Recess of 5-15 nm leads to shift in V_{th} from -1.5 to 1.49V. 5 to 300 ppm H_2 concentrations were tested at 240 oC with V_{DS} = 7V. The sensing response is evaluated at V_{DS}=5V and V_{GS}=0 at 240 °C, for sensors A-D, while VGS =2V for enhancement mode sensor E. An increased response of 13 to 145 % was obtained for sensor A to E with respect to conventional non-recessed design sensor. The transient response is evaluated at 240 °C for H_2 concentration of 10 to 250 ppm where V_{DS}=5V, V_{GS} =0V (VGS =1.5V for sensor E). The response and recovery time decreased for recessed designs. The sensors were also studied for repeatability with 250 ppm H_2 for 25 min and air purging for 60 min and repeatable responses were obtained. The power consumption reduced 48 times for the proposed sensor, which is very important for integrated sensors in real world applications depicting a recessed barrier layer under gate region is an effective way to improve H_2 gas sensing in AlGaN/GaN HEMT based sensor.

Yu et al [62] studied 10 nm Pd gate capacitive GaN honeycomb nanonetwork with Al back contact on silicon. Devices were tested for a range of temperatures from 25 to 130 ºC for optimal temperature; the capacitive sensor depicts negative capacitance variation when exposed to hydrogen while the initial capacitance depicted an increase as the operating temperature was increased. However, the variation in capacitance diminishes above a temperature of 80 ºC. H_2 concentration in the range of 1 to 5000 ppm was used for testing the capacitive sensor. For hydrogen concentration of 1000 ppm the response time was 3 sec at 50 ºC which decreased to 1.3 sec at 70 ºC. Also, very small concentrations could be detected with LOD of 500 ppb and 400 ppb for 50 and 70 ºC respectively. Using a passive device like capacitor for H_2 sensing has an advantage of being free of electric spark generation which could otherwise be hazardous because of hydrogen flammability along with its ease in integration with other systems.

J. Ahn et al [70] fabricated the HEMT with bilayer grapheme gate with 1nm Pt having 100nm SiO_2 gate oxide for H_2 detection. The testing of device was performed at V_{DS}=1V and the H_2 concentration were varied from 1 to 500 ppm. The transfer characteristics showed a negative shift and an increase in leakage current as H_2 concentration was increased. The sensitivity of the device was also tested in sub threshold regime by fixing gate voltage in range -2.8 to -3.3 V where response increases with increase in concentration of H_2 and saturates after H2 concentration above 1000 ppm was used. Also, the output response showed 15 times increase in response even for 1 ppm concentration. Various Pt thicknesses were used to observe the effect of Pt film and it is observed that thinner Pt film showed higher sensitive response. The sensor showed no change in response for different drain bias conditions however the gate bias is optimized. The sensor depicts excellent selectivity as the response for other gases (NH_3, H_2S and CO) was 1000 times lesser as compared to H_2 response depicting excellent resolution.

A simulation and modelling framework for the detection of hydrogen using a workfunction corresponding to Pd gate was proposed in [71]. A numerical model is developed by relating reaction rates and electric dipole at the adsorption sites on surface and metal/semiconductor interface for various gas concentrations. The electric dipole formed at the interface is emulated by considering an electric double layer of oxide with permittivity 2.25. The different gas concentrations are emulated through different interface charges and modulating gate work function which changes SBH and therefore current corresponding to different gas concentrations such as 100 ppm to few ppt.

T A Vuong et al [72] studied the optimization of AlGaN barrier thickness in source connected to gate and floating gate configurations. The sensitive response of the sensor improved when the gate had zero bias as compared to the floating gate configuration. A source connected to the gate configuration was studied as a two terminal device where a thin AlGaN barrier layer was used to enhance the transconductance of the device for better amplified response maintaining zero gate bias which exhibited an improvement in response from 13 to 19 %. The source connected with a thin barrier layer of thickness 9 nm depicted 85% and 20% response at 200 and 500 ºC respectively for a 4% hydrogen gas.

W C Chen et al [63] fabricated a catalytic Pt hybrid metal with Pt film and Pt nano particles (NP) to investigate the effect of film and nano particle strategy. The presence of Pt nano particles increases its surface to volume ratio. The solution-based process and a proper post annealing produce Pt NPs. SD ohmic contacts are made by thermal evaporation and annealed by RTP at 900 ºC for 2 min. A cylindrical chamber with coiled tube heater was used to test the device. The proposed sensor depicted lower values for response and recovery time as 17 and 23 seconds, respectively with a low detection level of 1 ppm-1% H_2 at 300K.

3.1.2 Detection of NH_3

Ammonia (NH_3) has been used in producing fertilizers, explosives and widely used as an industrial coolant while being an essential component for feedstock purpose in food industry. NH_3 is a colourless and toxic gas and a kind of stimulating in nature which can render people uncomfortable. NH_3 concentration in excess of 300 ppm can cause problems in the eyes, skin and damage of respiratory tract, while exposure to even higher concentration like 1000 ppm can lead to pulmonary edema. The other aspect related to NH_3 is that the presence of NH_3 in exhaled breath can act as an indicator of many diseases like kidney malfunction or stomach ulcers

which is caused due to the bacterial infection of stomach by helicobacter pylori. However, these sensors for medical use must have very low limit of detection in the range of 0.1-20 ppm so as to be commissioned in the medical diagnosis platform.

C Bishop et al [73] proposed the modelling and fabrication perspectives of 15 nm Pt gated GaN HEMT for different gas detection purpose. The sensor characterization is performed for a large range of NO, NO_2 and NH_3 concentration for a temperature range of 100 to 400 ^oC. The impact of gate dimension on the sensitive response is studied and an inverse relationship is observed between sensitivity and W/L ratio, whereas the sensitivity decreases for decreased gate length and increased width. W/L ratio of 200/2 µm is used in this work. The effect of AlGaN composition (thickness and mole fraction) on sensitivity is also studied depicting there is an optimum value to trade off current and sensitivity. The effect of Pt gate thickness is also studied and it is observed to detect all three gases the thickness of Pt should be less as the NH_3 and NO require pores in Pt surface to reach AlGaN surface so to be detected.

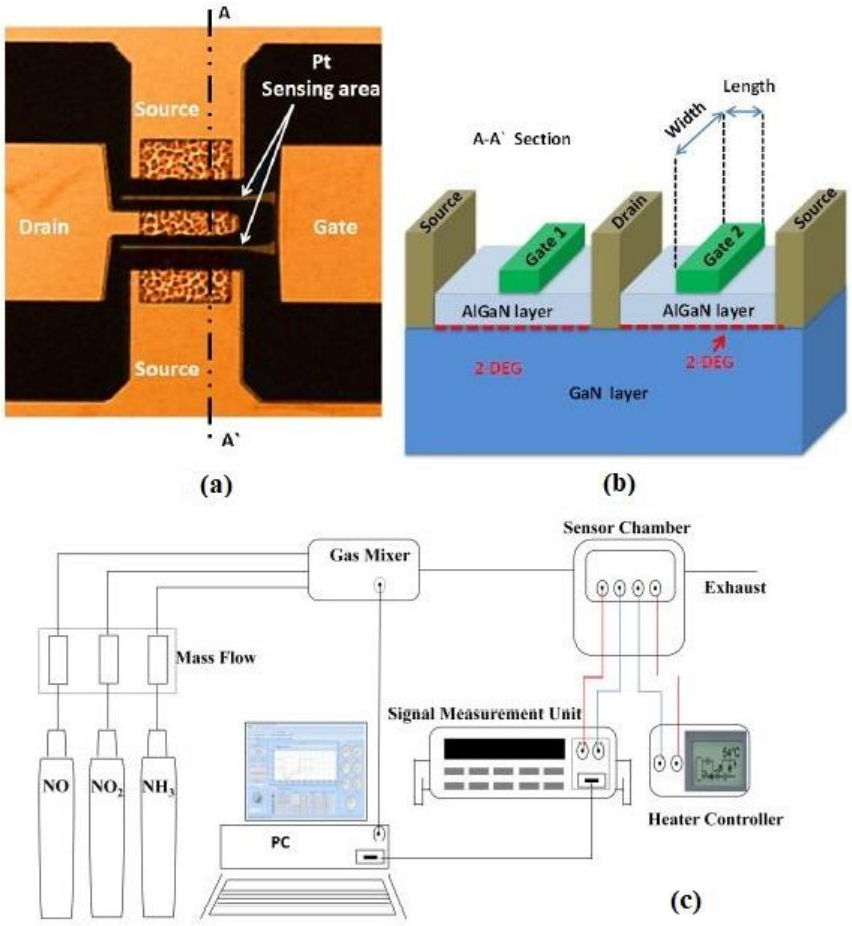

Figure 7: (a) Fabricated sensor micrograph (b) Device schematics and (c) Experimental set up for the gas detection showing various components of gas detection process [74].

Similar observations were also made by Yacine [74] who fabricated a Pt gated AlGaN/GaN HEMT for operation in harsh environment of diesel exhaust (600 ^oC). Gate is functionalized by Pt catalyst to embed gas sensing capability and the fabricated sensor depicts fast response of 1sec. Various devices were fabricated and the response of one sensor having dimension of 2x150 μm^2 is reported. Figure 6 (a) and (b) depicts the top view of fabricated sensor and the schematics of device in cross section, respectively. Figure 6 (c) Illustrates the experimental set up used for the testing purpose depicting various components of the testing system. The detection principle was illustrated for different gases like; NO_2 molecules reach AlGaN surface by segregating into oxygen ions and diffusing through Pt gate grain boundaries, NH_3 dissociates into hydrogen ions that diffuse

through Pt gate to Pt/AlGaN interface to form hydrogen dipole or it can also capacitively couple through pores in Pt layer, NO gas does not dissociate but interacts capacitively via pores in Pt film or through the traps at AlGaN surface. The evaluation is performed at V_{DS}=5V and V_{GS}=0V while the operating temperatures was 300 and 600 ºC. For NO and NO_2 the range of x detection is wide from 100 ppm to 900 ppm besides very low concentration of NH_3 can be detected (3 ppm). Figure 8 (a), (b) and (c) depict a change in current as different gas concentrations are used and the evaluation of response reveals a 12.8, 13 and 33% sensitivity for NO, NH_3 and NO_2, respectively. The comparison of the performance of the sensor for different gases and different temperatures was also reported revealing improvement in sensitivity and a decrease in response time which are desired qualities of a sensor. Figure 9 (a) depicts the sensitivity obtained from developed sensors for various gases at 300 ºC and 600 ºC. The sensitivities improve to 24, 38.5 and 33% for 900ppm NO, 900ppm NO_2 and 15ppm NH_3 respectively. Also, the response time is given in Figure 9 (b) depicting a reduction in response time of the order of 0.4, 1.2 and 0.45 min for 900ppm NO, 900ppm NO_2 and 15ppm NH_3 respectively, at 600 ºC.

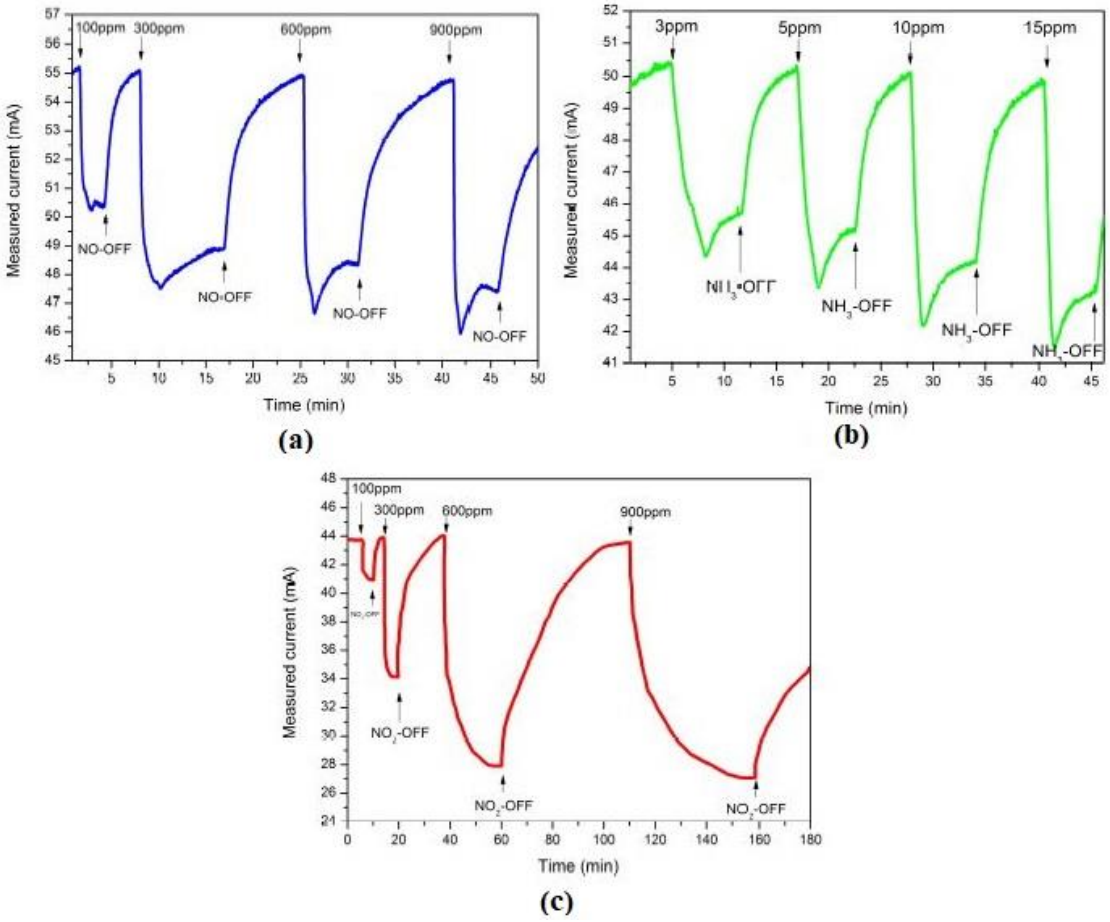

Figure 8 Transient response characteristics for various gases with different concentrations (a) NO, (b) NH_3 and (c) NO_2 [74].

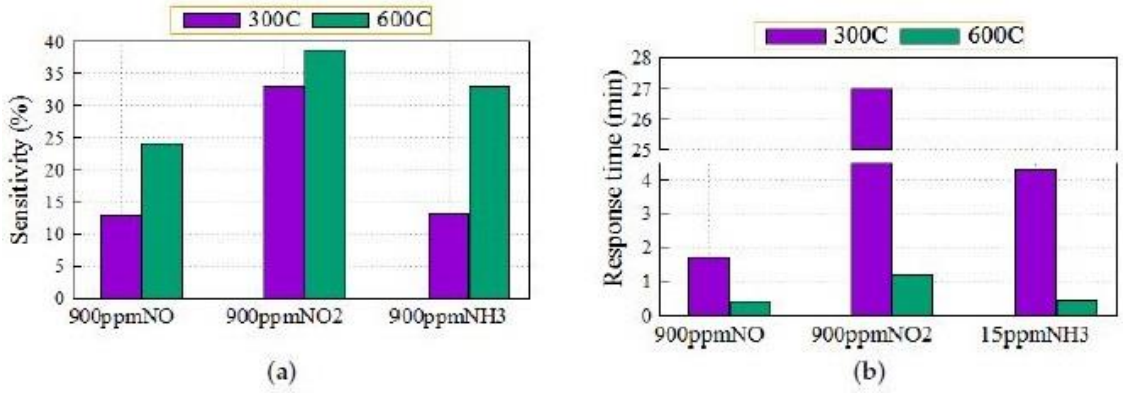

Figure 9 Performance of the sensor at different temperatures when exposed to different gases (a) Sensitivity comparison (b) Response time comparison [74].

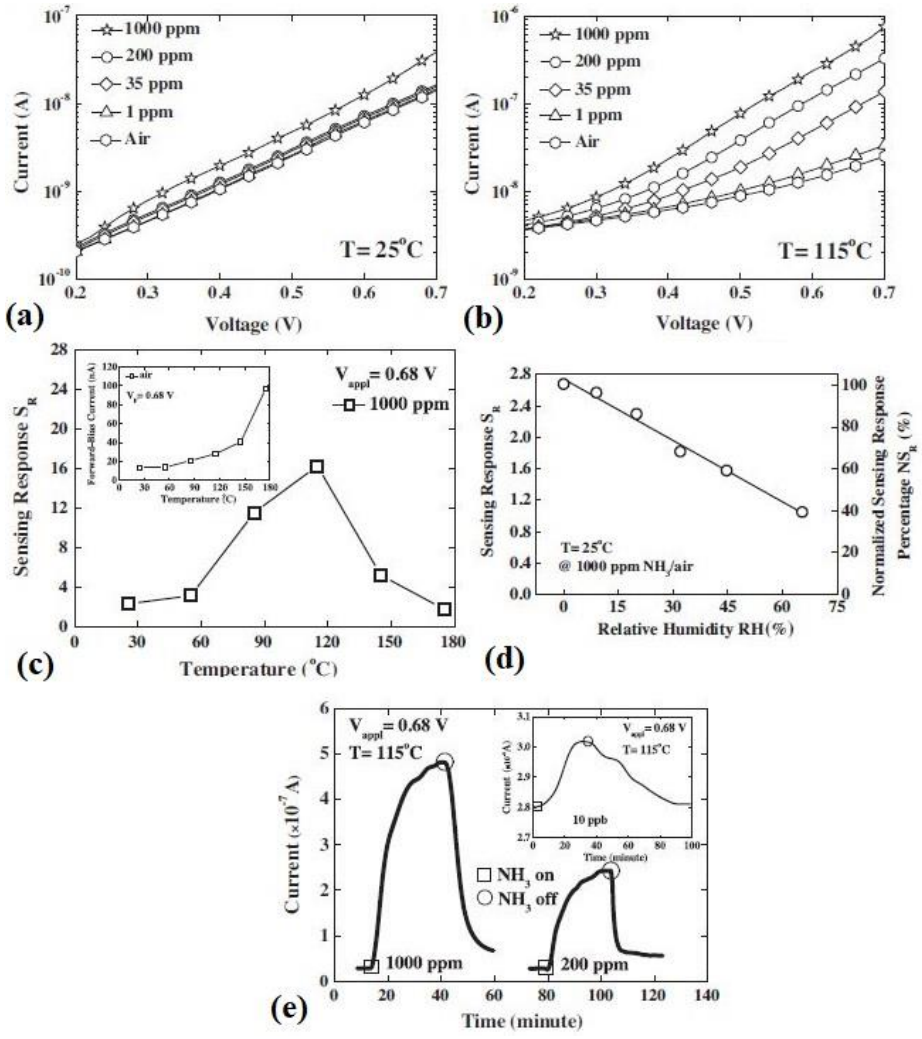

Figure 10 various characteristics of Pt gate AlGaN/GaN schottky diode (a) Current voltage characteristics at 25 °C, (b) Current voltage characteristics at 115 °C, (c) Temperature dependent sensing response for 1000 ppm ammonia concentration; inset shows response as a function of temperature in air ambient (d) Sensing response as a function of humidity and (e) Transient response of the sensor for different ammonia concentration at 115°C; inset depicts transient response at very low concentration of 10 ppb. Reprinted from [75], P. C. Chou et al., "Study of an electroless plating (EP)-based Pt/AlGaN/GaN Schottky diode-type ammonia sensor," Sens Actuators B Chem, vol. 203, pp. 258–262, 2014, doi: 10.1016/j.snb.2014.06.113. Copyright (2014), with permission from Elsevier.

P C Chou et al [75]demonstrated the Pt/AlGaN/GaN NH_3 sensor based on schottky diode which is fabricated by electroless plating (EP) technique. The precursor solutions were H_2PtCl_6, NaOH and NH_4OH and hydrazine was used as a reducing agent. The deposition of Pt gate was done at 40 ^oC. Figure 10 (a) renders the room temperature response of the device for varied ammonia concentrations showing an increase in current values as concentration increases. The change in current is more pronounced when temperature is increased to 115 ^oC as shown in Figure 10 (b). The increase in temperature enhances the sensitivity. The sensitivity decreases when the temperature is increased more than 115 ^oC as exhibited in case of 1000 ppm gas concentration at an applied bias of 0.68 V as depicted in Figure 10 (c). This type of response is attributed to the fact that when temperature increase from 25 to 115 ^oC It is associated with the increase in NH_3 dissociation while as the temperature is increased more than 115 towards 180 ^oC it is accompanied with desorption of NH_3 molecules. The sensing response also decreases with the increase in humidity as depicted in Figure 10 (d) and this is attributed to the chemisorption of water molecules which in turn diminishes the effective adsorbent sites for test gas. The transient response is also depicted in Figure 10 (e).

B Shen et al [76] fabricated in-plane GaN honeycomb nanonetwork grown on AlN/Si wafer by molecular beam epitaxy. 10 nm Pt gate GaN honeycomb nano network with large surface to volume ratio exhibited wide detection range upto 5000 ppm. Figure 11 (a), (b), (c) depicts the SEM images for the GaN nano honeycomb, the platinum layer over it and the ohmic contact respectively. XRD pattern of the GaN nano honeycomb is rendered in Figure 11 (d) while the wafer level micrograph of the final devices is depicted in Figure 11(e)and the enlarged view of one device is given for proper illustration of one dive showing various layers in Figure 11 (f). The sensor measurements were carried out at a drain bias of 0.5 V and the temperature is varied from 30 to 150 ^oC. The sensor showed response to NH_3 at RT also but the response time was large (577 sec for 500 ppm) while the best results were obtained when the operating temperature was 120 ^oC. The gate bias was varied from V_{GS}=0 V, V_{GS}= -1.5 V to floating gate configurations where it is observed that the response of sensor is 15 times more when V_{GS}=-1.5 V with respect to V_{GS}=0 V and floating gate configuration. The LOD of 0.31 ppm NH_3 was observed with 23 and 101 sec of response and recovery times. The conductance change for different concentrations of NH_3 gas with transient state was also studied as shown in Figure 12 (a), (b) and (c) depicting a clear change in conductance when the ammonia concentration was varied from 1-5000ppm. Figure 12 (d) renders the response of the sensor for the tested range of concentration and a linear relationship is established for the change in conductance. NH_3 selective response was observed with 2 – 9 times higher response with respect to other test gases; also 55% degradation in output response was observed after being tested a year later.

3.1.3 Detection of NO_2

NO_2 is also a by-product of incomplete combustion from thermal power plants, furnaces and automobile exhaust and is a volatile pungent red brown oxidizing toxic gas which can be detrimental for environment and humans [77] NO_2 in environment can undergo photo chemical reactions by absorbing light in ultra violet region <398 nm to form NO organic/inorganic nitrates and may react with other pollutant or water to form acid rain which is very harmful to many eco systems. Exposure to small concentration (<10 ppm) of NO_2 may cause nose, throat, eye irritation, pulmonary system diseases like lung tissue inflammation besides silo filler's disease and possible fatality. Prolonged exposure of plants to NO_2 may result in immature synthesis of chlorophyll which causes chlorosis. Higher concentration exposure to NO_2 may impair photosynthesis and also downgrade dyes and inks in textile industry [78], [79]

J. Sun et al [80] fabricated an AlGaN/GaN HEMT based tungsten oxide nano film modified gate along with a Pt micro heater. 80x40 μm^2 with 10 nm WO_3 was deposited over Pt gate as the functionalization material. The temperature and humidity measurements were carried out in the range of 263 to 353 K and RH of 5% to 90% while varying the drain bias from 0 to 10 V. Slight drop in current at higher drain bias is observed which is attributed to the scattering of the carriers. The current decreases as humidity increases, however, the effect of humidity becomes insignificant at higher temperature and this can be attributed to the desorption of water molecules at higher temperature making masked adsorbent sites again available for gas interaction.

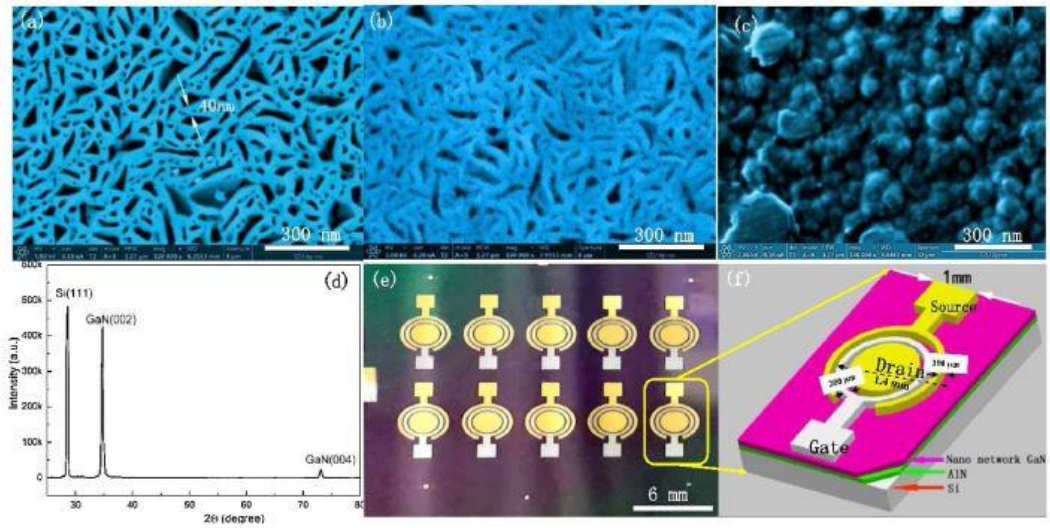

Figure 11 Figure: SEM images of; (a) GaN nano honeycomb, (b) Pt layer over honeycomb, (c) ohmic contact, (d) XRD pattern of GaN honeycomb, (e) fabricated sensors and (f) Enlarged view of ammonia gas sensor. Reprinted from [76], B. Shen, F. Li, Y. Xie, J. Luo, P. Fan, and A. Zhong, "High performance ammonia gas sensor based on GaN honeycomb nanonetwork," Sens Actuators A Phys, vol. 312, no. 2, 2020, doi: 10.1016/j.sna.2020.112172. Copyright (2020) with permission from Elsevier.

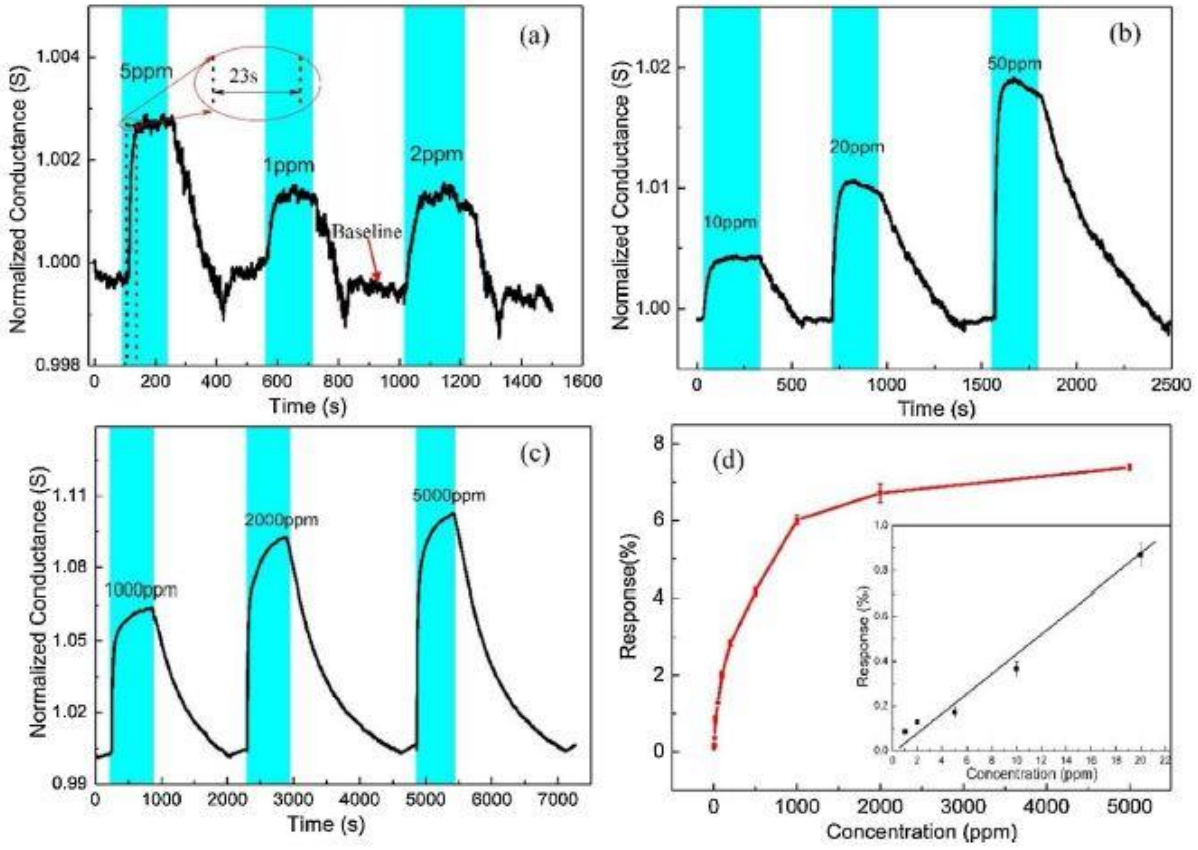

Figure 12 Figure: Normalized change in conductance pattern when the sensor is exposed to ammonia having concentrations (a) 1-5ppm, (b) 10-50ppm and (c) 1000-5000ppm, (d) Response of the sensor for different gas concentrations, where the inset depicts a linear relationship in sensor response at low concentration. Reprinted from [76], B. Shen, F. Li, Y. Xie, J. Luo, P. Fan, and A. Zhong, "High performance ammonia gas sensor based on GaN honeycomb nanonetwork," Sens Actuators A Phys, vol. 312, no. 2, 2020, doi: 10.1016/j.sna.2020.112172. Copyright (2020) with permission from Elsevier.

The response time of sensor for 10 ppm concentration improved from 423 sec to 91 sec when 10 nm WO_3 layer was used on Ti/Pt gate. Besides this the sensitivity increased with the increase in micro heater voltage.

The detection of NO_2 gas over the WO_3 surface can be ascribed to the chemisorption reaction resulting in the negatively charged gaseous ions that rapidly diffuse at the surface. The direct adsorption of NO_2 gas on the WO_3 surface and interacts as per following reactions:

$$NO2\ (gas) + e^- \rightarrow NO_2^-\ (ads) \quad (20)$$

$$NO_2^-\ (ads) + O^-\ (ads) + 2\ e^- \rightarrow NO\ (gas) + 2\ O^{2-}\ (ads) \quad (21)$$

V C Nguyen et al [81] fabricated a 30 nm Pd gate AlGaN/GaN HEMT in which the sensitivity was evaluated at different gate bias and the concentration of NO_2 was varied from 10 to 100 ppm. The fabricated device micrograph and the cross section is given in Figure 13 (a) and (b) respectively. The sensing device was tested from 25 to 300 ^oC where a stable operation was observed. The sensitivity of the sensor improved for higher operating temperatures as depicted in Figure 13 (c), (d) and (e) where the sensor was tested at 25 ^oC, 250 ^oC and 300 ^oC at a drain bias of 10V at different gate voltages to find the stable operating point. Figure 13 (f) depicts the effect of different gate biases on sensitivity when the response of sensor for 100ppm NO_2 gas was tested. The physical sensing mechanism is illustrated through simulations in TCAD by relating the change in gas concentration with the variation of band diagrams and carrier concentration. The sensing mechanism insights are given in Figure 14 (a) and (b) depicting the variation in conduction band profile when the device is tested at a gate voltage of 0V and -1V while the drain bias is 10V with a temperature of 300 ^oC, respectively. As the device is exposed to the gas it affects the conduction band profile which pulls the extent of conduction band edge up to reduce 2DEG as shown in Figure 14 (c) and thus current.

3.1.4 Detection of Carbon monoxide

Carbon monoxide is also a colourless and odourless gas having toxic nature due to the formation of carboxyhaemoglobin (COHb) in the blood due to its strong affinity to haemoglobin (230 to 260) which hampers the oxygen intake and exposure to concentration more than 100 ppm can lead to fatality, so it is also known as silent killer. CO is produced from the incomplete combustion of fuels and is added into atmosphere by emissions from industries, automobiles and domestic fuels. Even at lower levels like <70 ppm CO may lead to dizziness, headaches and fatigue while higher concentration 150 – 200 ppm may cause impaired vision, disorientation, confusion and may even cause death. The conventional method of CO detection uses conductance change in metal oxide as a performance parameter, however the oxide-based sensors exhibit low sensitivity and large response times. Therefore, devices with specific functionalized sensing materials at the gate region can serve as promising sensing platform for various gases [82].

Figure 15 depicts the sensing set up for CO gas where the sensor device is mounted inside tube and the gas is injected through controllers while parameter analyser is used for analysing the response. The device schematics are shown in Figure 16 (a) where the gate region is functionalized using ZnO nanorods which are exposed to the test gas and the response of the sensor at room temperature is depicted in Figure 16 (b) and (c) depicting an increase in current as the concentration of the gas increases. The sensor demonstrates an improvement in sensitivity from 0.09 to 0.34% with the increase in temperature with limit of detection of 50 ppm exhibiting fast response with response and recovery times of the order of 40 and 15 seconds respectively [83].

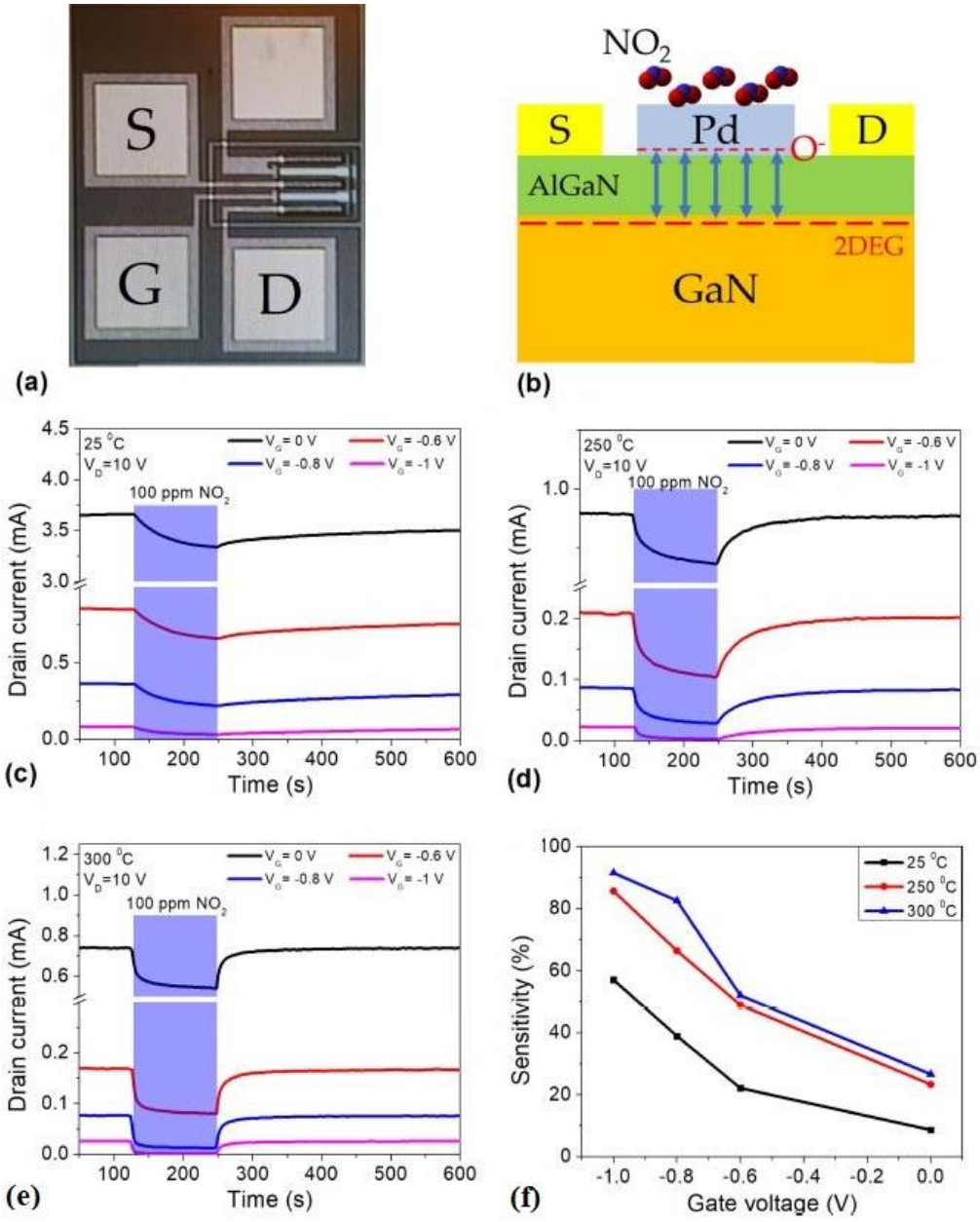

Figure 13 (a) Processed device micrograph, (b) Cross sectional view of device, Sensor response to 100ppm NO_2 at different gate biases with different temperatures (c) 25 **ºC**, (d) 250 **ºC**, (e) 300 **ºC** and (f) Sensitivity comparison for tested device at different temperatures [81].

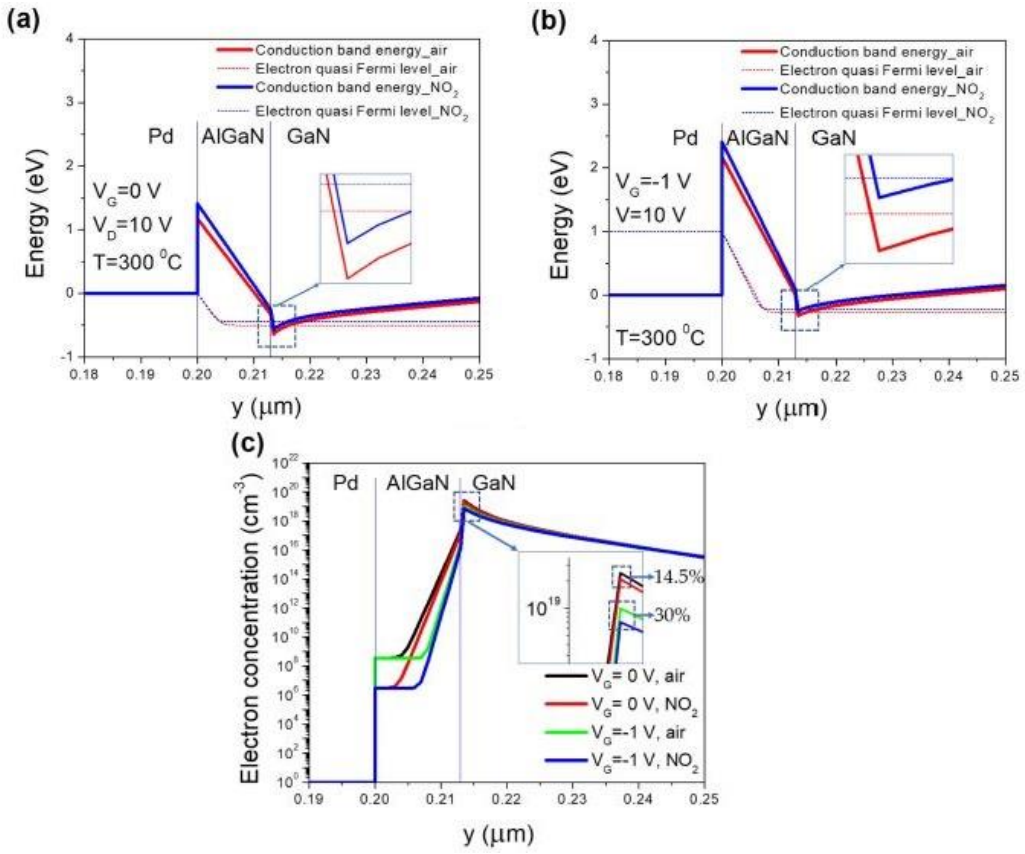

Figure 14 Gas sensing mechanism for the Pt-HEMT gas sensor (a) CB profile with and without gas ambient without gate bias, (b) CB profile with and without gas ambient using gate bias of -1V and (c) Variation of 2DEG density for different gate biases showing a decrease in 2DEG in presence of gas [81].

The effect of operating temperature on the detection of carbon monoxide (CO) for AlGaN/GaN HEMT is studied where it is observed that the sensitivity improves when temperature is increased from 25 to 150oC and

an increase more than 200 ºC decreased the sensitivity. The drain bias maintained in the testing is 0.5 V to minimize power consumption and the detection limit at RT ranges from 250 to 100 ppm. The detection sensitivities measured at 150 ºC and 250 ºC were 30 times higher than RT sensitivity and the LOD also improve to 30 ppm at 150 ºC with respect to 100 ppm at RT. The high sensitivity at higher temperature is due to the release of more electrons to the oxide surface as the dominant oxygen ion at higher temperature (300 ºC) is O^{2-}.

When the oxide surface adsorbs oxygen through chemisorption it reacts with CO to form CO_2 and releases an electron which results in more negative oxide surface inducing additional positive charges on the AlGaN surface in the sensitive region which manifests as an increase in channel 2DEG to enhance current as the CO gas concentration is increased. The surface reactions relevant could be written as:

$$CO + O^- \rightarrow CO_2 + e^- \quad (19)$$

$$2CO + O_2^- \rightarrow 2CO_2 + e^- \quad (20)$$

$$CO + O^{2-} \rightarrow CO_2 + 2e^- \quad (21)$$

S C Hung et al [84] studied the Polar/non polar ZnO nanowires grown on c/a plane GaN through chemical vapour deposition with good crystal quality which showed channel conductance variation following exposure to various concentrations of CO at RT. The diameter of ZnO nanowire was uniform of about 80 nm while 3.35 µm in length. The growth of ZnO nanorods increases surface to volume ratio so that improved catalytic activity occurs at surface and the subsequent reactions are given in Eq. (19), (20) and (21). The sensing region

dimension was 50x50 μm^2. Exposure to CO causes variation in surface charge in the sensing region leading to generation of positive charges on AlGaN surface thereby increasing 2DEG and hence current. The LOD for the polar and non-polar sensors is 400 and 3200 ppm, respectively. Similar results were also observed in ZnO functionalized 5 µm x 55 µm sensing region AlGaN/GaN HEMT when tested with CO concentration range of 50-500 ppm for temperature range of 25-250 ºC. The sensitive response increased at higher temperature and the LOD of 50 ppm and rapid response and recovery times were depicted by the sensor [85]. A bird's eye view of various earlier reports on gas sensing using AlGaN/GaN HEMT is given in Table III.

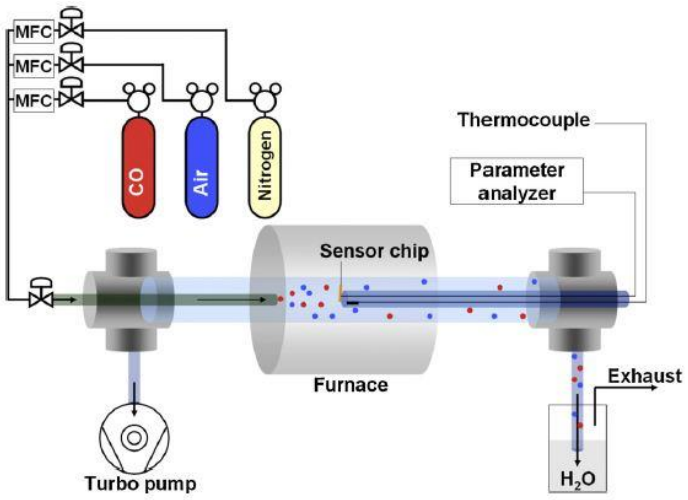

Figure 15 Illustration of Gas sensing system for Carbon monoxide. Reprinted from [83] C. F. Lo et al., "Effect of temperature on CO sensing response in air ambient by using zno nanorod-gated AlGaN/GaN high electron mobility transistors," Sens Actuators B Chem, vol. 176, pp. 708–712, 2013, doi: 10.1016/j.snb.2012.10.051. Copyright (2013) with permission from Elsevier.

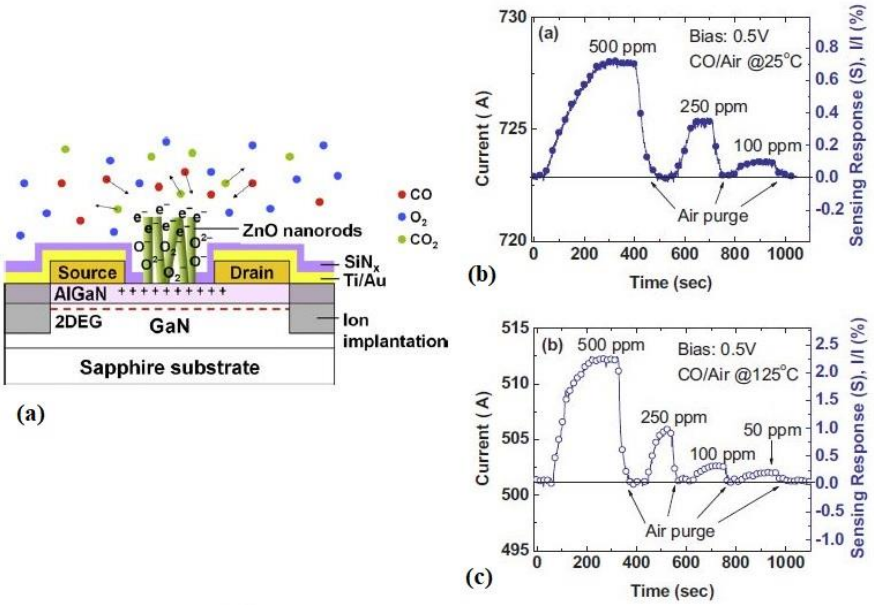

Figure 16 Figure: (a) Device schematics of ZnO functionalized AlGaN/GaN HEMT and Real time measurement of sensor response in terms of output drain current at (b) 25 oC and (c) 125 oC. Reprinted from [83] C. F. Lo et al., "Effect of temperature on CO sensing response in air ambient by using zno nanorod-gated AlGaN/GaN high electron mobility transistors," Sens Actuators B Chem, vol. 176, pp. 708–712, 2013, doi: 10.1016/j.snb.2012.10.051. Copyright (2013) with permission from Elsevier.

Table III Details of some of the Gas sensing reports in the literature

Author, Year, Reference	Details	Type of work	Type of sensor	Remarks
Schalwig, 2002 [33]	Pt gate GaN HEMT	Experimental	H_2 gas sensor	Demonstration of feasibility of AlGaN/GaN HEMT with Pt gate as gas sensor.
C F Lo, 2011 [83]	The effect of operating temperature on the detection of carbon monoxide (CO) for AlGaN/GaN HEMT is studied	Experimental	CO sensor	The sensitivity improves when temperature is increased from 25 to 150 ^oC and an increase more than 200 ^oC decreased the sensitivity. The chemisorbed oxygen on the oxide surface reacts with CO to form CO_2 and releases an electron which makes the oxide surface more negative resulting in inducing additional positive charges on the AlGaN surface in the sensitive gate region which manifests as an increase in channel 2DEG to enhance current as the CO gas concentration is increased.
I. Ryger, 2012 [86]	Pt/Pt-IrO_2 gated HEMT are fabricated and tested for H_2 gas	Experimental	H_2 gas sensor	Thin oxide of IrO_2 is used to supress unwanted reactions, which improves sensitivity by 12 times
S T HUNG, 2012 [66]	20 nm SnO_2 was deposited by hydrothermal method on gate to detect 1% H2 at 50 oC.	Experimental	H_2 gas sensor	The SnO2 oxide functionalized gate was used for H_2 detection, non-annealed sample was insensitive to H_2. Samples annealed at 300 ^oC showed 3 times increase in sensitivity with respect to sample annealed at 200 ^oC.
H. Kim, 2013 [87]	Pt nano networks with 2-3 nm diameter	Experimental	H_2 gas sensor	Pt thin film and Pt nano network gate HEMTs were fabricated and tested at RT for 500 ppm. Nano network sensor depicted higher sensitivity due to its reduced SBH which increases channel conductance.
S C Hung, 2013 [88]	Polar/non polar ZnO nanowires were grown on c/a plane GaN by chemical vapour deposition.	Experimental	CO sensor	Polar and non-polar ZnO nanowire modified gate is proposed which showed channel conductance variation following exposure to various concentrations of CO at RT. ZnO nanowire is grown by chemical vapour deposition with good crystal quality with a diameter of about 80 nm while 3.35 um in length.
P C Chou, 2014 [75]	Pt/AlGaN/GaN schottky diode type NH_3 sensor is fabricated by electroless plating technique.	Experimental	Diode type, NH_3 sensor	The increase in temperature enhances the sensitivity while the sensing response decreases with the increase in humidity and this is attributed to the chemisorption of water molecules which in turn diminishes the effective adsorbent sites for test gas.
Chris Bishop, 2016 [73]	15 nm Pt gated GaN HEMT modelling and fabrication is presented for gas sensing,	Modelling/ Experimental	NO, NO_2, NH_3 sensor	Different gases behave differently on Pt gate and each gas has a specific optimal temperature for detection. The sensor characterization is performed for a large range of NO, NO_2 and NH_3 concentration and temperature range 100 to 400 ^oC. Effect of gate dimension, AlGaN barrier layer thickness and of Pt gate thickness is reported.
Yacine, 2016 [74]	Pt gated HEMT for operation in harsh environment of diesel exhaust (600 oC)	Experimental	NOx and NH_3, Environmental monitoring	Sensors capable of working in harsh environment of diesel exhaust systems are proposed for improved sensitivity to NO, NO_2 and NH_3. Gate is functionalized by Pt catalyst to embed gas sensing capability with fast response of 1sec.
S Jung, 2017[89]	Humidity is critical issue in respect to sensitivity in ambient. Spin coated PMMA is used for water blocking and mitigate humidity effects.	Experimental	H_2 gas sensor	Encapsulated devices don't show any decrease in response in presence of water and detection limits upto 100 ppm were obtained. PMMA encapsulated layer prevented water molecules to reach platinum gate and block adsorbent site while it allowed the permeation of hydrogen molecules without any decrease in sensitivity.

H I Chen, 2018 [65]	Sputtered HfO_2 is used to form Pd/HfO_2/GaN MOS type schottky diode.	Experimental	H_2 gas sensor	The response and recovery times are decreased as the temperature increases from 300 to 383K. The response time decreased from 39 sec to 5.3 sec while recovery time decreased from 42 sec to 2.5 sec when operated at elevated temperature of 383K. LOD= 5 ppm.
J. Sun, 2019 [80]	Tungsten oxide nano-film is modified as gate along with Pt micro heater	Experimental	No_2 sensor	Tungsten oxide nano-film is modified as gate along with Pt micro heater to act as a sensor platform. Detection of 100 ppb NO_2/NO at 300 ^oC is observed with response and recovery times of 88 and 132 sec respectively.
R. Sokolovskij, 2020 [69]	Impact of gate recess on Pt gate HEMT	Experimental	H_2 gas sensor	Study of Pt electrode gate recess (5-15 nm) where recessed device shows 145% increased response along with LOD of 5 ppm in air.
R. Sokolovskij, 2020 [90]	Gateless GaN HEMT for diesel soot characterization	Experimental	Particulate matter, environmental	Gateless GaN HEMT sensor was fabricated for particulate matter detection in diesel soot.
B Shen, 2020 [76]	In-plane growth of GaN honeycomb nanonetwork was grown on AlN/Si wafer by molecular beam epitaxy.	Experimental	NH_3 sensor	10 nm Pt gate GaN honeycomb nano network with large surface to volume ratio and exhibited wide detection range upto 5000 ppm. The sensor measurements were carried out at drain bias of 0.5 V and the temperature is varied from 30 to 150 ^oC. The best results were obtained when the operating temperature was 120 ^oC.
J Ahn, 2021 [70]	100 nm Sio_2 oxide based GaN HEMT with a bilayer graphene gate and 1 nm Pt.	Experimental	H_2 gas sensor	Ultra-high sensitive (1 ppm) GaN HEMT with Graphene gate decorated with Pt for H_2 detection was fabricated. Various Pt thicknesses were used to observe the effect of Pt film and it is observed that thinner Pt film showed higher sensitive response.
Arathy, 2021 [71]	AlGaN/GaN HEMT with gate workfunction as that of Pd	Simulation/Modelling	H_2 gas sensor	Modelling and simulation of GaN HEMT for H_2 detection through interface charge variation at RT.
T A Vuong, 2021 [72]	Optimized AlGaN barrier thickness in source connected to gate and floating gate configuration	Experimental	H_2 gas sensor	Ultra-thin AlGaN barrier of 9 nm exhibited 85% improved performance at 200 ^oC. The sensitivity response of normally on HEMT based sensor improved when the zero bias was applied to the gate as compared to the floating gate configuration.
W C Chen, 2021 [63]	Catalytic Pt hybrid metals with Pt film and Pt nano particles	Experimental	H_2 gas sensor	Presence of Pt nano particles gives spill over effect to increase its surface to volume ratio. Widespread detection range upto 1 ppm-1% H_2/air and operating temp 300-523K. most tests under RT.
Nguyen, 2021 [81]	24 x 120 um 30 nm Pd gate was e-beam evaporated	Experimental	No_2 gas sensor	The sensing device was tested for a temperature range from 25 to 300 ^oC where a stable operation was observed. The physical sensing mechanism is illustrated through simulations in TCAD by relating the change in gas concentration with the variation of band diagrams and carrier concentration.
Yu, 2021 [62]	Capacitive sensor with 10 nm Pd gate capacitive GaN honeycomb nanonetwork	Experimental	H_2 gas sensor	Using a passive device like capacitor for H_2 sensing has an advantage of being free of electric spark generation which could otherwise be hazardous because of hydrogen flammability, ultra-fast response which decreases with the increase in temperature.

3.2 Biosensors

As per IUPAC biosensor is a device that uses specific biochemical reactions mediated by isolated enzymes, immunosystems, tissues, organelles or whole cells to detect chemical compounds usually by electrical, thermal or optical signals. Simply put together, we can say a biosensor is an analytical device that detects changes in biological processes and converts them into a detectable signal which can be later displayed on a handheld device for point of care testing (POCT) applications [1]. GaN has been actively studied for its biosensing application due to its superior material properties such as high 2DEG density, high saturation velocity, high mobility, radiation hardness, proven non-toxicity to living cells desired for in vivo implantations and chemically inert to etching due to high bond strength making it resistant to harsh environments like highly acidic or alkaline, high temperature, nuclear power systems and outer space exploration systems among others. Silicon is widely used due to its mature fabrication but the problems associated with silicon is that it gets easily corroded in harsh environment besides it low temperature operation restriction (upto 200 ^{o}C), Gallium arsenide material system provides very high mobility and fast device response but the presence of arsenic makes it toxic for biosensing applications. The wide band gap nature of SiC and GaN has the advantage of less intrinsic concentration of $8.2x10^{-9}$ /cm^3 and $1.6x10^{-10}$ /cm^3 respectively, which translates into high signal to noise ratio as the lesser intrinsic concentration is associated with lower leakage and noise [2]. However, SiC suffers from low mobility (900 cm^2/Vs) and lack of heterojunction formation capability. Thus, GaN seems to have best properties which are a very important performance parameter for a robust biosensor. The formation of hetero junction of AlGaN/GaN adds piezoelectric polarization besides spontaneous polarization of AlGaN and GaN. The total polarization in the GaN material system leads to the formation of high density, mobility and saturation velocity 2DEG at the heterojunction which is balanced with the surface states. Any change in the charge state at surface will cause a change in surface potential and consequently a change in the 2DEG density in the channel and hence device performance making it a highly sensitive sensor platform.

The immune system in humans is really complex and is beyond the level of understanding. Antibodies comprise of sulphide bonded poly peptide amino acid chains, both heavy and light. These proteins are capable of selectively binding antigen molecules at the receptor sites and the sensors that work on this principle are called immunosensors. These sensors act as diagnostic tools to quantify the human body about how well the human immune system functions. Si based systems rather ISFET's have already been commercialized and they replace conventional sensor systems, the pH meters. However, the Si based systems face limitations of poor stability in aqueous solutions, requirement of bio-membranes and reference electrode. Unlike Si based devices, GaN based devices exhibits high chemical stability; the only known chemical is NaOH solution at 450 ^{o}C that can etch GaN. This inherent chemical and temperature stability of the material can be attributed to its wide band gap. In GaN, the ionic bond between Ga and N easily attracts protein molecules on to its surface. This forms the reason for GaN based systems being useful over a longer lifetime unlike the Si based systems that requires a bio-membrane specific coating for accomplishment of the same goal besides biomarker functionalization. The HEMT bio-sensors developed in the past decades is summarized in Table IV along with their transduction/sensing mechanisms. AlGaN/GaN HEMT is used in different configurations for biosensing purpose where some times the top GaN cap is functionalized, some other material like ZnO nanorods or 2D material are grown on GaN cap or a gold gate is functionalized for detecting a particular bio material. Usually, a linker molecule is drop casted first to attach antibody which can specifically bind to the antigen. A general representation of biosensing is given in Figure 17, where different antibody can be functionalized for the detection of a particular biomolecule of interest. Some of the earlier reports on AlGaN/GaN HEMT used for biosensing are given in Table IV.

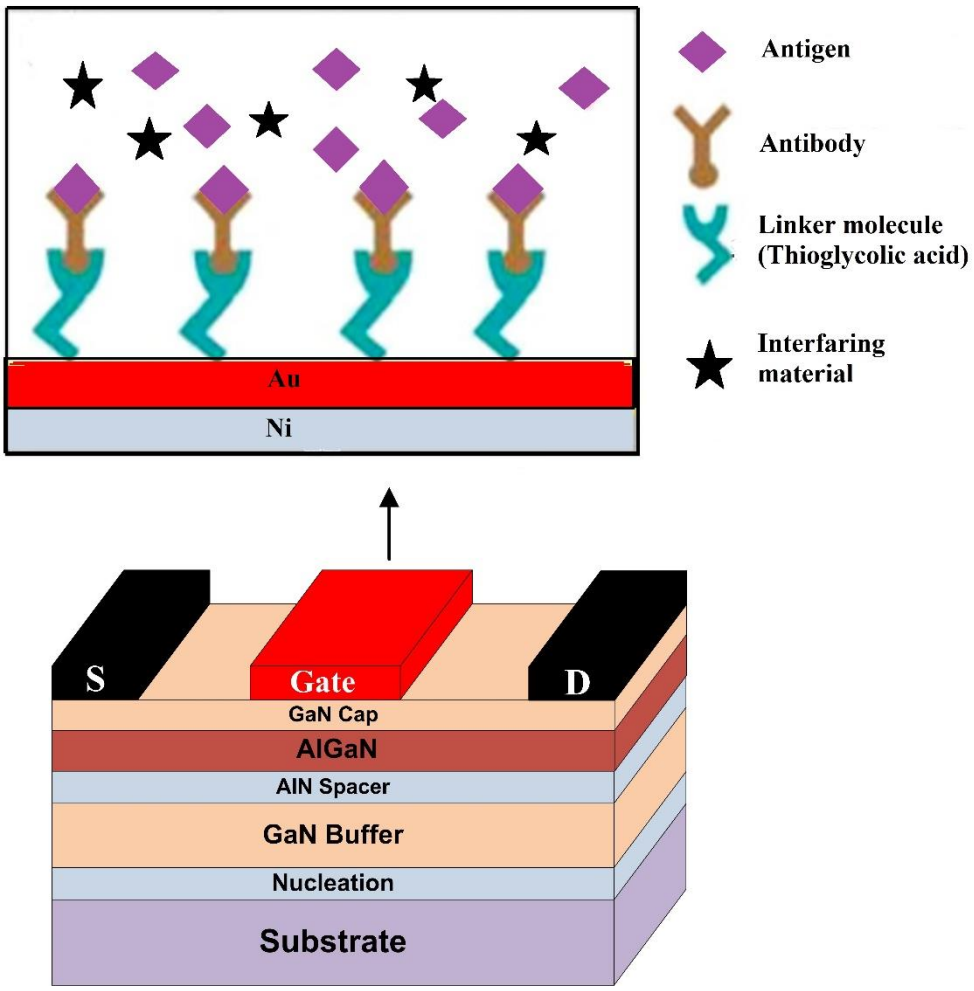

Figure 17 Representation of Biosensor functionalization used for the detection of biomolecule

3.2.1 GOx (Glucose oxidase enzyme) detection:

In this work, ZnO nano rods were grown selectively at the gate region through low temperature hydrothermal method to immobilize glucose oxidase (GOx) for the electrical detection of glucose. Using ZnO nano rods improves the surface to volume ratio which enhances the sensitivity and a rapid response of less than 5 seconds is observed when GOx solution at pH of 7.4 was exposed at ZnO sensing region. The sensor depicted a linear response for concentration range of 0.5 nM to 14.5 µM and the experimental limit of detection was 0.5 nM. GOx immobilization was performed by exposing 5 µl of GOx solution on sensing surface and the device was kept at 4°C in the solution for 48 hours and then the incubated for 30 minutes at 37°C. Afterwards different glucose concentrations were applied at sensing surface to measure its response at a drain bias of 250 mV where a decrease in current was observed as the concentration of glucose was increased. Glucose detection using glucose oxidase enzyme (GOx) as biomarker reported by Chu et al [11] reports sensitivity analysis for glucose concentrations varying from 0.5 nM to 125 µM. Kang et al. [91] reports sputter deposited ZnO nano rods at the gate/sensing area of the device for GoX detection. ZnO nano rods are used due to its nontoxic nature, bio compatibility and low fabrication costs involved. Both the devices used drain current modulation due to enzyme promoted reaction as the sensing metric. The variation in drain current with bio immobilization due to the variation in channel conductance (g_d) is used as sensing metric mostly, as this is easy to extract. However recent works shows that variation in channel conductance, and conductance to current ratios can effectively be used as sensing metrics. The device showcased excellent performance compared to FET counterparts. The drain current and conductance-based sensitivity of the device per mmol/l concentration of bio immobilization is found to be 0.206mA and 44.25mS/mm respectively in Varghese et al.[92].

3.2.2 Biomarker detection (C-erbB-2 (breast cancer) and PSA (Prostate Specific antigen for prostate cancer)):

Chen et al. reported the detection of breast cancer biomarker c-erbB-2 from human saliva in 2008. Biomarkers like ERBB2, HER2, CD340 etc can be effectively used for active screening of breast cancer and few of its variants that are dangerous. The glycoprotein expression increases by 25 to 30 % when affected by this disease. Hence, this biomarker can be used for early-stage detection and active surveillance of this disease. This protein concentration in human saliva and serum are in the range of few micrograms per ml and requires sensors with very high sensitivity and resolution. With introduction of c-erbB-2 antigen to the antibody functionalized HEMT gate, the device showed a rapid decrease in ON current with response time lower than 5s. The device showed sensitivity in the range of 0.25 µg/ml to16.7 µg/ml and nonlinear change in drain current was observed [93].

PSA (aliases: KLK3, APS, hK3, gamma seminoprotein, kallikrein-3) is a kallikrein related peptiside secreted by the prostate gland epithelial cells. In healthy men, PSA is present in small quantities in serum elevated quantities of PSA can be used as an indicator of prostate cancer and its aggressive variants like prostatitis and benign prostatic hyperplasia. Besides detection the monitoring of PSA is also required in affected patients in follow ups, therefore an ultra-sensitive PSA detector is necessary. Kang et al. [10] developed a HEMT Prostate Specific Antigen sensor for detection of prostate cancer. The physical sensing was achieved through lowering of drain current when PSA antibody binds through ester bonds (carboxylate succinimdyl ester) to the GaN sensing area functionalized with thioglycolic acid. The sensor shows a rapid response of less than 5 seconds while the current decreases as the concentration of prostate specific antigen is increased. The sensor could sense wide range of antibody concentrations ranging from 10pg/ml to 1 µg/ml depicting a decrease in current with increase in PSA concentration. The limit of detection (10pg/ml) is two orders lower than concentration cut off value of PSA for clinical detection of prostate cancer depicting a highly sensitive sensor. Research shows that if the rate of increase of PSA or the PSA velocity is >0.35ng/ml per year this can be used as a more specific biomarker than the level specific detection. Shuai Yang et al [94]reported a disposable gate HEMT design for trace level PSA detection which has a separate sensing platform easing the sensor reusability. The sensor was developed with the functionalization of cysteamine and glutaraldehyde which exhibited good linearity and specificity in response with LOD of 100 fg/mL. In order to have a feasible design of HEMT sensor simulations and modelling of the sensor is a pre requisite to analyse its sensitivity and feasibility of design before going into actual fabrication and sensor development. Varghese et al.[92] presented a mathematical model for sensitivity enhancement and device optimization. The theoretical findings present enhanced sensitivities of 0.91 mA/ngml^{-1}.

3.2.3 DNA (Deoxyribonucleic acid) detection:

Functionalized gold gated AlGaN/GaN HEMT was proposed by Kang [2006] for the detection of hybridization of DNA sequences through. Thiol based label free single stranded gate functionalization was encapsulated with PMMA except the sensing region. The thiol modified oligonucleotides are immobilized on gold gate to act as binding sites for the target DNA sequences in aqueous solution and thiol linking was confirmed by X-ray photo electron spectroscopy (XPS). The real time transient response depicts an increase in current from baseline device current when the thiol is added to the device, also the current decreases from thiolated value when the target DNA was exposed on sensing surface. The non-specific DNA was also tested and it showed a comparatively small change in current depicting a good specificity. R. Thapa et al. [9] demonstrated label-free detection of DNA hybridization using a GaN HEMT based transducer. The physical detection was achieved through immobilization of DNA, both amine modified and single stranded on SAM of mercaptoundecanoic acid. The drain-source current in the device substantially dropped on introduction of complementary DNA into the device gate well depicting DNA hybridization.

3.2.4 Zika virus and HIV (Human Immuno deficiency Virus) detection:

J. Yang et al. 2018 [95] reported a GaN HEMT sensor employing a cover glass as the sensing region thereby ensuring reusability. The bio functionalized gate could detect zika virus in the range 0.1 ng/ml to100 ng/ml. The antigen to antibody binding efficiency was found to be 0.013 to 0.84. A mathematical model for the same has also been reported which models the static and dynamic output current using spring like elastic relaxation model and Langmuir extension model. This work uses a disposable gated design where the sensing gate is a separate

entity that is bonded to the HEMT sensor through an interconnect. The disposable cover glass with large surface area is functionalized in this case to detect the viral biomarker with high selectivity and specificity. The bio signals are minute and when they travel through this medium, the signal losses and noise interferences become prevalent. Hence there is huge scope for improving sensitivities of these sensors by integrating the sensing surface on to the sensor there by increasing the proximity and reducing the signal losses along with noise.

Advancement in technology seems necessary for detection of HIV during AHI (Acute Human Immuno deficiency virus infection) acquisition and seroconversion phases. The concentration of this viral biomarker is very low during these phases and cannot be detected using conventional sensing devices or mechanisms with low resolution levels. Y. W Kang et al. [96] used HIV-Reverse Transcriptase (HIV-RT) immobilization on the gate electrode for the effective detection of binding of the bio-analyte to aid in drug development. It was reported from the investigation that a huge amount of time and cost overheads can be eliminated when AlGaN/GaN HEMT and the site-binding models are used in drug development.

3.2.5 CVD (Cardio Vascular Disease) detection:

Cardio vascular diseases can be detected at early stages through detection of levels of C-Reactive Protein. In order to overcome the limitations of having a sensing set up where the sensor has to be loaded on bulky semiconductor device analyser, [19] presents use of a null balancing circuitry to measure the variation in gate potential and output device currents. Pt gated transistors integrated with differential circuits reduces the noise signals by 97 % and improves the limits of detection of C-Reactive Protein [97]. The limit of detection of these devices were found to be 10 pg/ml providing a wide detection range of 0.01 ng/ml to 1000 ng/ml. Further double gating mechanisms proves to have advantages over conventional gating as they yield higher sensitivities through efficient charge screening increasing the resolution and specificity [98]. This system packaged in polymer is cheap and reliable to be used as Point of care test device and the application is not limited to hospitals or clinics. They can be used as personal healthcare equipment and are developed focusing on futuristic healthcare requirements.

3.2.6 Circulating Tumor Cells Detection:

An array of sensors has been proposed and demonstrated by A K Pulikkathodi et al. in 2017 that showcases high sensitivity and selectivity. These sensors have been used in the enumeration of CTCs (Circulating Tumor Cells) which are important markers for the diagnosis and prognosis of cancer metastasis. The proposed device design exhibits high resolution of even a single cell binding detection which is ascribed to the new electrical sensing technique where the output current shows a change when aptamer immobilized the CTC while using HCT-8 colorectal cancer cell line as a receptor [99].

3.2.7 Cardiac Troponin I Sensor:

Troponins have been used for acute myocardial infarction and other cardio related disease detection as it is released into blood quickly after cardio muscle damage and thus can be used as a clinical biomarker to monitor myocardial tissue. An electrical double-layer gated GaN HEMT Troponin I detector assay has been realized in I. Sarangadharan et al. [100]. The high sensitivity and gain in high ionic concentration of clinical levels can be ascribed to the unique EDL FET-based design and the assay turn-around time reduced to 5 min. A quantitative troponin detection from serum sample is presented here and the biosensor presented with its unique structure has the potential of being the future's economic and fast cardiovascular diseases biomarker assay.

3.2.8 NT ProBNP (N-terminal pro-B type natriuretic peptide) Sensor:

Tse-Yu Tai et al. 2019 demonstrates a promising aptamer functionalized biosensor with high and tunable sensitivities for selective detection of the clinical biomarker amine-terminated brain natriuretic peptides (NT-ProBNP). Detection is performed in a physiological salt environment and the sensor design overcomes the limitations of charge screening without limiting the sensitivities as the sensor is designed in such a manner that the space between the gate and the sensing area is maintained minimal and a higher gate voltage operation [101]. This study reports a methodology to avoid a very critical issue of Debye screening and therefore allowing direct detection of biomarkers at physiological concentrations for buffer and clinical serum samples without any pre-treatment.

3.2.9 Cortisol detection:

The adrenal cortex on kidney secretes a steroid hormone which acts as a biomarker for the psychological chronic stress and mental related issues and the sample for analysis can be taken through invasive method from blood or urine and non-invasively from saliva. The potential of GaN HEMTs for direct detection of a stress hormone known as cortisol through c-mAb (cortisol monoclonal antibody) binding is presented in [102]. The immobilization of biomarker is achieved through antibody-antigen binding while the sensor exhibits high sensitivity and resolution. Further, the performance enhancement has been achieved through use of illumination (532 nm Green laser light) as it helps to detrap electrons improving sensitivity and decreasing the limit of detection to 1 pM.

3.2.10 C-erbB2 detection:

In this study AlGaN/GaN HEMT sensing platform is developed for the detection of breast cancer through its specific biomarker C-erbB2. The device used for sensing purpose is a common drain two-finger gate design with a width of 125 µm and gate length of 5 µm. After the device fabrication the gate region is functionalized with organic linker self-assembled monolayers of thioglycolic acid which form Au-S bond for linking and was confirmed from Fourier transform infrared spectroscopy (FTIR) and energy dispersive spectroscopy (EDS) analysis. After this the functionalization is performed using a phosphate buffer saline (PBS) of 200 µg/ml C-erbB2 monoclonal antibody for 4 hours, and later tested with C-erbB2 positive human cancer cells. The device current shows an increase after thioglycolic acid incubation and then a decrease after antibody functionalization which decreases further when the positive cancer cells are exposed at the sensing region depicting a 31 % change in drain current implying the feasibility of the developed sensing platform for early stage disease diagnosis and prognosis [103].

3.2.11 C3G Sensor:

The sensor presented in P. Kacchawa et al. [104] uses extended source, drain pads and interdigitated gate electrodes to detect low concentrations of C3G from bio samples. C3G is a protein which belongs to the guanine nucleotide exchange factor (GEF) family responsible for proper functioning of various cellular activities and its imbalance is ascribed to tumorigenesis. Then antigen-antibody conjugation at the functionalized interdigitated gate is demonstrated through thioglycolic acid binding and EDC/NHS (N-ethyl-N'-(3-(dimethylamino)propyl) carbodiimide/N-hydroxysuccinimide) chemistry to activate the functional groups for reaction. The functionalization confirmation was established from the water contact angle measurement and the antibody-antigen immobilization was confirmed from atomic force microscopy measurement. After antigen-antibody immobilization, the output current increases and a maximum of 36.2% change in current is observed. The limit of detection of these biosensors are in the range of few hundreds of pg/ml with enhanced resolution in milliamperes.

3.2.12 HER-2 Sensor

S. Mishra et al. presents the design and development of a common drain AlGaN/GaN HEMT label free detection of HER-2 (human epidermal growth factor receptor-2) proteins for diagnosis of breast cancer. Antigen-antibody binding has been used for detection and the gate has been functionalized using cysteine methyl ester (CME) to link HER-2 antibody receptor which is highly selective to disease causing HER-2 antigen through less invasive process by using human serum which was confirmed from ELISA method [105]. The detection range here is few 100's of fg/ml to 10's of µg/ml. Also, the exposure of HER-2 antigen the output drain current increases and a maximum of 1.7 mA change in current is observed at a drain bias of 5V. The results reveal a promising alternate for diagnosis and prognosis purpose due to its high sensitivity, selectivity, rapid response time and low sample requirement.

Table IV HEMT based bio sensors, their functionalization and transduction mechanism.

Author, Year, Reference	Detected Quantity	Gate Material	Gate Functionalization	Sensing/transduction Mechanism
B. S Kang, 2007 [91]	Glucose	Sputtered ZnO nanorods	GOx	Enzymatic reaction
B. S Kang, 2007 [10]	Prostate Specific Antigen	Au metallization	PSA antibody functionalized gate	Antigen-antibody binding
H. T Wang, 2007 [106]	KIM-1	Au metallization	KIM-1 antibody functionalized gate	Antigen-antibody binding
K. H Chen, 2008 [93]	c-erbB-2	Au metallization	c-erbB-2 antibody functionalized gate	Antigen-antibody interaction
Y. L Wang, 2008 [107]	Botulinum toxin	Au metallization	Botulinum antibody functionalized gate	Antigen-antibody binding
B. H Chu, 2008 [108]	Lactic acid	Sputtered ZnO nanorods	Lactic Oxidase enzyme	Enzymatic reaction
Y. Song 2012 [109]	Uric acid	Nanotetrapods ZnO based	Uricase functionalized gate	Enzymatic reaction
R. Thapa, 2012, [9]	DNA	Au metallization	Thiolated DNA	DNA Hybridization
Y. W. Kang, 2013 [96]	HIV	Au metallization	Reverse Transcriptase immobilization	Antigen-antibody binding
H. F Huq, 2016 [110]	MIG	Au metallization	MIG antibody functionalized gate	Antigen-antibody binding
H. H Lee, 2015 [19], 2016 [97]	CVD	Pt metallization	C-Reactive Protein antibody functionalized gate	Antigen-antibody binding
A. K. Pulikkathodi 2017, [99]	Circulating tumor cells	Au metallization	Cell-specific functionalized gate	Cell binding
J. Yang, 2018 [95]	Zika virus	Au metallization	Thiolated RNA	RNA Hybridization
I. Sarangadharan 2018, [102]	Cardiac Troponin I	Au metallization	Thiolated Troponin specific aptamer functionalized gate	Aptamer-protein binding
T. Y. Tai 2019, [101]	NT-ProBNP	Au metallization	Thiolated DNA	Aptamer Protein Binding
K. Woo 2020, [102]	Cortisol	Au metallization	c-mAb functionalized gate	Antigen-antibody binding
N. Chaturvedi, 2021, [103]	C-erbB2	Au metallization	C-erbB2 monoclonal antibody	Antigen-antibody binding
P. Kachhawa 2022, [104]	C3G protein	Au metallization	C3G antibody functionalized gate	Antigen-antibody binding
S. Mishra 2022, [105]	HER-2	Au metallization	HER-2 antibody functionalized gate	Antigen-antibody binding

Simulation and Modeling methodologies for biosensors

The theoretical simulations of AlGaN/GaN HEMT for different sensing applications are also reported in literature with different approaches. The simulations for pH sensing are performed by utilizing the site binding model (SBM) and Guoy-Chapman-Stern (GCS) theory [111]. Simulations facilitate exploration of the device's full range and identify device optimized parameters. This will save a lot of time and cost before a sensor is actually fabricated. Also, it is better to develop a model which can predict the behaviour of a sensor to give more insightful knowledge about AlGaN/GaN HEMT device intricacies and try to optimize its response and then use that design for fabricating the sensor. Earlier reports performed the simulations to observe the effect of binding sites and reaction rates though not incorporating stern layer [112]. Others studied different oxide materials for sensing surface feasibility using a surface potential-based approach only. The other group investigated the effect of drain bias, gate length and surface binding sites through physics-based modelling using Florida object-oriented device simulator (FLOODS) framework [113], [114]. The simulations for pH sensor involve the definition of electrolyte through an intrinsic semiconductor whose mobility and band gap are modified to emulate electrolyte. The interaction between device sensing surface and electrolyte leads to the formation of stern layer and a diffuse layer, collectively known as electrical double layer (EDL). The stern layer is emulated through an oxide in such a way that its capacitance is 20 $\mu F/cm^2$. When a pH sample comes in contact with the sensing surface it will protonate or deprotonate the surface altering the interface charge density according to the pH value. The acidic pH will protonate the surface while the basic pH will deprotonate the surface and consequently increase or decrease of 2DEG in the channel to increase or decrease the drain current which can be used as a sensing metric [115]–[117]. Similarly, if reference electrode system is used the protonation or deprotonation will result in negative or positive shift in threshold voltage which can be another sensing metric. A number of studies have been reported using different designs to improve the sensitivity where the shift in threshold voltage or change in drain current was used to investigate the sensing behaviour of a sensor. Likewise, many simulation reports are there where the researchers have attempted to emulate the biological entities like proteins, DNA, antibodies etc in the simulation platform to investigate the biosensing attributes of the sensor. The various approaches include the representation of neutral biomolecules through its dielectric constant and for charged biomolecules like DNA it is represented by the dielectric constant as well as the charge associated to the biomolecule [118]–[121]. There are many designs reported in the literature such as nanogap embedded cavity, dual cavity, underlap and open gate designs. The other approach includes the charge deduction methodology where the charge associated to a biomolecule is calculated and same is introduced as an interface charge to investigate its effect on the device characteristics or the potential equivalent of that charge is calculated and applied on gate contact to check its sensitivity response. Various studies are also reported in terms of modelling the sensor response to different pH, biomolecules, gases etc in an attempt to optimize the device design for highly sensitive sensor [122], [123].

3.3 pH sensors

The site binding model (SBM) was proposed by Yates [124] in 1973 which unravelled the insights into the oxide-electrolyte interface. The adsorbed counter ion species interact with the oxide surface charge groups to form interfacial ion pairs which in turn alters the surface potential in accordance with the ionic concentration. The operation of FETs used for sensing applications is illustrated in terms of the site dissociation model and the variation of potential across the insulator-electrolyte interface. The voltage drop across this interface depends on the pH of the electrolyte which itself is a function of point of zero charge pH and a sensitivity parameter. The study by Bousse [125] in 1983 reveals that the flat band voltage is a very important characteristic which itself depends on the various charges associated with the insulator and insulator-electrolyte interface. The pH sensing mechanism can be understood from the SBM through the protonation (SOH_2^+) and deprotonation (SO^-) of the amphoteric surface sites (SOH) as given in Eq. (22) and (23). These reactions result in positive or negative

interface charge density which modulates the channel charge carrier concentration accordingly and consequently the output drain current.

$$SOH_2^+ \leftrightarrow SOH + [H_s^+] \tag{22}$$

$$SOH \leftrightarrow SO^- + [H_s^+] \tag{23}$$

P. Bergveld, studied the underlying operation mechanism for the ISFETs and proteins where remarkable similarities were observed consequently leading to important conclusion of similarity between oxide and protein molecule for the design of ISFET biosensors [126]. The pH sensitivity, buffer capacity of solution, acid-base properties of proteins and experimental measurements are reported. The changes in ionic concentration tend to cause a change in ionic charges in the supporting electrolyte which depends on the sensitivity parameters and double layer capacitance. This leads to the change in surface charge and eventually surface potential. It is also observed that for a larger difference in the bulk pH and the iso-electric pH of the protein the output response will be mainly dominated by the presence of protein molecule. A general theory regarding the potential at the surface of oxide and electrolyte solution interface was proposed by P Bergveld in 1996 [111]. The change in electrostatic potential is explained in terms of the variation in the double layer capacitance and the intrinsic buffer capacity. When an electrolyte is put on an oxide, surface reactions will take place which leads to the emergence of charge at the oxide surface. These charges at surface will develop potential difference between surface and the bulk related via Poisson-Boltzmann (PB) statistics. The activity of proton at surface is related to the bulk activity through PB equation:

$$H_s^+ = H_b^+ \exp\left(-\frac{q\psi_o}{KT}\right) \tag{24}$$

Where, H_s^+ is the proton activity at surface, H_b^+ is the bulk proton activity, q is the elementary charge of electron, ψ_o is the electrostatic potential near oxide/electrolyte interface, T is temperature and K is the Boltzmann constant. The surface reactions and equilibrium equations are described by the site dissociation model approach where we can get a resultant surface charge density. Using charge neutrality and site binding model equations the resultant surface charge density can be derived as:

$$\sigma_0 = q\, N_s \left(\frac{[H_s^+]^2 - K_a K_b}{[H_s^+]^2 + K_a K_b + [H_s^+]K_a}\right) \tag{25}$$

Where, K_a and K_b are the acid and base dissociation constants explained elsewhere [111]. The change in this surface charge density due to an infinitesimal change in in surface pH is referred to as intrinsic buffer capacity, which depicts the capability to maintain a specific pH of a solution and its value should be as high as possible. The oxide surface charge variation manifests in the change in double layer charge which could be calculated from Guoy-Chapman-Stern (GCS) model. The formation of charge distribution at the surface immersed in solution leads to emergence of charge devoid Stern layer and the diffuse layer which is formed by the attraction of counter ions from the solution to screen surface charge. This charge is screened by equal and opposite charge at a certain distance forming inner Helmholtz plane (IHP) while the layer containing counter charges has a maximum approach to certain distance known as outer Helmholtz plane (OHP). The random thermal motion counteracts to attraction forces which tends to equalize ionic concentration of the solution which is possible as the attraction forces become weaker with the increase in distance from surface where the thermal motion dominates. This equilibrium between surface attraction and random thermal forces produces the diffuse layer, where the ionic concentration of supporting electrolyte is given as in Eq. (26):

$$n_i(x) = n_b^o \exp\left(-\frac{qZ_i\psi_x}{KT}\right) \tag{26}$$

Where, $n_i(x)$ is the molar concentration of species at a distance x with respect to bulk, n_b^o is the bulk concentration and Z_i is the valency of ions. The total charge per unit volume at a distance x from bulk is given as:

$$\rho\,(x) = \sum n_i\,(x) Z_i q = \sum \mathrm{n_b^o}\ \exp\left(-\frac{\mathrm{qZ_i\psi_x}}{\mathrm{KT}}\right) Z_i q \tag{27}$$

This charge is related to potential through Poisson equation and can be written as in Eq. (28):

$$\rho\,(x) = -\epsilon\epsilon_o\ \frac{d^2\psi}{dx^2} \quad \text{or} \quad \frac{d^2\psi}{dx^2} = -\frac{\rho\,(x)}{\epsilon\epsilon_o} \tag{28}$$

Solving this, we get

$$\frac{d\psi}{dx} = -\sqrt{\frac{8KTn_o}{\epsilon\epsilon_o}}\ \sinh\frac{\mathrm{qZ\psi_x}}{\mathrm{KT}} \tag{29}$$

Therefore, using Poisson-Boltzmann statistics and gauss's law the surface potential and charge density relationship is established. From Gauss's law, we have

$$E = \frac{Q}{\epsilon\epsilon_o} = \frac{\sigma_O}{\epsilon\epsilon_o} \tag{30}$$

$$\sigma_O = \epsilon\epsilon_o\ E = -\epsilon\epsilon_o\ \frac{d\psi}{dx} = -\epsilon\epsilon_o\ \sqrt{\frac{8KTn_o}{\epsilon\epsilon_o}}\ \sinh\frac{\mathrm{qZ\psi_x}}{\mathrm{KT}} \tag{31}$$

$$\sigma_O(Charge\ density\ on\ oxide) = -\sigma_{dl}(Charge\ density\ on\ EDL)$$

Therefore, the relationship between surface potential and surface charge density on oxide is given as in Eq. (32):

$$\sigma_O = \sqrt{8KT\ \epsilon_o\epsilon_w\ n_i^o}\ \sinh\frac{\mathrm{qZ\psi_x}}{\mathrm{2KT}} \tag{32}$$

However, as the ions have finite size and can't approach the surface any closer than ionic radius, a plane of closest distance for the centres of the ions at distance x_2 exists called as OHP. The field strength at x_2 is given as;

$$\frac{d\psi}{dx} = -\sqrt{\frac{8KTn_i^o}{\epsilon\epsilon_o}}\ \sinh\frac{\mathrm{qZ\psi_2}}{\mathrm{2KT}} \tag{33}$$

As there is no ion in OHP, the field is constant and potential drop is linear. The interfacial potential can be related to double layer charge as:

$$\begin{aligned}\sigma_O = -\sigma_{dl} = -\epsilon\epsilon_o\left(\frac{d\psi}{dx}\right)_{x=x_2} &= -\sqrt{\frac{8KTn_i^o}{\epsilon\epsilon_o}}\ \sinh\frac{\mathrm{qZ\psi_2}}{\mathrm{2KT}} \\ &= \sqrt{8KT\ \epsilon\epsilon_o\ n_i^o}\ \sinh\frac{\mathrm{qZ}\left(\psi_0 + \frac{x_2\,\sigma_O}{\epsilon\epsilon_o}\right)}{\mathrm{2KT}}\end{aligned} \tag{34}$$

Therefore, equating the SBM and GCS model final solution for the surface charge density can be obtained which can relate the interfacial potential to every bulk pH. Also, the sensitivity of the FET to the pH is given by:

$$\psi_{o=-log_e 10} * \delta_w * \frac{KT}{q} * \left(pH - pH_{pzc}\right) \tag{35}$$

Where the terms used are explained in our earlier work [115]. The other important parameter of interest is the differential capacitance, defined as the ability of the electrolyte to store charge in response to the change in

electrostatic potential and its low value is desired for higher sensitivity. Various oxides like SiO_2, Al_2O_3 and Si_3N_4 are studied for different molar concentrations of the electrolyte to study the effect of different oxides and ionic strength on sensitivity. The oxide with higher binding sites and ionic strength solution showed higher sensitivity. Some of the earlier reports on AlGaN/GaN HEMT used for pH sensing are discussed and a bird's eye view is also given in

Table V.

A model was presented by Landheer in 2005 [127] for the sensitivity analysis of FET based sensors using potential diagram to detect charged species in the electrolyte while considering amphoteric surface sites on the oxide. This method is equally valid to the functionalized semiconductor surface or metal gate where the charged biomolecules are depicted through an ion permeable membrane whose potential variation follows Poisson-Boltzmann equation. The application of the concept has been extended to illustrate the operation of BIOFET with some insights on effects of thermal noise and noise associated with trapping/detrapping through tunnelling of carriers at the electrolyte-oxide interface.

An earlier review on silicon-based FETs by Shinwari in 2015 [128] provides comprehensive insights into the physics of FETs, mechanism and application of ISFETS in biosensing along with the detailed analysis of electrolyte-oxide interface. The electrochemistry of ionic solutions is described by illustrating dissociation reactions for water besides that bulk charge transport in electrolytes is also highlighted. The structure of electrolyte insulator semiconductor field effect transistor (EISFET) is described along with its potential diagram, charging of insulator surface and the extension of EISFET as pH sensor and a BIOFET for DNA sequencing application with its circuital analysis. Various aspects of noise in the FETs which can lead to random fluctuations in output signal are highlighted so that remedial measures can be taken which include thermal noise due to carrier in transistor and electrolyte, flicker noise and other faradaic process-based sources. This study provides a concise description of basic theories of MOSFET, EISFET, surface electrochemistry and interactions associated with the oxide-electrolyte interface and sensing membrane surface.

Stutzman et al in 2002 [129] reported one of the first review reports highlighting the ability of AlGaN/GaN HEMT heterostructure for sensing applications. This stems from polarization established in the III-V nitride which makes it sensitive to the changes in surface charge states caused due to the adsorption of ions, wetting of liquids, catalytic schottky contact exposure to gases and mechanical strain to name a few. The basic electrostatics of polarization was discussed which is helpful in understanding the basic physics and highlights the shallow 2DEG is highly sensitive to the changes in surface charges and for any adsorbed positive or negative ion an electron in 2DEG is added of lost. The various samples tested in this work were isopropanol, acetone, methanol, hydrogen, fibroblast cell and piezoresistive pressure or strain.

Steinhoff et al [130] fabricated GaN HEMT, oxidized GaN HEMT and GaN cap AlGaN/GaN HEMT by plasma induced molecular beam epitaxy (PIMBE) and studied their response to various pH environments at the surface. The native and thermally grown oxide devices were tested for different pH and a response of 58.7 mV/pH is obtained which is close to Nernst limit of sensitivity with a pH resolution 0.05 depicting that a native oxide is responsible for pH sensitivity.

The open gate AlGaN/GaN HEMT design with sensing region dimension (WxL= 500x10 µm) was used for liquid phase wet environment measurements which showed proper output characteristics with distinct linear and saturation regions for V_{GS}=0 to -2 while varying V_{DS} from 0 to 1V [131]. The output current sensitivity for variation in pH value from 4 to 10 was observed to be 33 µA/pH. The threshold voltage sensitivity was investigated by an electrochemical cell measuring circuit through reference electrode measurements depicting a pH response of 57.5 mV/pH. The Open gate AlGaN/GaN HEMT were also fabricated with Sc_2O_3 oxide as sensing membrane having dimensions of (WxL= 150x2 µm) to test its pH response[41] . The polar electrolyte causes variation in surface charge density which manifests as change in 2DEG to change current when the pH is varied from 3 to 10. The transient measurements were carried out at V_{DS}=0.25 V and an average sensitivity of 37 µA/pH was observed while using Sc_2O_3 as oxide with a pH resolution of less than 0.1 pH over the entire range of pH. Also, a comparative investigation is performed for different gate oxides [132]. The native oxide

device showed higher current sensitivity of 70 µA/pH with a resolution of 0.4 pH, Sc_2O_3 oxide device showed a current sensitivity of 37 µA/pH with pH resolution of 0.1 pH while the UV Ozone established oxide showed intermediate results with a resolution of 0.2 pH. Another study on AlGaN/GaN HEMT open gate design with various sensing dimensions is reported in [133]. Both reference electrode and without reference electrode configurations are studied for their pH response which exhibited a stable operation in aqueous electrolytes. The device with area 490x40 µm depicts best sensitivity value of 1.9 mA/pH at V_{DS}=5 V and V_{GS}=-5.

Due to the chemical inertness diamond has been a largely used material in biosensing regime. Dipalo reported on the integration of boron doped diamond as electrochemical gate to accrue the benefits of stability of diamond and the high transconductance HEMT to render a highly sensitive sensor of the order of 50mV/pH [134]. After fabrication the device is covered with epoxy and the contacts and sensing gate region are opened for characterization and pH sample exposure. The measurement set up is depicted in Figure 18 (a) and the response for exposure of sensing region to the pH of 1 and 13 is obtained as shown in Figure 18 (b) depicting a positive shift in threshold voltage.

The methods to predict and consequent optimization of charge sensitivity for ungated AlGaN/GaN HEMT was reported in [135], [136]. The numerical simulations are performed and validated with different barrier layer composition fabricated devices. The main observations were that a thinner barrier layer and lower Al mole fraction in AlGaN layer render highest sensitive device for pH sensing applications by ensuring near zero threshold voltage. For a near zero threshold voltage and maximum transconductance to be at zero reference voltage and achieve a maximum sensitivity for reference free electrode platform, the threshold voltage is adjusted by using photoelectrochemical (PEC) oxidation of GaN cap layer as illustrated in [136]. The investigated device structure schematic and fabricated device micrograph is shown in Figure 19 (a) and (b) respectively.

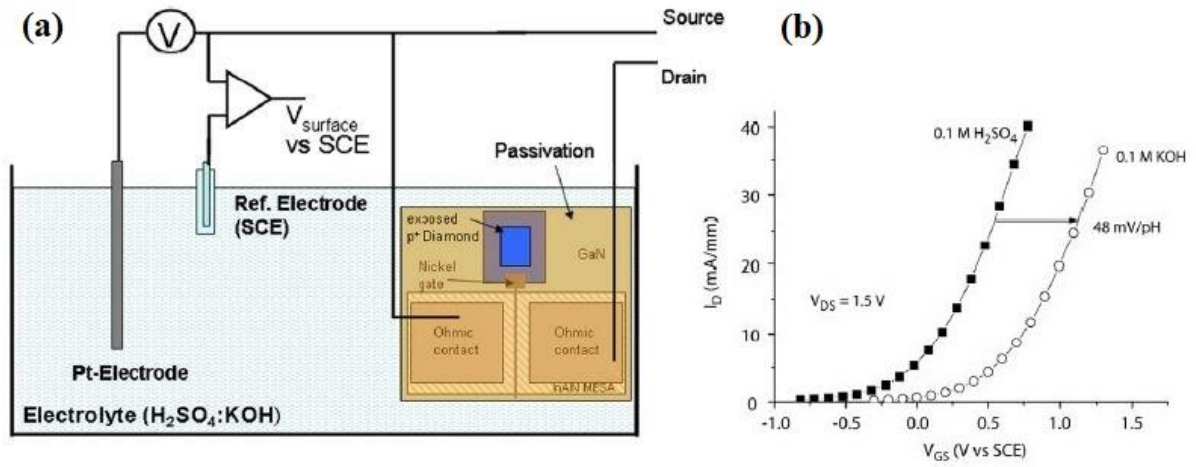

Figure 18 Figure: (a) Set up of electrochemical cell (b) Transfer characteristics of the sensor when exposed to pH=1 and pH=13 at a drain bias of 1.5V. Reprinted from [134], M. Dipalo et al., "Combining diamond electrodes with GaN heterostructures for harsh environment ISFETs," Diam Relat Mater, vol. 18, no. 5–8, pp. 884–889, 2009, doi: 10.1016/j.diamond.2009.01.011. Copyright (2009) with permission from Elsevier.

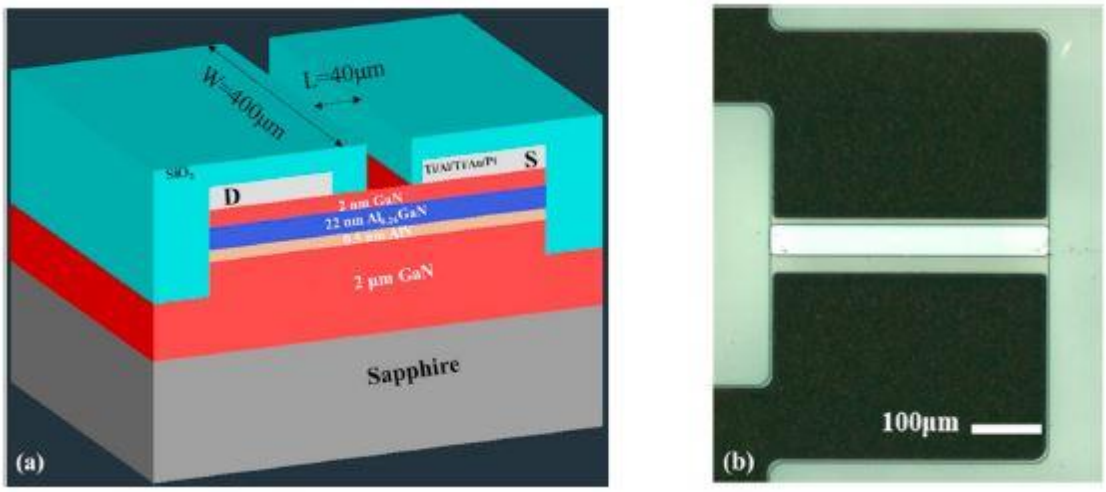

Figure 19 Figure: (a) Schematic of the device structure depicting its layer structure (b) Fabricated device image. Reprinted from [136], D. Xue et al., "Enhancing the sensitivity of the reference electrode free AlGaN/GaN HEMT based pH sensors by controlling the threshold voltage," Sens Actuators B Chem, vol. 306, no. December 2019, p. 127609, 2020, doi: 10.1016/j.snb.2019.127609. Copyright (2020) with permission from Elsevier.

The sensing area used in this study is 400x40 µm and the pH resolution was 0.5 pH. Figure 20 (a) and (c) depict the output characteristics for once and thrice PEC etches when exposed to pH of 4, 7 and 10. The current depicts a decrease when higher pH is used and the relative change in this current is used as performance metric called as current sensitivity. Similarly, Figure 20 (b) and (d) depict the shift in transfer characteristics and increase in transconductance when the PEC etch duration is increased in terms of number. The transfer characteristics shows a positive shift with the increase in PEC oxidation time, however as the PEC oxidation treatment time is increased the oxide thickness increases which becomes resistant to further oxidation reaction. The reason for the right shift is the conversion of GaN cap into Ga_2O_3 oxide which has higher band gap that results in the improved solid-liquid interface barrier. The shift in threshold voltage observed was from -3.46 to -1.15 V which corresponds to the maximum transconductance shift from -2.6 to -0.1 V. Also, the change in current per pH observed for conventional reference free electrode sensor was 0.7 µA which increased to 14 µA for PEC treated sensor indicating 20 times increase in sensitivity.

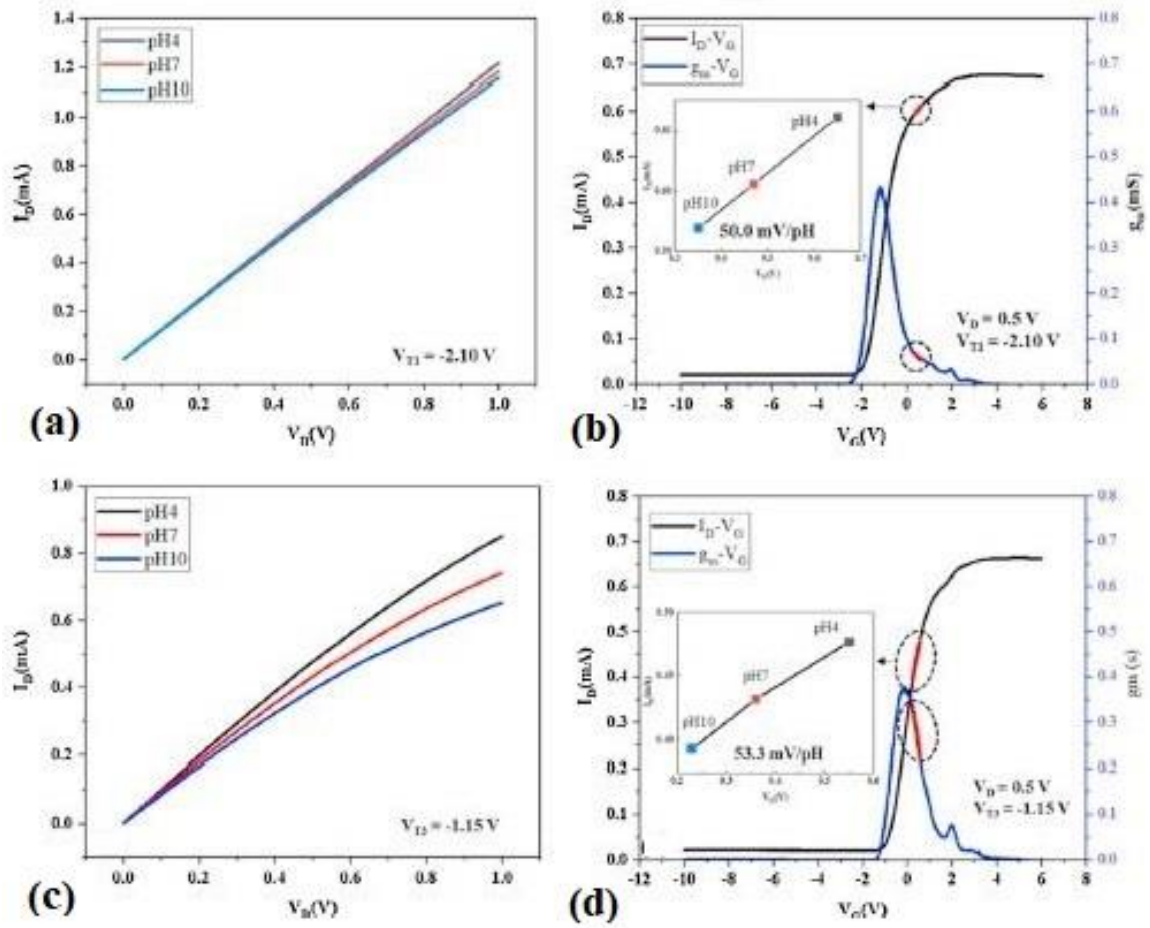

Figure 20 (a) Output characteristics of the sensor after one photo electrochemical etch for pH of 4, 7 and 10, (b) Transfer characteristics for DI water at drain bias of 0.5V, (c) Output characteristics after three times of PEC and (d) Transfer characteristics of the sensor with reference electrode configuration at drain bias of 0.5V. Reprinted from [136], D. Xue et al., "Enhancing the sensitivity of the reference electrode free AlGaN/GaN HEMT based pH sensors by controlling the threshold voltage," Sens Actuators B Chem, vol. 306, no. December 2019, p. 127609, 2020, doi: 10.1016/j.snb.2019.127609. Copyright (2020) with permission from Elsevier.

The role of oxide as a sensing membrane and the growth process of oxide were investigated in various studies. Al_2O_3 was used as an oxide for passivation and sensing membrane (sensing region of 200x50 µm) with some devices without passivation for reference [39], [137]. The Al_2O_3 passivated devices showed 32% increase in output current. The voltage sensitivity measurements are performed by applying reference voltage through the electrolyte and the corresponding sensitivities for unpassivated and passivated devices are 41.6 and 55.2 mV/pH, while the output current sensitivity for these two sensors is 42.8 and 55.8 µA/pH, respectively. The transient analysis is also reported where a constant decrease in drain current is observed as the pH increases from 4 to 10. The transient time of passivated device is less and hence faster in response. The various other aspects of sensors like the hysteresis and drift in measurements are also studied. Passivated sensor has less hysteresis value of 4.8 mV with respect to 8.7 mV for unpassivated sensor along with lesser drift depicting a clear advantage in using passivated device for pH sensing applications. Some used atomic layer deposition (ALD) to grow Al_2O_3 and investigate its sensitivity. Al_2O_3 based ISFET exhibits two order less gate leakage current improving the device stability. Proper transfer and output characteristics are observed with a corresponding shift in characteristics depending on the pH sample tested. The I_{DS}-V_{REF} characteristics for the normal ISFET and ALD deposited Al_2O_3 ISFET are depicted in Figure 21 (a) and (b) respectively, where a positive shift in characteristics is observed that is plotted for proper depiction in Figure 21 (c). The use of ALD Al_2O_3 as sensing film improves the surface properties by providing a smooth surface with RMS roughness of 0.6 nm and lowering contact angle to allow more ionic species to link the binding sites and consequently enhance the response from 48.4 mV/pH to 57.8 mV/pH [138].

The effect of thermal oxidation on the growth of Al_2O_3 was also studied as the AlGaN/GaN HEMT based devices are fabricated and then thermally oxidized at a temperature of 600, 700 and 800 ^oC to have an oxide layer as a sensing membrane [139]. It is observed that the treatment temperature is crucial in determining the transformation of hydroxide into oxide, while Al_2O_3 is formed at lower temperature Ga_2O_3 if formed at higher temperature and both can coexist at 800 ^oC. From AFM scans it is observed that the roughness of the oxide surface also depends on growth temperature of oxide, while smooth surface is observed for sample oxidized at 700 ^oC while the oxide grown at 800 ^oC showed some needle like peak protuberances.

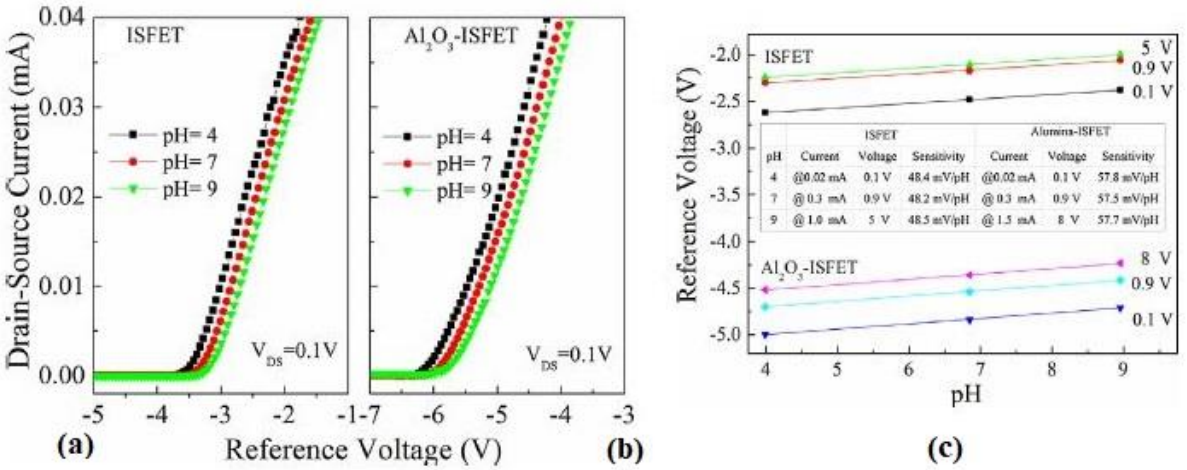

Figure 21 Transfer characteristics of (a) ISFET, Al2O3–ISFET and (c) Reference voltage for different pH. Reprinted from [138], L. Wang, L. Li, T. Zhang, X. Liu, and J. P. Ao, "Enhanced pH sensitivity of AlGaN/GaN ion-sensitive field effect transistor with Al 2 O 3 synthesized by atomic layer deposition," Appl Surf Sci, vol. 427, pp. 1199–1202, 2018, doi: 10.1016/j.apsusc.2017.09.072. Copyright (2017) with permission from Elsevier.

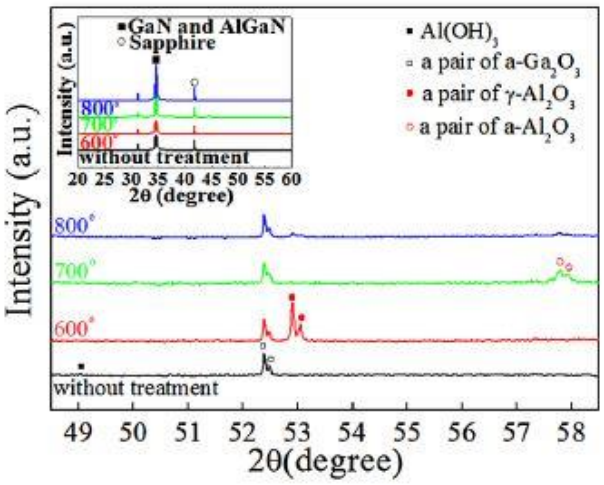

Figure 22 ISFET surface XRD spectra revealing the constituents of surface material, inset shows same XRD spectra at wider scan range. Reprinted from [139], L. Wang, Y. Bu, L. Li, and J. P. Ao, "Effect of thermal oxidation treatment on pH sensitivity of AlGaN/GaN heterostructure ion-sensitive field-effect transistors," Appl Surf Sci, vol. 411, pp. 144–148, 2017, doi: 10.1016/j.apsusc.2017.03.167. Copyright (2017) with permission from Elsevier.

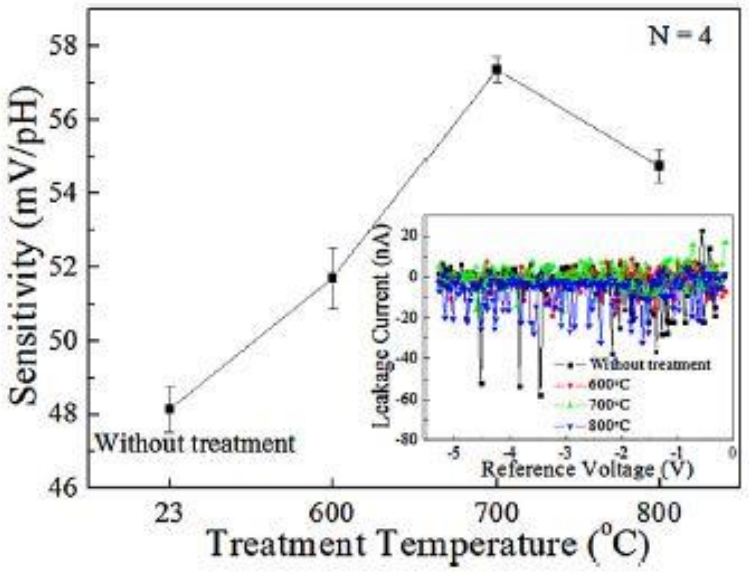

Figure 23 Effect of thermal oxidation on average sensitivity after treatment at 600, 700 and 800 oC, inset shows the leakage current behaviour. Reprinted from [139], L. Wang, Y. Bu, L. Li, and J. P. Ao, "Effect of thermal oxidation treatment on pH sensitivity of AlGaN/GaN heterostructure ion-sensitive field-effect transistors," Appl Surf Sci, vol. 411, pp. 144–148, 2017, doi: 10.1016/j.apsusc.2017.03.167. Copyright (2017) with permission from Elsevier.

It is also seen that as the oxide growth temperature increases the surface hydroxide will initially transform to γ-Al_2O_3 and then to a more stable phase α-Al_2O_3 as observed from XPS analysis resulting in higher sensitivity as shown in Figure 22. Therefore, oxide growth temperature is a critical parameter to tune the interface and surface properties for better sensitivity [140]. The sensitivity increases as the oxidation temperature is increased till 700 and decreases thereafter due to the formation of α-Al_2O_3 as shown in Figure 23.

X Ding et al [51] developed a molecular gated HEMT in which the gate region or sensing region was modified with 3-aminopropyltriethoxysilane (APTES) to improve binding sites or receptors. The successful immobilization is confirmed from SEM images where the GaN surface having amine terminated APTES and gold nano particles having carboxyl-terminated groups can be seen anchored. The APTES modification of sensing region will render hybrid detection sites in terms of hydroxyl and amine groups which help to enhance the sensitivity from 22.25 to 37.17 µA/pH. The modified sensor exhibits good transient response to both acidic and basic pH. Similar work was also reported by Zhiqi Gu[31]. However, in their work, the sensing region is modified by the functionalization of ethanolamine to provide extra binding amine sites on the surface so that large number of ionic or bio species are linked and thereby increase the sensitive response implying a proper surface modification strategy could be used to enhance the sensitivity of the device. The modified device was first analyzed for the response to different pH and an improved sensitivity and linearity in response was obtained for both acidic and basic pH solutions. A current sensitivity of 83.51, 79.42 and 80.92 µA/pH is observed for neutral, acidic and alkaline pH solutions, respectively. The same device was further modified by functionalization with glutaraldehyde and Prostate specific antibody to detect prostate specific antigen and a good response was observed with a very low limit of detection of the order of 1fg/ml.

H Zhang et al [141] reported on possible optimization strategy through gate geometry. In this study the effect gate geometry on the sensitive response of packaged device is investigated to render optimized device design. It is observed that the series resistance is key parameter affecting the current sensitivity is of packaged sensor which depends on the aspect ratio (W/L) of gate structure. If the aspect ratio is small, the channel resistance dominates the total resistance in the system and the sensitivity increases as aspect ratio is increased further. If aspect ratio is large, the series resistance of the packaged sensor dominates total resistance and the sensitivity

decreases as the aspect ratio increases depicting there is an optimum aspect ratio to be maintained for better sensitivity.

N Sharma et al [42] proposed a high-resolution electrochemical sensor for pH and chloride ion detection. A two-finger common drain AlGaN/GaN HEMT is fabricated and used for testing in dry environment like air and wet environment like DI water, pH and salinity of NaCl in DI water. The sensing mechanism is explained from the band bending, when different pH solutions are exposed on the sensing surface it leads to the adsorption of ionic species on gate surface which alters the surface charge and consequently the channel 2DEG. The pH sensitivity of 4.32 µA/mm-pH was observed at V_{DS}=1V and V_{GS}=0V, while a sensitivity of 6.48 and 2.02 mA/mm-molar for NaCl in DI water was observed at V_{DS}=1 and 5V respectively, with V_{GS}=0V. Also, a fair response time of 250-350 ms was observed.

Q. Cheng et al [142] reported a planar dual gate HEMT having a dual gate configuration to provide tunable gain and eventually desired amplification capability as shown in Figure 24. This configuration lets the use of sensor in very narrow pH ranges like in human blood (7.35-7.45) and a wide range pH like in sweat (4-6.8) easily. The device is implemented like an inverter and the sensitivities are deduced from the voltage transfer characteristics (VTC) for blood pH and sweat pH. The effect of output load resistor, reference electrode bias and second gate bias are also shown depicting a clear shift in curves which could be adjusted to obtain maximum sensitivity. The ability to tune the sensor for detecting small and wide range pH make it an attractive option to be inducted as a next generation sensor platform. The sensitive response is adjusted by tuning the gate voltage which increased the sensitivity from 45 mV/pH to 2.06 V/pH and its maximum is determined by the value of load resistor.

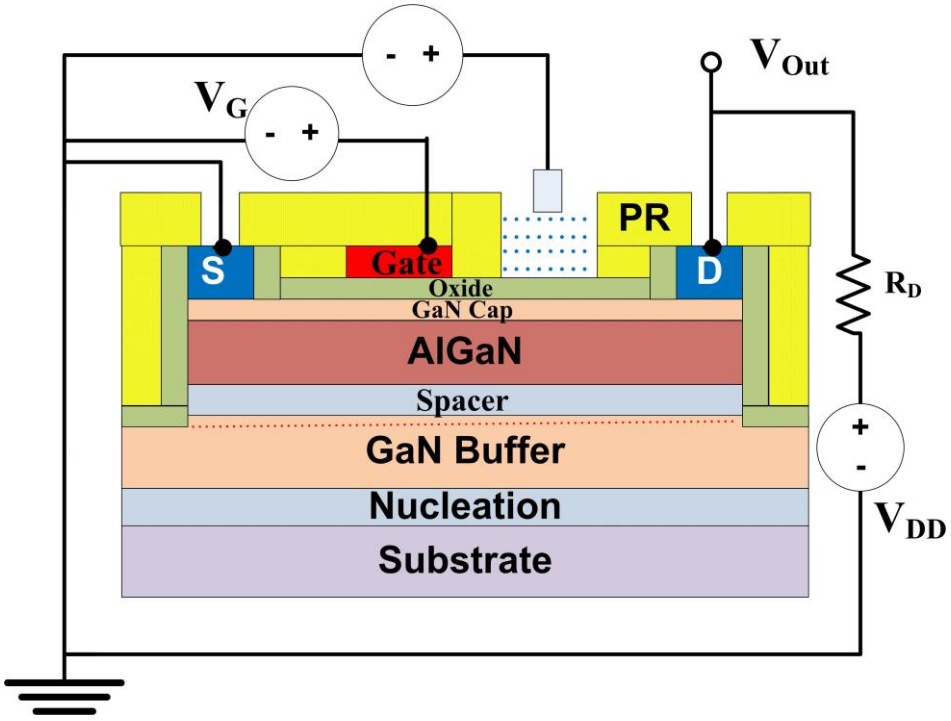

Figure 24 Illustration of a dual gate AlGaN/GaN HEMT pH sensor design

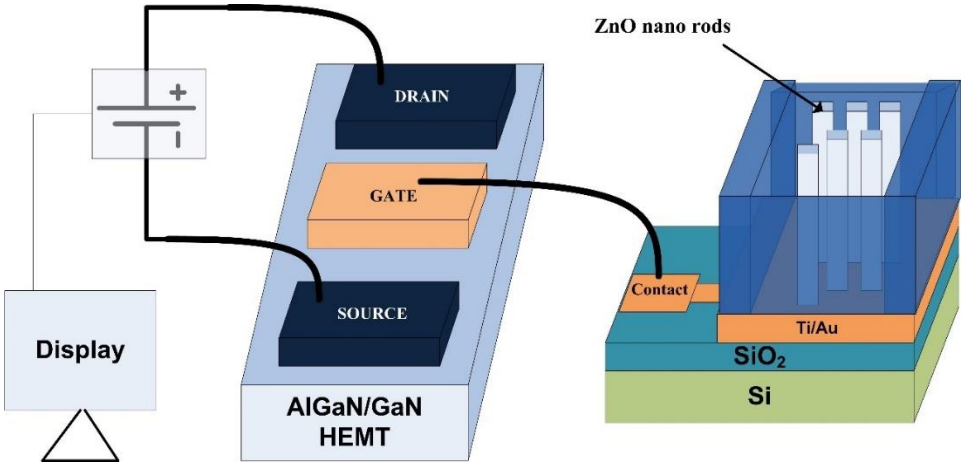

Figure 25 Illustration of an extended/disposable gate AlGaN/GaN HEMT pH sensor design

To enhance the stability and sensitivity of the normal HEMT based sensor a structurally improvised sensing platform is proposed having reference HEMT device integrated with the normal sensing HEMT device. The new structure improves the voltage sensitivity from 49.43 mV/pH to 54.38 mV/pH with a 20% increase in stability with respect to conventional counterpart. The performance is analysed using double layer model integrated into the equivalent circuit model and it is observed that the equivalent resistance and electrical noise is reduced which enhances stability of testing signal. The sensing area comprises of 250x30 µm [143]. Another strategy pursued in research is the extended or disposable gate design as shown in Figure 25. where the sensing part is separated from the active device. This separated device and sensing part has the advantage of ease in measurement and reusability of the sensor. AlGaN/GaN HEMT with an extended SnO_2 sensing platform is reported for pH sensing applications [52]. A 3 nm ALD deposited Al_2O_3 oxide is used to reduce leakage current of the active device, while the sensing membrane is on separate platform where testing can be done easily and later disposed and the main HEMT transducer can be reused. The sensing area dimension are 6x50 µm and the pH sensitivity is analysed from transfer characteristics considering a reference current of 1 nA where a linear shift in threshold voltage of 56.39 mV/pH is observed at V_{DS}=0.05 V. The transient time analysis also shows a nice real time response with a sensitivity of 20.48 µA/pH. Similar work regarding an extended disposable gate sensing platform strategy was proposed for pH sensing [144] where ZnO nanorods are grown on the sensing platform to increase its surface to volume ratio which is further functionalized with ethanolamine to protect ZnO nanorods from dissolution due to the acidic and alkaline environment and eventually improve its stability and sensitivity as shown in Figure 25. ZnO nanorods are realized through a two-step hydrothermal method using zinc acetate, sodium hydroxide, zinc nitrate and hexamethylenetetramine as precursors. The ethanolamine modification not only prevents the nanorod dissolution in strong acid or base but also improves the pH sensitivity from 12.17 µA/pH for bare nanorods platform to 22.86 µA/pH for the ethanolamine functionalized sensing membrane. The selectivity of the sensor was also verified where other ions like K^+ and Na^+ were tested and the device was insensitive to them implying a selective response to H^+ ions.

In order to achieve beyond Nernst limit sensitivity in HEMT, a resistive coupling network is used comprising of coplanar control gate and sensing gate, where an extended configuration is used, as shown in Figure 26 (a) and (b) respectively. Figure 26 (c) depicts an equivalent model of the fabricated design. The amplification for pH sensitivity beyond Nernst limit is achieved by the change in the magnitude of resistance between the sensing and control gate. By varying the ratio of resistance between control and sensing gate from 1:1, 2:1 and 3:1 the corresponding voltage sensitivities are 56, 112 and 167mV/pH, respectively as rendered from Figure 27 (a-d). A disposable gate platform is also demonstrated that avoids direct contact of sensor to wet environment which prevents damages to the sensor while improving its reliability [145].

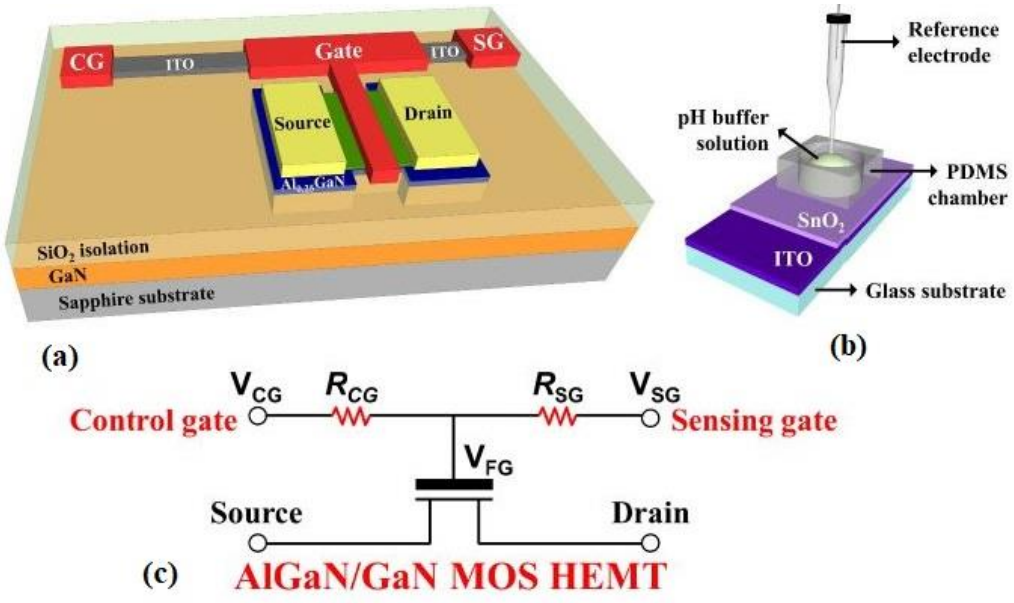

Figure 26 Figure: Device structure schematic of co-planar AlGaN/GaN HEMT and (b) Extended gate or sensing unit [145]

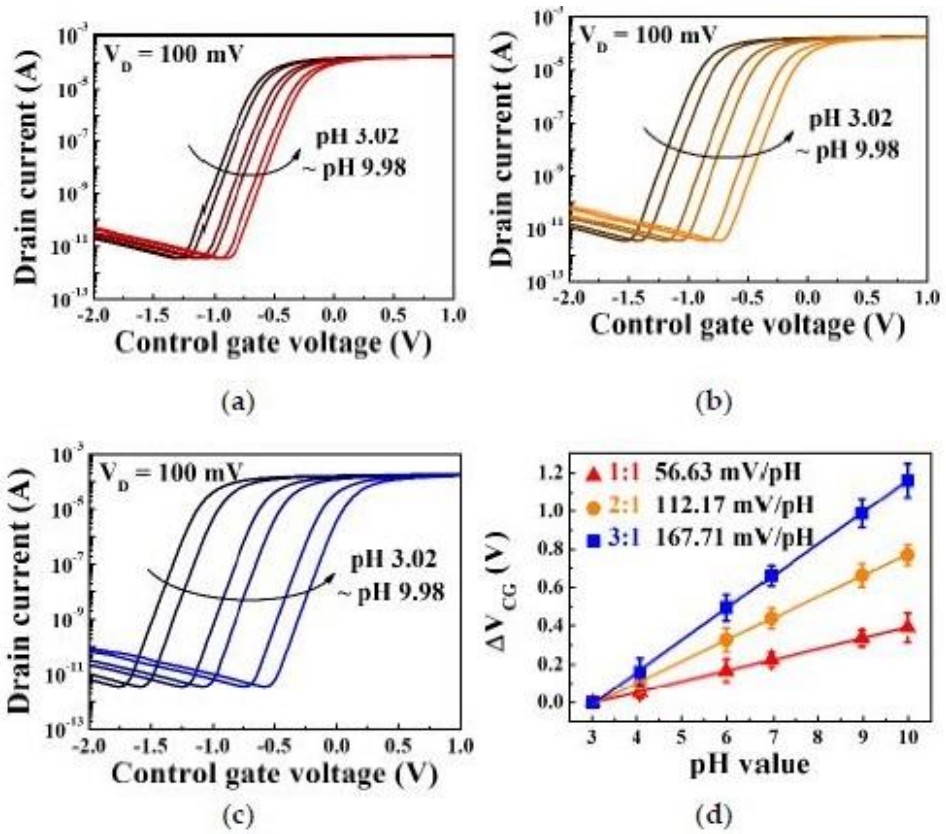

Figure 27 Transfer characteristics for various pH samples with different ratio of control gate and sensor gate (R_{CG}:R_{SG}) (a) 1:1, (b) 2:1 and (c) 3:1 (d) Change in control voltage with the change in pH [145]

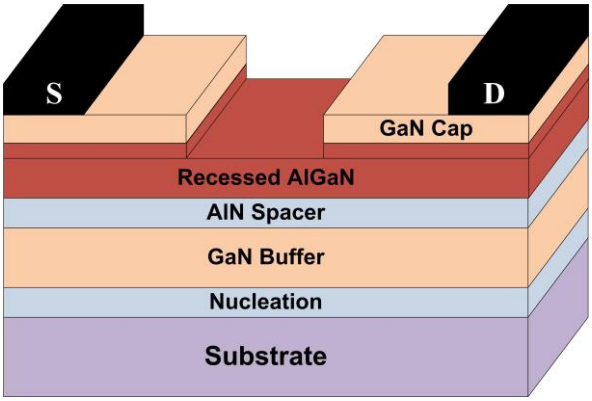

Figure 28 Device schematic of Recessed barrier layer AlGaN/GaN HEMT

The conventional, recessed and recess with ammonium hydroxide treatment devices were fabricated and tested for pH response where the structure of recessed AlGaN schematic is given in Figure 28. The sensitivity was evaluated from relative shift in drain current and threshold voltage. The recessed device with ammonium hydroxide treatment depicted the best result for sensitivity. To understand the dependence of response on the surface and the type of response obtained XPS study was performed which revealed a large change in the content of nitrogen atoms by varying the ratio of Ga-N and Ga-O bonds. Also, the dry etching for recess creates N vacancies under the gate forming virtual gate with a negative shift in threshold voltage. However, ammonium hydroxide treatment fills some N vacancies improving the threshold voltage sensitivity. In terms of sensitivity a 61% increment is observed for the recessed with NH_4OH treated device. This can be attributed to enhanced transconductance and improvement in potential sensitivity due to combined use of recess to decrease 2DEG channel to surface distance and NH_4OH treatment to improve surface condition, respectively [146].

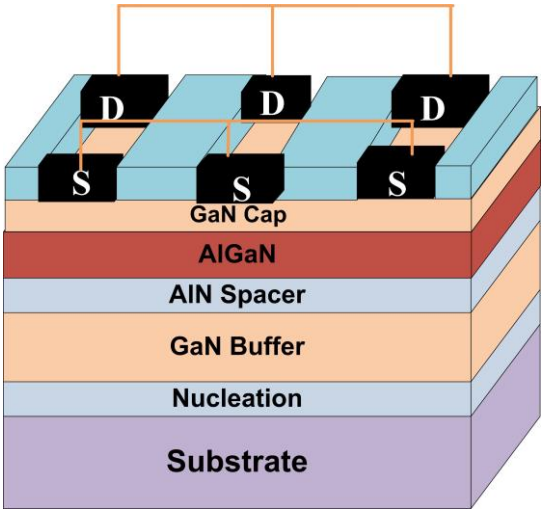

Figure 29 Device schematic of Planar Multi channel AlGaN/GaN HEMT for pH sensing

Recently highly sensitive sensor was developed by integrating multi-channel configuration as shown in Figure 29 with 365 nm UV light coupling mechanism together to enhance the sensitivity by 30 times with respect to conventional design [147]. This improvement can be attributed to the increase in sensing area and effective channel resistance decrease for parallel multi-channel design. The length and width of the channels is 900 and 50 µm respectively. The sensor with multi-channel design when used without UV coupling renders a sensitivity of 10.37 µA/pH, while the peak sensitivity of 37.04 µA/pH is obtained when coupled with UV light. Also, a small hysteresis width of 6 µA and a rapid response of 1 second was observed along with a stable output where only a drift of 7-9 nA/hour is observed depicting a degradation of 0.71% after a month implying a robust design.

Summary of Modelling, Simulation and Fabrication approaches to investigate pH sensing capabilities of AlGaN/GaN HEMT

A theoretical model was developed to depict the sensitivity of AlGaN/GaN HEMT towards different values of electrolyte pH [148]. The surface charge density and associated reactions are incorporated using SBM while as the electrolyte is modelled based on the solution of Poisson-Boltzmann equation for potential. The values for dissociation constants, material properties and the concentration of surface sites are obtained from the experimental results and a good agreement with experimental results was observed. This model also predicted an improved response for the N-face polarity GaN heterostructure, decreasing Al mole fraction and increasing the sensing region or area. Many reports are there which provided other different ways to simulate the behaviour of the sensor for pH sensing to predict sensor output and use the optimized design for actual fabrication of sensor. A simulation methodology for pH sensing application of AlGaN/GaN HEMT is studied providing insights into many aspects of the sensing. The developed simulation methods are used to predict the device behaviour by studying the effect of available binding sites, adsorbed charge, and surface potential that translates into change in current where from sensitivity can be deduced by evaluating change in output current in regards to reference [112], [113]. The proposed methodology takes the advantage of SBM to express the surface reactions of ionic species and the results of modelling depict a close match with the experimental results validating the model authenticity. The electrolyte semiconductor boundaries are defined through the Poisson's equation while the carrier and ionic species transport is captured by using drift diffusion equations, the electrical double layer is represented by an oxide and the electrolyte-semiconductor interface interactions are captured through reaction as per site binding model. The device is investigated for voltage sensitivity depicting a pH resolution of 58.6 mV/pH and current sensitivity of 4.7 mA/mm-pH at 5V. The other study investigates and provides some key insights into the effect of gate length and drain bias on the sensitivity of the sensor to find out the optimum design and operating condition for measurement [114]The study reveals an increase in the sensitivity with the increase in drain bias however, a trade-off with the power consumption must be considered as per the application and availability.

Recently some studies have been reported for modelling and simulations of AlGaN/GaN HEMT for pH sensing applications. The pH sensor simulation methodology is proposed for predicting the response of AlGaN/GaN HEMT device. The electrolyte is emulated through semiconductor whose material properties are modified in accordance to the electrolyte. The charge associated with a pH is calculated through the model and that charge is introduced as the interface charge to analyse the effect of corresponding pH solution. Analysis of without reference electrode device exhibits lower sensitivity with respect to the reference electrode configuration where the device can be tuned to maximum transconductance condition for higher g_m and eventually higher sensitivity [115]. The other study is an extension of our previous work on pH sensor simulation model. The device response sensitivity is studied and some important results are reported which are quintessential to be considered while designing a pH sensor. The AlGaN barrier composition is studied where the barrier thickness and Al composition are varied to analyse the effect of each parameter on the sensitivity. It was observed that a thinner barrier and lower Al composition resulted in higher sensitivity due to the increment in transconductance for the thinner barrier which is attributed to better gate coupling to the 2DEG channel carriers [149]. The other group also reported somewhat similar results with modelling aspects and some important conclusions are given [117], [150], [151]. In these works, an analytical model for pH sensing analysis is demonstrated using AlGaN/GaN HEMT material system. The electrolyte is modelled through semiconductor and is defined in a nano gap embedded cavity under gate region. The 2DEG charge concentration, threshold voltage and drain current models are proposed and verified with the simulation results where a good match is observed. The effect of sensing region length and barrier layer thickness was evaluated and a larger sensing region and thinner barrier exhibited higher sensitive behaviour. A bird's eye view of earlier reported work is given in

Table V.

Table V Some insights and Performance comparison of various pH sensor designs reported earlier

Author, Year, Reference	Abstract of work	Type of work	Sensitivity V	Sensitivity I	Remarks
D. E Yates, 1973 [124]	SBM of EDL at oxide-electrolyte interface	Theoretical			The SBM was proposed which provided the insights into the oxide-electrolyte interface
P. Bergveld, 1996 [111]	A general model	Theoretical/Analytical			A general theory regarding the potential at the surface of metal oxide and electrolyte solution interface is proposed. The change in electrostatic potential is explained in terms of the variation in the double layer capacitance and the intrinsic buffer capacity.
M. Strutzman, 2002 [129]	GaN heterostructure for sensing applications	Experimental			This is one of the first review reports highlighting the potential of AlGaN/GaN HEMT heterostructure for sensing applications. The various tested samples are that of isopropanol, acetone, methanol, hydrogen, fibroblast cell and piezoresistive pressure or strain sensor.
G. Steinhoff, 2003 [130]	pH response of GaN surfaces	Experimental	58.7 mV /pH		In this report a GaN FET, oxidized GaN FET and GaN cap AlGaN/GaN HEMT were grown by PIMBE and studied for their response to pH changes at the surface.
M. Bayer, 2005 [148]	Theoretical study of electrolyte gate AlGaN/GaN HEMT	Theoretical/Analytical			A theoretical model has been developed to depict the sensitivity of AlGaN/GaN HEMT towards different pH values of an electrolyte. The surface charge density and associated reactions are incorporated using SBM while the model for electrolyte depends on the solution of Poisson-Boltzmann equation for potential.
D. Landheer, 2005 [127]	Study of various aspects of sensing	Theoretical			A model is presented for the sensitivity analysis of FET based sensors using potential diagram to detect charged species in the electrolyte while considering amphoteric surface sites on the oxide.
T. Kokawa, 2006 [152]	Open gate liquid phase sensor	Experimental	57.5 mV /pH	33 µA/pH	The liquid phase wet environment measurements were performed with an open gate AlGaN/GaN HEMT. The device showed fast and stable response when exposed to polar liquids and the drain current linearly decreased with the increase in normalized electric dipole moment.
Shinwari, 2007 [128]		Review			This study provides a concise description of basic theories of MOSFET, EISFET, surface electrochemistry and interactions associated with the oxide-electrolyte interface and sensing membrane surface.
B S Kang, 2007 [37]	Response to pH variations by a Sc_2O_3 sensing film	Experimental		37 µA/pH	Open gate AlGaN/GaN HEMT were fabricated with Sc_2O_3 oxide depicting a pH resolution of less than 0.1 pH over the entire range of pH.
B S Kang, 2008 [132]	Role of gate oxide in pH sensors	Experimental		37 and 70 µA/pH	In this report a comparative investigation is performed for different gate oxides. The native oxide device showed higher current sensitivity of 70 µA/pH with a resolution of 0.4 pH, Sc_2O_3 oxide device showed a current sensitivity of 37 µA/pH with pH resolution of 0.1 Ph while the UV Ozone established oxide shoed intermediate results with a resolution of 0.2 pH.
M S Z Abidin, 2011 [133]	Open gate pH sensor	Experimental		1.9 mA/PH	Open gate HEMTs with various sensing dimensions are defined by photolithography. Both reference electrode and without reference electrode configurations are studied for their pH response which exhibit a stable

					operation in aqueous electrolytes.
A Podolska, 2015 [115]	Methods to predict and optimize sensitivity of open gate HEMT device	Experimental/ Simulation			Thinner chosen barrier layer and lower Al mole fraction will render highest sensitive device by ensuring near zero threshold voltage for pH sensing applications.
H Y Liu, 2015 [117]	H_2O_2 grown Al_2O_3 sensing membrane	Experimental	41.6-55.2 mV/pH	42.8-55.8 µA/pH	Both unpassivated and passivated devices were fabricated and the Al_2O_3 passivated devices showed better performance due to a greater number of binding sites. The transient time of passivated device is less and hence fast in response.
E. Patrick, 2015[113] ,	Open gate pH sensing simulations	Simulation	58.6 mV/pH	0.14, 2.8, 4.7	This report describes the simulation methodology which can be used as a simulation framework to investigate the sensing response of chemical sensors before going into actual fabrication.
M. Sciullo, 2016 [112]	GaN HEMT optimization for chemical sensing	Simulation		1.4 mA/mm-pH	This study investigates and provides some key insights into the effect of gate length and drain bias on the sensitivity of the sensor. The study reveals an increase in the sensitivity with the increase in drain bias however, a trade-off with the power consumption must be considered as per the application and availability.
L Wang, 2017 [139]	Effect of thermal oxidation on pH sensitivity	Experimental	57.5 mV/pH		It is observed that the thermal treatment temperature is critical in determining the transformation of hydroxide into oxide. It was observed that as the oxide growth temperature increases the surface hydroxide will initially transform to γ-Al_2O_3 and then to a more stable phase α-Al_2O_3 as observed from XPS analysis resulting in higher sensitivity.
X Ding, 2018 [51]	Molecular gated HEMT for pH sensing applications	Experimental		37.1 µA/pH	Molecular gated HEMT has been fabricated and modified with APTES to furnish amphoteric amine groups that act as the receptors for pH detection exhibiting good transient response to both acidic and basic pH.
L Wang, 2018 [138]	Al_2O_3 by ALD	Experimental	48.4-57.8 mV/pH		The use of ALD Al_2O_3 as sensing film improves the surface properties by providing RMS roughness of 0.6 nm, less gate leakage current and lower contact angle allowing more ionic species to bind the binding sites and consequently sensitivity
J Y Pyo, 2018 [52]	Extended gate HEMT with SnO_2 as sensing membrane for PH sensing application.	Experimental	57.6 mV/pH	20.84 µA/pH	AlGaN/GaN HEMT with an extended SnO_2 sensing platform is reported for pH sensing applications. A 3 nm ALD deposited Al_2O_3 oxide is used to reduce leakage current of the active device, while the sensing membrane is on separate platform where testing can be done easily and later disposed and the main HEMT transducer can be reused.
Z Qui, 2019 [144]	Ethanolamine modified HEMT for pH and bioassay applications.	Experimental		79.4-83.5 µA/pH, LOD for PSA 1fg/ml	Ethanolamine modified molecular gate platform is proposed where the GaN surface (sensing region) is modified to render amphoteric amine groups for pH and probe molecular immobilization of PSA. The device also shows an improved response when used for PSA detection with LOD of 1fg/ml.
L Li, 2019 [140]	Normally OFF HEMT based ISFET	Experimental	48.5-56.3 mV/pH		Photoelectrochemical etch process is used to etch AlGaN barrier and transform into oxide in order to realize a normally off HEMT.
M. Sciullo, 2019 [112]	Review on GaN HEMT pH sensors	Review			The developed simulation methods are used to predict the device behaviour by studying the effect of available binding sites, adsorbed charge, and change in surface potential on the channel charge which translates into change in current where from sensitivity can be deduced.

Niketa, 2020 [42]	High resolution electrochemical sensor	Experimental		4.32 µA /mm-pH	A two-finger common drain AlGaN/GaN HEMT is fabricated and used for testing in dry environment like air and wet environment like DI water, pH and salinity of NaCl in DI water.
Q. Cheng, 2020 [142]	Planar dual gate HEMT with tunable sensitivities	Experimental	45 mV/pH, 2.06 V/pH		A planar dual gate HEMT having a dual gate configuration to provide tunable gain and eventually desired amplification capability in order to use the sensor in very narrow pH ranges like in human blood and a wide range pH like in sweat.
Y. Dong, 2020 [143]	Enhancing pH sensitivity by reference HEMT device	Experimental	49.4-54.3mV /pH		To enhance the stability and sensitivity of the normal HEMT based sensor a structurally improvised sensing platform is proposed having reference HEMT device integrated with the normal sensing HEMT device.
D. Xue, 2020 [137]	Enhancing voltage sensitivity of reference electrode free HEMT	Experimental		7-14 µA/pH	In order to achieve a near zero threshold voltage for the maximum transconductance to be at zero reference voltage and achieve a maximum sensitivity for reference free electrode platform, the threshold voltage is adjusted by using photoelectrochemical oxidation of GaN cap layer.
S K Cho, 2021 [145]	Co planar gate HEMT for improved sensitivity	Experimental	167 mV/pH		To achieve beyond Nernst limit sensitivity in HEMT, a resistive coupling network is used comprising of coplanar sensing gate and a control gate.
P pal, 2021 [88]	pH sensing model	Model/Simulation	950 mV/pH	9300 µA/mm-pH	An analytical model for pH sensing analysis is demonstrated using AlGaN/GaN HEMT material system. The effect of sensing region length and barrier layer thickness was evaluated and a larger sensing region and thinner barrier exhibited higher sensitive behaviour.
A M Bhat, 2021 [115]	pH sensor simulation model	Model/Simulation	110 mV/pH	17 mA/mm/pH	A pH sensor simulation methodology is proposed for predicting the response of AlGaN/GaN HEMT device. The electrolyte is emulated through semiconductor whose material properties are modified in accordance to the electrolyte.
A M Bhat, 2021 [149]	pH sensor sensitivity optimisation	Simulation	162 mV/pH	15 mA/mm/pH	It was observed that a thinner barrier and lower Al composition resulted in higher sensitivity due to the increment in transconductance for the thinner barrier which is attributed to better gate coupling to the 2DEG channel carriers.
Yue He, 2021 [146]	Recessed HEMT for pH sensing	Experimental	39.5-55.8 mV/pH	52.2-78.8 µA/pH	Conventional, recessed and recess with ammonium hydroxide treatment devices were fabricated and tested for pH response. Recessed device with NH_4OH treatment depicts enhanced transconductance and improvement in potential sensitivity due to combined use of recess to decrease 2DEG channel to surface distance and NH_4OH treatment to improve surface condition, respectively.
Z. Guo, 2021 [144]	Ethanolamine functionalized ZnO nanorods based Disposable AlGaN/GaN HEMT	Experimental		12.1-22.8 µA/pH	An extended disposable gate sensing platform strategy is proposed for pH sensing; where ZnO nanorods are grown on the sensing platform to increase its surface to volume ratio which is further functionalized with ethanolamine to protect ZnO nanorods from dissolution due to the acidic and alkaline environment and eventually improve its stability and sensitivity.
X. Yang, 2021 [147]	Enhancing pH Sensitivity with multi-channel and UV light	Experimental		37.04 µA/pH	In this work, a highly sensitive sensor is developed by integrating multi-channel configuration with 365 nm UV light coupling mechanism together to enhance the sensitivity by 30 times with respect to conventional design which can be attributed to the increase in sensing area and effective channel resistance decrease for parallel multi-channel design.

3.4 Heavy metal ion sensors

Heavy metals can be categorized as the metals whose density varies between 3.5 to 7 g/cm^3. During earth's core formation the heavy metals descended deep however, they can find course to ecosystem through water bodies, mining and other industrial processes. While some heavy metals are necessary for biological and physiological processes their excess amount may lead to detrimental effects. Therefore, the monitoring of such heavy metals is essential especially in drinking water as higher amounts of mercury can have toxic effects on physiological systems like digestive, nervous, reproductive, immune, endocrine etc [153]. Excess of lead can cause harmful effects on renal, nervous, cardiovascular systems and exposure to foetus can cause miscarriage, premature and low body weight births. Similarly, excess in zinc makes a person more vulnerable to gastro intestinal and respiratory tract disorders while higher doses can cause prostate cancer [154]. The bird's eye view of the earlier reported work is rendered in Table VI.

Mercury (Hg) is a toxicological pollutant cation posing toxic and chronic environmental threats. Hg enters the ecosystem through various routes such as fertilizers, mining, fossil fuels, industrial effluents, solid waste incineration and volcanic emissions causing contamination of water and soil which bio accumulate in the food chain. The world health organisation (WHO) and environmental protection agency (EPA) prescribe a standard limit of 1 and 2 ppb Hg ion concentration in drinking water respectively. Therefore, the higher concentration of Hg in human body can be detrimental and has a number of health issues associated to it like neurodegenerative diseases, respiratory issues like pulmonary edema and nephrotic syndrome. Also, DNA strands have a thymine nucleotide bonding with cytosine, the presence of Hg can lead to Hg-thymine complexes causing alterations in DNA replication mechanism. Conventional methods of Hg detection have drawbacks of time-consuming testing at specific labs, thus non portable and costly.

H T Wang et al [155] reported gold gated AlGaN/GaN HEMT and analyzed its response to Hg ions using two different designs such as bare gold gate and thioglycolic acid (TGA) functionalized gate surface. TGA functionalized sensors depicted better response than bare gold gate sensors (2.5 times). TGA improves hydrophillicity by reducing contact angle from 58.4^o to 16.2^o which enables more ionic species adhesion and consequently larger effect on channel carriers, current and sensitivity. A response time of 15 s and 5 s was observed for bare and TGA functionalized sensors respectively as the sensors were exposed to a concentration of 10^{-5} M of Hg. The TGA functionalized sensor showed a LOD of 27 ppb (10^{-7} M) and a 100 times higher selectivity over Na^+ and Mg^{2+}. This sensor could be operated at low power (8 µW, 0.5 V, 80 µA at 11Hz) and harnessed in portable hand held systems.

An oligonucleotide functionalized GaN cap layer AlGaN/GaN HEMT sensor is demonstrated for Hg detection taking advantage of Thymine-Hg-Thymine binding interaction to enhance detection upto trace amounts [156]. The functionalization with 5' amino modified oligonucleotides was followed by UV oxidation for 30 minutes, which was later functionalized with APTES and followed by amine group activation by glutaraldehyde. The binding of Hg increases current due to Hg accumulation at sensing surface and the LOD of the sensors was estimated to be 10^{-14} M Hg concentration depicting a highly sensitive sensor. The sensor also depicted a good selectivity when other ions such as Co^{2+}, Zn^{2+}, Mn^{2+} and Pb^{2+} were introduced in the sensing region.

MoS_2 is formed by S-Mo-S covalent bonds via weak van der Waal's force of attraction and it comes under the category of transition metal dichalcogenides (TMDCs) and has excellent properties such as good conductivity, fast electron transport, tunable band gap, thermal stability, natural abundance as molybdenite and high surface to volume ratio making it an outstanding contender for future electronic systems. Therefore, functionalization of gold gate was performed with 20 mg/ml MoS_2 to enhance the detection of Hg^{2+} ions under UV illumination besides normal light. The device with a gate length of 50 µm and source to drain separation of 100 µm were fabricated where MoS_2 was synthesized through hydrothermal process and the gate was functionalized with micropipette through drop casting. The mechanism of operation can be understood from the response observed which shows an initial increase in current due to the chemical adsorption process where the transfer of electrons

occurs between MoS_2 and Hg^{2+} ions which reduces the net negative surface charge on MoS_2 and consequently increases gate potential to enhance current. As the concentration of Hg^{2+} is increased the current shows a decrease due to the further adsorption of Hg^{2+} ions through physical electrostatic interaction as MoS_2 may still have negative charges due to higher S atoms and thus a decrement in current. The sensor exhibits a very good response of 0.618 µA/ppb and the LOD is in the range of 15.13 ppt which is well below the WHO prescribed limit of 1 ppb [14].

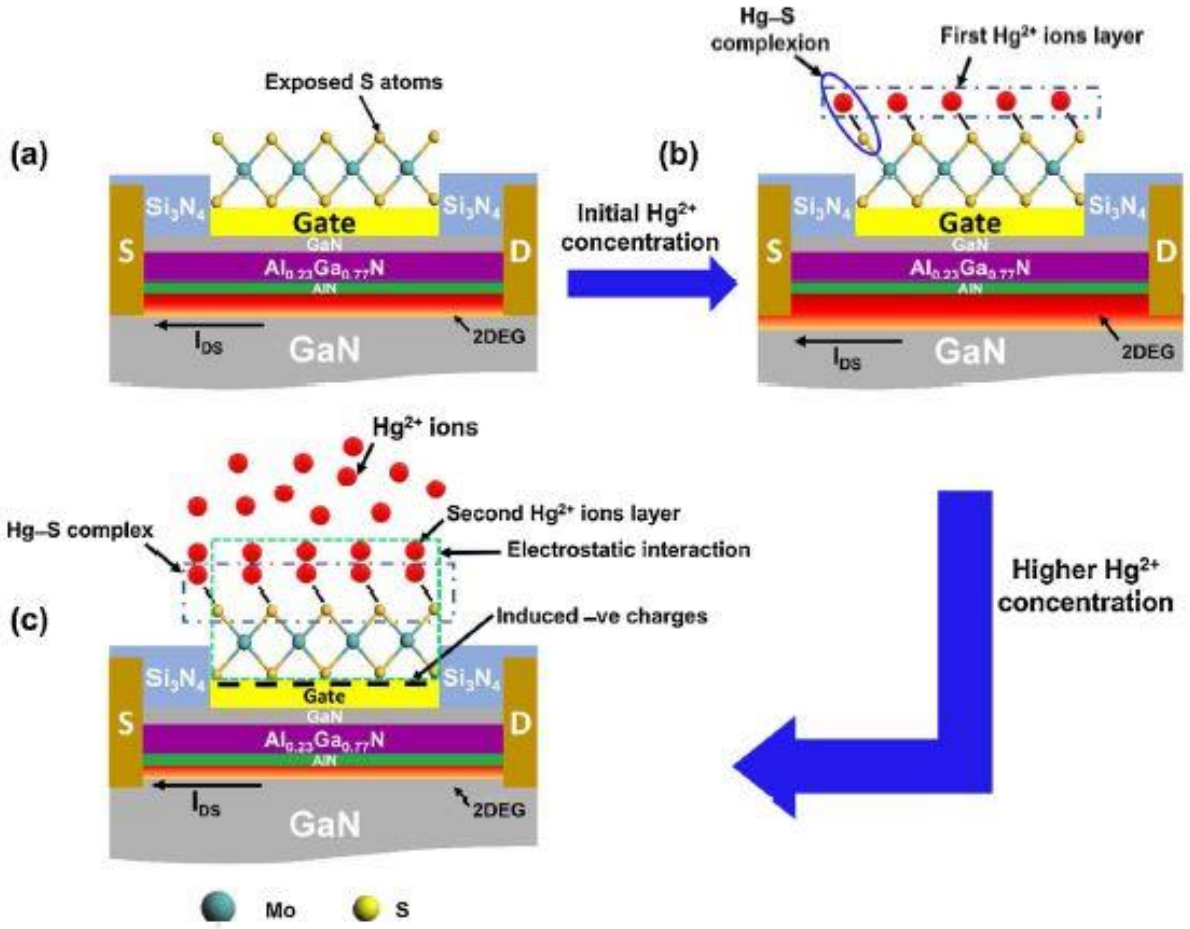

Figure 30 Mercury ion sensing mechanism of AlGaN/GaN HEMT (a) MoS_2 functionalization, (b) Low concentration mercury forming Hg^{2+}-S complex and (c) Electrostatic interaction between MoS_2 and Hg^{2+} under High concentration of mercury. Reprinted from [157], A. Nigam et al., "Real time detection of Hg^{2+} ions using MoS_2 functionalized AlGaN/GaN high electron mobility transistor for water quality monitoring," Sens Actuators B Chem, vol. 309, no. January, p. 127832, 2020, doi: 10.1016/j.snb.2020.127832. Copyright (2020) with permission from Elsevier.

This group furthered the research and prepared flower shaped MoS_2 hydrothermally which was used for functionalization of gold gate through drop casting using a micropipette. The synthesized MoS_2 was ground to powder form for 30 min and a 20 mg/ml solution in IPA was prepared which was ultrasonicated for 2 hours and then drop casted on gate region and the device was annealed for 15 min at 80°C. SEM morphology analysis depicted flower like MoS_2 nanostructure formed by many curved nano flakes [157]. The mechanism of sensing can be understood from Figure 30, where Figure 30 (a) depicts the functionalization of gate by MoS_2. Figure 30 (b) shows the Hg-S complex formation after the initial exposure to low Hg concentration in which adsorption goes on till all binding sites are occupied. Since S is a natural reducer so it donates electrons to Hg^{2+} to form Hg-S complex and depletes electrons from MoS_2 surface which causes increase in gate potential. As the Hg^{2+} concentration is further increased the physical electrostatic interaction phenomenon causes adsorption of

more Hg^{2+} as shown in Figure 30 (c) which induces more negative charge on MoS_2 reducing the gate potential and thus current. The output of the sensor is given in Figure 31, where Figure 31 (a) depicts the output current at different stages for bare device, MoS_2 functionalized device and in presence of Hg ion showing a decrease in current. The real time response is given in Figure 31 (b) depicting a decrease in current with the increase in Hg concentration while Figure 31 (c) depicts the sensor response and calibration curve. The relative change in current and response ratio for various ions is given in Figure 31 (d) and (e) respectively. Figure 31 (f) depicts the transient response of the sensor where the response time and recovery time of the sensor are obtained. The developed sensor showed repeatable and reproducible response as shown in Figure 31 (g) and (h) respectively, implying a dependable sensor. The sensitivity of sensor in terms of current change was 0.64 µA/ppb and the LOD was 0.01152 ppb or 11.2 ppt with a fast response time of 1.8 seconds at 1 ppt. The selectivity of the sensor was also evaluated in presence of other ions such as Pb^{2+}, Zn^{2+}, Ni^{2+}, Cr^{3+} and Cu^{2+}. The sensor also exhibited repeatable and reproducible response and these are all desired qualities of a good sensor.

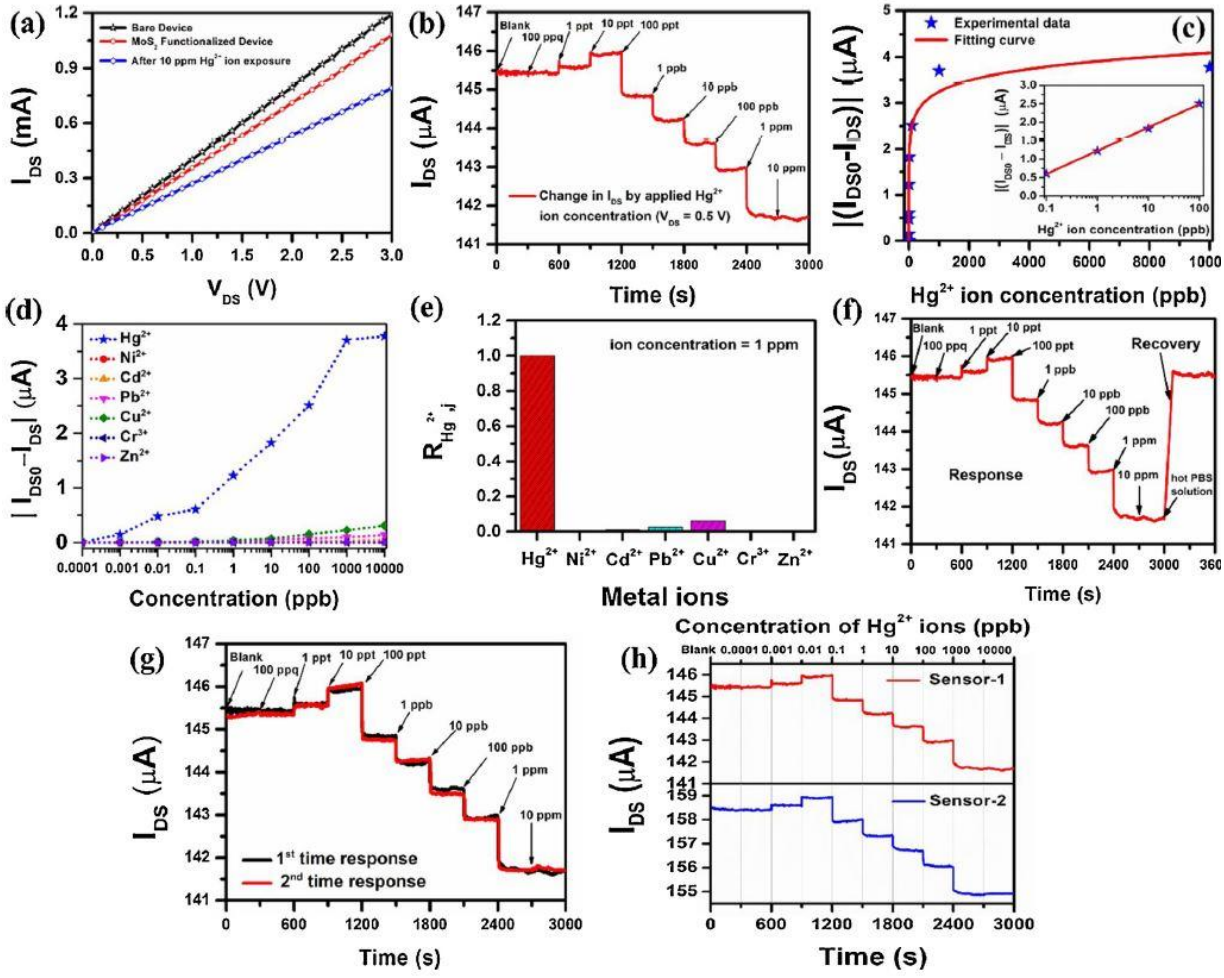

Figure 31 (a) Output characteristics of bare and functionalized device, (b) Real time sensor response to Hg exposure, (c) Sensor response along with calibration curve ; inset showing response at lower concentration for detection of lower limit, (d) Relative change in current of sensor under different Hg concentrations, (e) Response ratio in presence of undesired ions, (f) Transient response indicating response and recovery times, (g) Sensor response depicting repeatability and (h) Sensor responses depicting reproducibility. Reprinted from [157], A. Nigam et al., "Real time detection of Hg^{2+} ions using MoS_2 functionalized AlGaN/GaN high electron mobility transistor for water quality monitoring," Sens Actuators B Chem, vol. 309, no. January, p. 127832, 2020, doi: 10.1016/j.snb.2020.127832. Copyright (2020) with permission from Elsevier.

The other methodology used was that Silver nanowires (AgNW) were mixed to improve conductivity of MOS_2 nano composite (1:4) grown through hydrothermal process has been utilized to functionalize the ungated

sensing region to enhance the sensitivity [56]. The inclusion of AgNW highly increases the surface area and conductivity due to which a sensitivity of 1.6 mA/ppb and a LOD of 20 ppt was observed. The sensor response was not affected by other ions and exhibited good selectivity with ions like Pb^{2+}, Zn^{2+}, Ni^{2+}, Cr^{3+} and Cu^{2+}. Also the response and recovery times of the sensor were 2.1 s and 100 s, respectively which are very small and thus making the real time detection very fast. The sensor developed was further used in real time data acquisition for water quality monitoring in an IOT system using a programmed Arduino Uno and a WiFi module to append the data to cloud storage and can be forwarded to a smart device used for data analysis.

Cadmium is a heavy metal and can find course to the food chain through automobile exhaust, mining waste, paints, coal and other industries. Due to its carcinogenic effects and toxicity higher amount of Cd exposure in humans can lead to numerous health issues like pulmonary fibrosis, osteoporosis, fatigue, weight loss and kidney dysfunction. The WHO and EPA has set permissible standard Cd limit of 3 and 5 ppb respectively, in drinking water which is considered to be safe for human consumption. The conventional methods of detection are costly and time consuming, therefore AlGaN/GaN HEMT based Cd^{2+} ion sensor provides an effective alternate in terms of sensitivity, rapid response and portability. Mercaptopropionic acid (MPA) and glutathione (GSH) are used for gate functionalization to detect Cd^{2+} ions [158]. The gate functionalization commenced with the mixing of 5 ml water and ethanol with 10 M MPA followed by incubation for 12 hours at room temperature, afterwards the activation of carboxyl terminus was ensured by treatment with 4 mM NHS and 20mM EDC in 100 2-(N-morpholino)-ethane sulfonic-acid (MES) buffer for 1 hour. The intended functionalization layer of MPS-GSH was formed by immersion in 50 mg/mL GSH solution at 4^{o}C for 12 hours. The sensor shows a decrement in current with the increase in Cd^{2+} ion concentration demonstrating a sensitivity of 0.241 µA/ppb and LOD of 0.255 ppb when operated at a drain bias of 0.5V, which is well below the limits prescribed by WHO. The sensor also exhibited selective response to Cd^{2+} ions in presence of other interfering ions of valency 2 and 3 such as Cu^{2+}, Ni^{2+}, Pb^{2+} and Cr^{3+} respectively.

L Zhao et al [159] reported on the feasibility of AlGaN/GaN HEMT device for the detection of ionic pollutant such as Fe^{2+}, besides Fe^{2+} is the largest trace element found in human body implying its importance in biological domain. The sensor design consists of two extended gate HEMTs where one is used as reference and the other is functionalized for ion detection purpose in a differential method to reduce the noise effects. The extended gate of sensing device is functionalized with 2-mercaptosuccinic acid while the reference device has bare gold gate. The ion solution is drop casted in sensing chamber enclosing and reference device extended gates. The sensor was tested at a drain bias of 1V a real time response depicting a decrease in drain current due to the chelation of Fe^{2+} ion with the carboxyl terminus as the Fe^{2+} ion concentration is increased while the reference device maintained same current response for different Fe^{2+} ion concentrations. The detection range of the developed sensor was wide varying from 10 fM to 100 µM with a LOD of 10 fM.

Zinc is an essential biological second largest trace element next to iron which plays an important role in survival of human beings such as in neurotransmission, gene expression, cell metabolism and other pathological processes on many diseases including Alzheimer's, epilepsy etc. WHO recommends a concentration limit of 76 µM in drinking water and a physiological content of 10 µM in human serum. Any variation from these limits can be related to different problems and thus it is urgent to develop a sensing platform that can monitor or detect Zn^{2+} with high sensitivity, selectivity and rapid response. Thus, a Schiff's base functionalized extended gate HEMT sensor platform as shown in Figure 32 is presented [160] where the different concentration zinc solution is poured in the sensing chamber to detect Zn^{2+}. With increase in zinc concentration (1 fM to 1µM) the drain current exhibits a decrease due to the interaction of zinc and Schiff base that causes a surface potential change and modulates 2DEG in the channel. The sensor depicted high sensitivity, rapid response time (10 sec) and LOD as 1 fM. The sensor also depicted selective response to zinc as the output was not affected by the other ions such as Na^{+}, K^{+}, Cu^{2+}, Fe^{2+}, Al^{3+} and Mg^{2+}. The change in pH also did not change the response of sensor indicating a stable operation in pH range of 5-8.

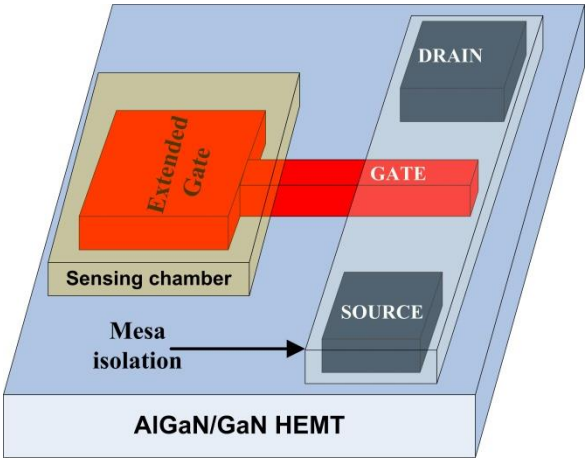

Figure 32 Device schematic for extended gate AlGaN/GaN HEMT sensor for zinc ion detection.

The maximum concentration of Cu^{2+} considered to be permissible in the drinking water such that it is not harmful to human body by the WHO is 2 mg/L. Excessive concentration of Cu^{2+} can cause a number of problems such as Alzheimer's, Menkes, Wilson and Parkinson's diseases affecting the cell metabolism. Therefore, a highly sensitive AlGaN/GaN HEMT sensor with gate functionalized by L-cysteine forms an excellent Cu selective sensor platform. The testing was realized through drop casting Cu^{2+} solution on L-cysteine modified gate region and its response was analysed by observing the changes in drain current. The concentration of Cu^{2+} used in investigation varied from 0.01 to 20 mg/L while the output current depicted a decrease from 2.72 to 1.32 mA, respectively. The real time transient analysis was also performed at V_{DS} of 6V and 8V which also showed the same trend of decreasing current as the Cu^{2+} concentration is raised from 0.01 to 20 mg/L. This decrease in current is attributed to Cu^{2+} trapping and the formation of complexes that reduces the conductivity and 2DEG concentration of channel carriers and thus current. The LOD of the proposed sensor platform is 0.01 mg/L which is well beyond the WHO recommended Cu^{2+} limit (2 mg/L) in drinking water [161].

Phosphate is part and parcel of all living organisms as it is involved in the metabolic process such as the formation of adenosine tri phosphate (ATP) which acts as the energy packet in the body. The normal phosphate level in humans for proper physiological functioning is 25-45 mg/l in blood serum and any variation from this can lead to pathological and physiological changes in human body. The phosphate concentration is also important for aquatic ecosystem, a high phosphate level can lead to eutrophication which causes reduction in dissolved oxygen in water bodies and consequently reduces oxygen levels in the water which will suffocate the aquatic animals and even their death. Thus, the monitoring and maintaining of phosphate levels in permissible limits is essential. The conventional methods of phosphate detection include fluorometry, chromatography and spectrophotometry which are costly, slow, laborious and require skilled personnel for operation. In such a scenario AlGaN/GaN HEMT based sensors emerges as a desirable alternate with high sensitivity and rapid response characteristics. X. Jia et al [162] reported a molecular imprinted technology using molecularly imprinted polymers (MIPs) to create recognition sites which act as artificial antibodies or receptors on ungated surface of AlGaN/GaN HEMT sensor to detect or recognize the phosphate ion as shown in Figure 33 (a). The output characteristics of the bare device and in the phosphate ambient is given in Figure 33 (b) while the response to different anions is shown in Figure 33 (c). The real time response of the sensor at a drain bias of 0.5 mV for different phosphate ion concentrations is depicted in Figure 33 (d) showing a decrease in output current when ion concentration is increased. Figure 33 (e) depicts the sensor response and calibrated curve for different phosphate ion concentrations where the sensor shows a linear response and later saturates at higher concentrations as it has limited binding sites. The response current decreases as the phosphate ion concentration increases and sensitivity of 3.19 µA/mg/l is observed with a LOD of 1.97 µg/l for the proposed sensor. Similarly, the nitrate detection was reported using a open gate design engineered for near zero threshold voltage operation such that device operates with high transconductance to render high sensitivity [163]. The devices

were encapsulated with PVC based membrane containing a plasticizer and an ionophore for nitrate detection. Kelvin four probe method was used for measurements and the sensor exhibits fast response of <60 seconds with LOD of 10^{-6} M and a linear range of 10^{-6} -10^{-3} M.

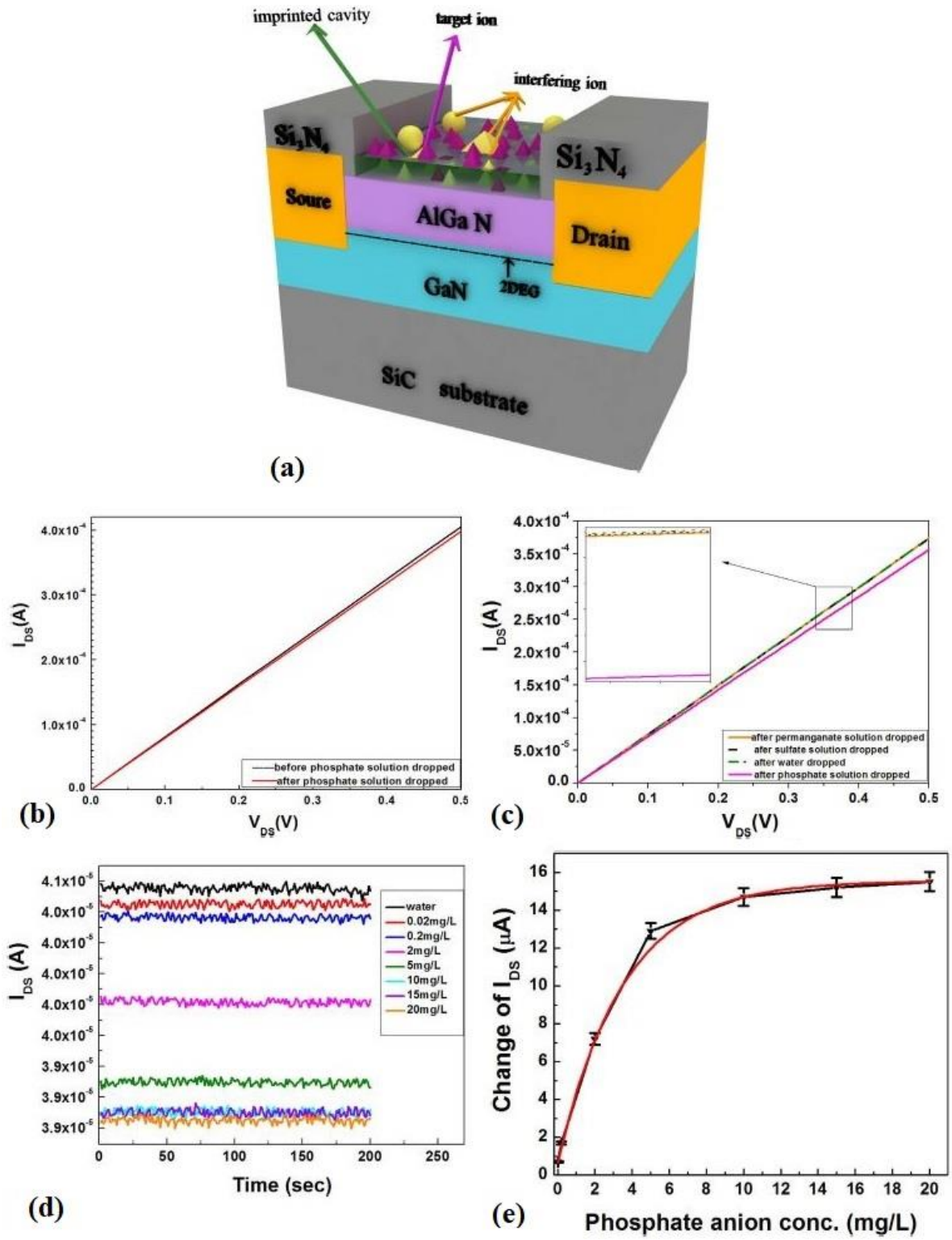

Figure 33 (a) Schematic of the ungated functionalized ion imprinted polymer AlGaN/GaN HEMT based phosphate ion sensor, (b) Output current characteristics of the sensor before and after phosphate ion exposure, (c) Output characteristics for different anions, (d) Current response of the sensor for different phosphate ion concentrations at a drain bias of 50 mV and (e) Change in current for different phosphate ion concentrations [162].

AlGaN/GaN HEMT wearable device was recently demonstrated for the detection of pH and potassium ions in the sweat [164]. Gateless AlGaN/GaN HEMT devices with sensing area of 300*100 μm^2 were fabricated where 5 nm Al_2O_3 was used as sensing membrane for pH detection in one device and the other device was functionalized with ion selective film to detect potassium ions. The real time transient analysis reveals a decrease in current when pH of solution is increased or the concentration of potassium ions increases. The sensitivity of the sensor to acidic pH and basic pH was 45.72 and 51.07 µA/pH, respectively while the potassium ion sensitivity was 4.94 µA/log(α_k^+). Furthermore, the sensor showed a stable response for 28 tests and a good reliability with the relative standard deviation (RSD) of 2.6 % and 7.3 % for pH and potassium ions respectively. Moreover, the hysteresis measurements were performed for 7 → 8 → 9 and 9 → 8 → 7 loop which showed RSD of 2.1% while hysteresis test for potassium ion depicted a RSD of 1.4%. The sensors also depicted good repeatability and stability.

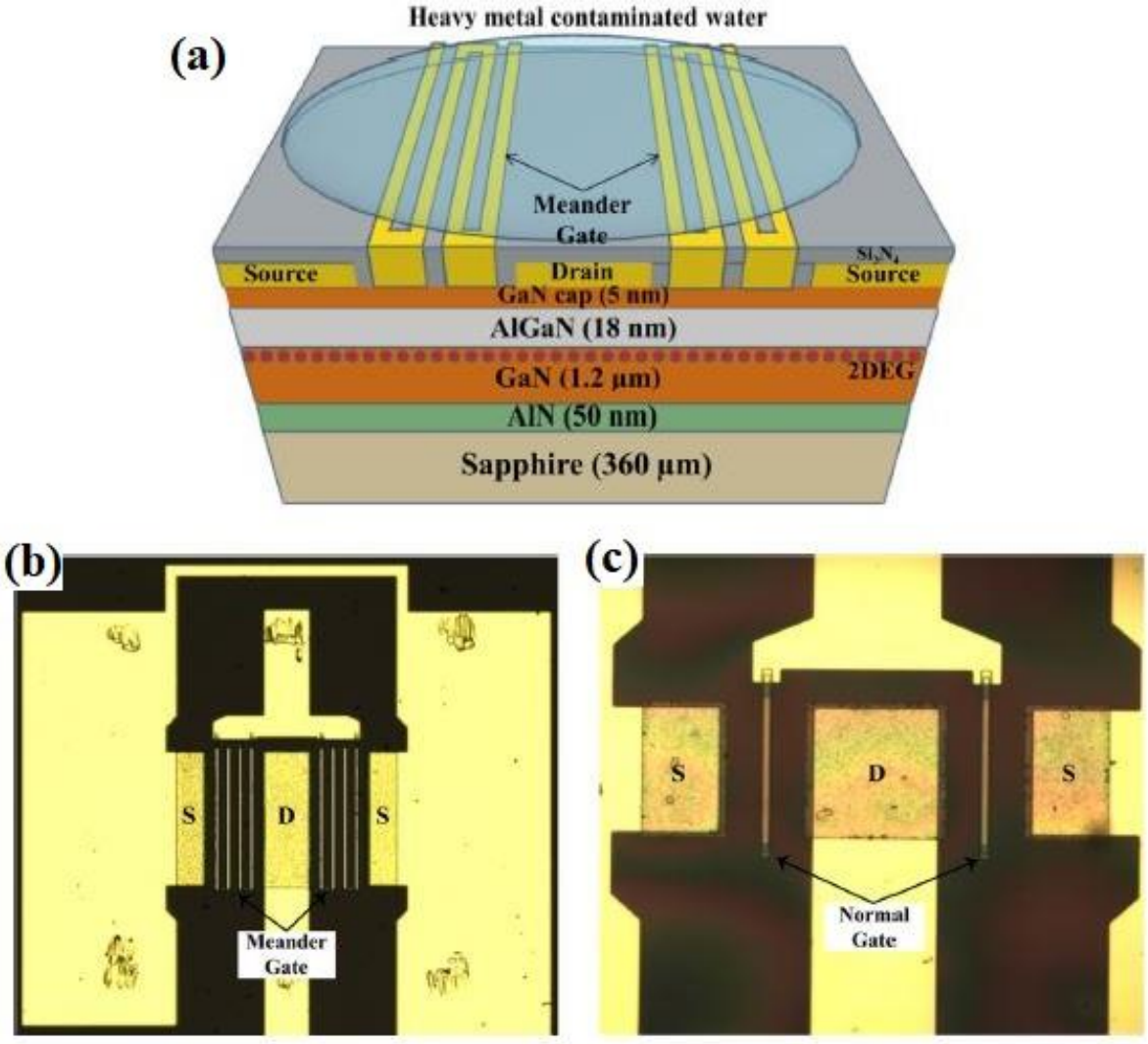

Figure 34 (a) Device schematic for meandered gate AlGaN/GaN HEMT, Fabricated device micrograph of (b) Meandered gate structure and (c) Conventional two finger gate device. Reprinted from [154], S. Mishra, P. Kachhawa, R. R. Thakur, A. K. Jain, K. Singh, and N. Chaturvedi, "Detection of heavy metal ions using meander gated GaN HEMT sensor," Sens Actuators A Phys, vol. 332, p. 113119, 2021, doi: 10.1016/j.sna.2021.113119. Copyright (2021) with permission from Elsevier.

AlGaN/GaN HEMT based sensors have been fabricated and used to detect different heavy metal ions such as lead, Zinc, Copper and Mercury [154]. The device schematic of the proposed sensor design is shown in Figure 34 (a) while the fabricated proposed meandered gate and normal gate designs are shown in Figure 34 (b) and (c), respectively. The real time response of the sensor when exposed to different ions such as mercury and copper is depicted in Figure 35 (a) where the response current increases with the increase in ion concentration. Figure 35 (b) renders a comparison in performance of the sensors when different gate design is used for sensing analysis showing a clear advantage of high sensitivity in using a meandered gate design due to its increase in sensing area. The drain current response of sensors used for different ion detection at varied concentrations along with their linear fitted curves is shown in Figure 35 (c). The response analysis of the sensor is performed at a drain bias of 5V and a distinct real time transient output is observed for different ion concentrations. Two different gate structures are designed one with conventional two finger gate configuration and other with meandering gate design which provides a sensing area of 200 μm^2 and 900 μm^2 respectively. Both configurations were fabricated with a source to drain separation of 25 µm and 50 µm and the meandered gate configuration with smaller S-D separation design exhibited better sensitivity. The sensor operation is described on the basis of capacitance model, where the capacitive coupling to the 2DEG channel varies the carrier concentration as a test solution is exposed on the sensing surface. The binding and detaching of ions is confirmed from SEM, EDS and Raman shift analysis implying durable and re-usable sensor platforms. The calibration curves for different ions were derived to extract the sensitivity values and the sensitivity corresponding to Zinc, Copper, Mercury and Lead are 35, 38, 31 and 24 mV/dec[M].

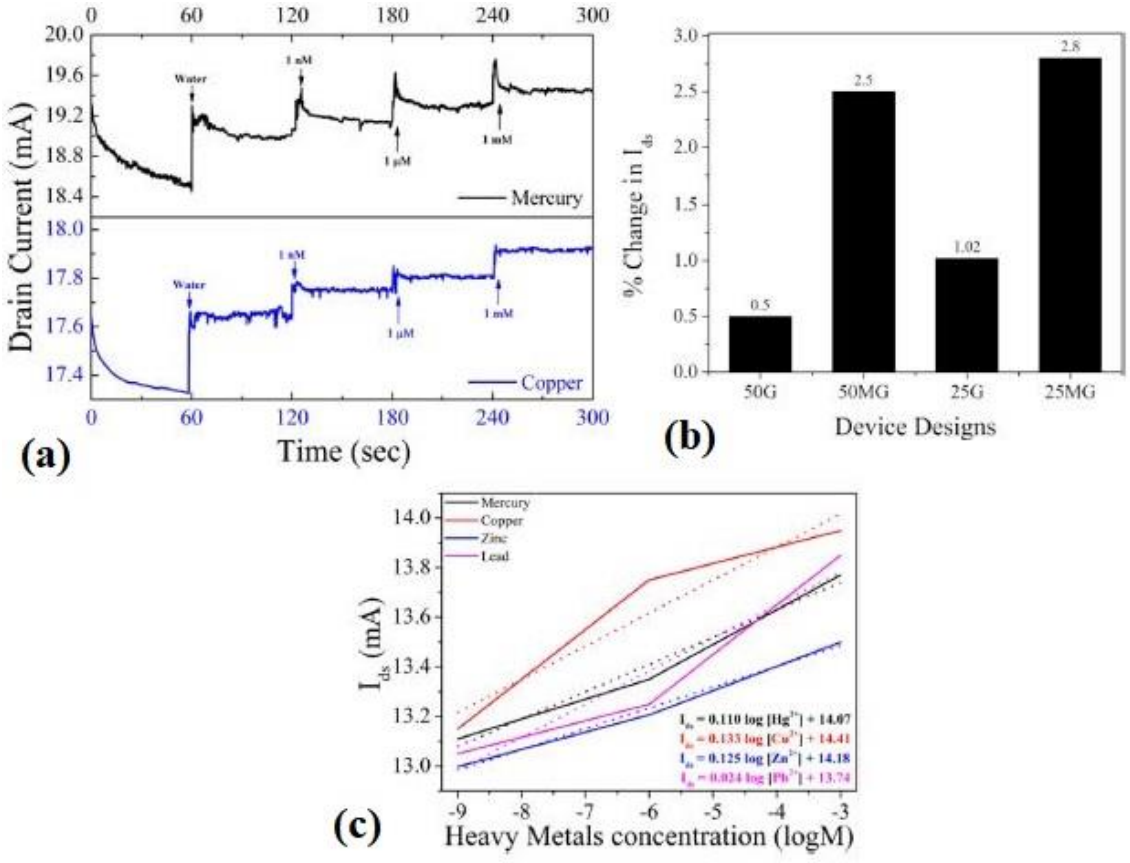

Figure 35 (a) Sensor transient response when exposed to different ions like mercury and copper, (b) Performance comparison of the developed sensor designs-meandered gate (MG) and normal gate (G) and (c) Output drain current response for various ions at different concentration. Reprinted from [154], S. Mishra, P. Kachhawa, R. R. Thakur, A. K. Jain, K. Singh, and N. Chaturvedi, "Detection of heavy metal ions using meander gated GaN HEMT sensor," Sens Actuators A Phys, vol. 332, p. 113119, 2021, doi: 10.1016/j.sna.2021.113119. Copyright (2021) with permission from Elsevier.

Table VI Bird's eye view of some of the earlier reported heavy metal ion sensors

Author, Year, Reference	Details	Type of work	Sensitivity	Remarks
H T Wang, 2007 [155]	Fast electrical detection of Hg(II) ions	Experimental	Sensors detected low concentration of 10-7 M	Bare gold gate and TGA functionalized gate surface was analyzed for its response to Hg ions. TGA functionalized sensors depicted a 2.5 times larger response than bare gold gate sensors.
S. Rabbaa, 2012 [165]	pH and Dipole moment sensing	Modelling/Simulation	55.4-55.7 mV/pH and 0.053 – 0.109 mA/pH	A theoretical triangular quantum well model is proposed and the electrical characteristics are validated with the previous experimental work for application in biosensing, chemical sensing, pH sensing and polar liquid dipole measurement.
J Cheng, 2014 [156]	Ultrasensitive detection of Hg using oligonucleotide functionalized HEMT	Experimental	Dynamic linear range from 10-14 to 10-8 M	An oligonucleotide functionalized GaN cap layer AlGaN/GaN HEMT sensor is demonstrated for Hg detection taking advantage of Thymine-Hg-Thymine binding interaction to enhance detection upto trace amounts.
A. Nigam, 2019 [157]	Hg detection for water quality measurement	Experimental	0.64 µA/ppb with LOD of 0.1152 ppb	Hydrothermally prepared flower shaped MoS_2 was used for functionalization of gold gate through drop casting using a micropipette. The developed sensor depicts excellent response sensitivity and a fast response time of 1.8 seconds.
A. Nigam, 2019 [158]	Cd ion detection	Experimental	0.241 µA/ppb, LOD of 0.255	Mercaptopropionic acid (MPA) and glutathione (GSH) are used for gate functionalization to detect Cd ions. The sensor shows a decrement in current with the increase in Cd ion concentration demonstrating sensitivity which is well below the limits prescribed by WHO.
X Jia, 2019 [162]	Phosphate ion detection	Experimental	3.191 µA/mg/L LOD of 1.97 µg/L.	In this work, molecular imprinted technology using molecularly imprinted polymers (MIPs) was used to create recognition sites to act as artificial antibodies or receptors on ungated surface of sensor by phosphate ion imprinted polymer for detection of the phosphate ion.
L Zhao, 2019 [159]	Differential extended gate real time detection of ionic pollutant (Fe^{2+})	Experimental	Sensitive from 10 fM to 100 µM with a LOD of 10 fM.	The feasibility of AlGaN/GaN HEMT device is tested for the detection of ionic pollutant such as Fe^{2+}. The sensor design consists of two extended gate HEMTs where one is used as reference and the other is functionalized for ion detection purpose in a differential method to reduce the noise effects.
Le Gu, 2019 [160]	AlGaN/GaN HEMT for Zn^{2+} detection	Experimental	Sensitive from 1 fM to 1µM	A Schiff's base functionalized extended gate AlGaN/GaN HEMT sensor platform is developed for Zn^{2+} detection.
A Nigam, 2020 [55]	Ultra-sensitive detection of Hg under UV illumination of MOS_2 functionalized GaN HEMT	Experimental	of 0.618 µA/ppb and the LOD is in the range of 15.13 ppt	AlGaN/GaN HEMT gold gate was functionalized with MoS_2 to enhance the detection of Hg ions under UV illumination besides normal light. The sensor exhibits a very good response which is well below the WHO prescribed limit of 1 ppb.
X Liu, 2020 [164]	Wearable platform for pH and potassium detection	Experimental	45.72 and 51.07 µA/pH	AlGaN/GaN HEMT wearable device is demonstrated for the detection of pH and potassium ions in the sweat. Gateless AlGaN/GaN HEMT devices with 5 nm Al_2O_3 was used as sensing membrane for pH detection in one device and the other device was functionalized with ion selective film to detect potassium ions.
H Guo, 2020 [153]	AlGaN/GaN HEMT for water quality	Review		A comprehensive review on heavy metal ion detection for water quality monitoring discussing various structure designs, sensing mechanism and fabrication aspects.

	monitoring			
S Mishra, 2021 [154]	Detection of heavy metal ions using meander gated AlGaN/GaN HEMT	Experimental	Sensitive from 1 nM to 1 mM with 24 to 38 mV/dec [M]	AlGaN/GaN HEMT based sensor has been used to detect heavy metals like lead, Zinc, Copper and Mercury. Conventional two finger gate and meandering gate design were fabricated where the meandered gate design with smaller SD separation exhibited better sensitivity.
N Sharma, 2021 [56]	Hg detection for IOT enabled smart water analysis	Experimental	1.604 mA/ppb and LOD of 20 ppt	AgNW were mixed to improve conductivity of MOS_2 nano composite (1:4) to functionalize the ungated sensing region to enhance the sensitivity. The inclusion of AgNW highly increases the surface area and conductivity.
X. Jiang, 2022 [161]	AlGaN/GaN HEMT for Cu^{2+} detection	Experimental	Sensitive from 0.01 to 20 mg/L	AlGaN/GaN HEMT sensor with gate functionalized by L-cysteine forms an excellent Cu^{2+} selective sensor platform with LOD of 0.01 mg/l.

3.5 Radiation sensors

The human desire to become interplanetary species, urge for renewable energy, smart grid and the electric automobile endeavours has ignited a great amount of interest in the GaN based devices. GaN based devices can be operated at higher frequency and thus it is attractive alternate device for high frequency converters which need less passive storage elements reducing the size, weight, cost and enhances the reliability. THz spectroscopy and imaging provide a promising substitute to the ionizing harmful X-ray and invasive chemical characterization methods. THz time domain spectroscopy can emerge as an alternate technology for imaging of packaged objects, material analysis, non-destructive inspection of composite materials, industrial output quality control, 3D imaging, concealed weapon detection, thickness measurement, bio medical applications and holography. FET based THz detectors exhibit advantages like rapid response, high sensitivity and operation capability in harsh environment like nuclear systems and high temperature. Schottky diode, Bolometer, pyro electric detector and Golay cells are widely used in THz detection in contemporary times. Bolometers work in low temperature, pyro electric detector and Golay cells work well upto room temperature, this constraint is however due to its intrinsic dependence of operating temperature where a higher temperature will increase the background noise and reduce sensitivity besides, portable issues. Schottky diodes and FET based detectors work well at room temperature, but the GaN based HEMT devices have an extra window in terms of operating temperature due to its wide band gap. The wide band gap ensures lower intrinsic concentration and thus low leakage current so that GaN HEMT can be used in extended ranges of temperature.

There are many reports revealing that GaN has high resistance to ionizing radiations and thus can be a choice of material for devices in radiation applications such as space besides its high temperature durability. GaN exhibits desirable material properties for radiation applications. When a GaN based material system is placed under energetic irradiation environment the properties of the material get changed due to the creation of defects such as frenkel pairs in Ga and N sublattice in the band gap. These defects produced lead to the emergence of acceptor and donor states respectively. The Ga vacancies producing acceptor states leads to the decrease in carrier concentration as the acceptor states will trap electrons as they are produced. The production of defect levels and associated trapping effects shift the fermi level, decrease carrier concentration and consequently has an impact on sheet resistance and specific resistance which eventually translates into decreased current and the amount of decrease can be normalized and the corresponding irradiation intensity can be calculated [166]

The pioneering theoretical work in the field of THz detectors and the basic concept description of non-resonant THz detection in FETs was put forward as Dyakonov-Shur theory [167].

$$\Delta U = \frac{qU_a^2}{4m\,s^2} \tag{36}$$

Where, ΔU is the induced terahertz signal, s is plasma wave velocity and the complete terahertz response including the effect of temperature can be given as:

$$\Delta U = \frac{U_a^2}{4} \frac{1}{\left(V_{T\,ln}\left[1 + exp\left(\frac{V_o}{V_T}\right)\right] + V_{th}\left(\frac{n_i}{n_o}\right)\right)\left[1 + exp\left(-\frac{V_o}{V_T}\right)\right]} \tag{37}$$

Where, the terms have usual meaning and can be further understood from earlier work [167].

It is observed that there is a steep degradation of the response in silicon-based FETs and others like GaAs or InP FETs as the temperature is increased. GaN based HEMT has however shown the least degradation in response demonstrating its inherent advantage of larger band gap and low intrinsic carrier density. A fabricated GaN HEMT with nano antenna structure as shown in Figure 36 is proposed for THz detection capable of operating upto 200ºC at 0.14 THz [167]. For the fabricated GaN HEMT we observe a degradation of current from 31 mA/mm at 30ºC to 17 mA/mm at 200ºC with a corresponding decrease and broadening in transconductance (from 34 to 10 mS/mm) characteristics along with a negative shift in threshold voltage from -4.5V to -5.5V

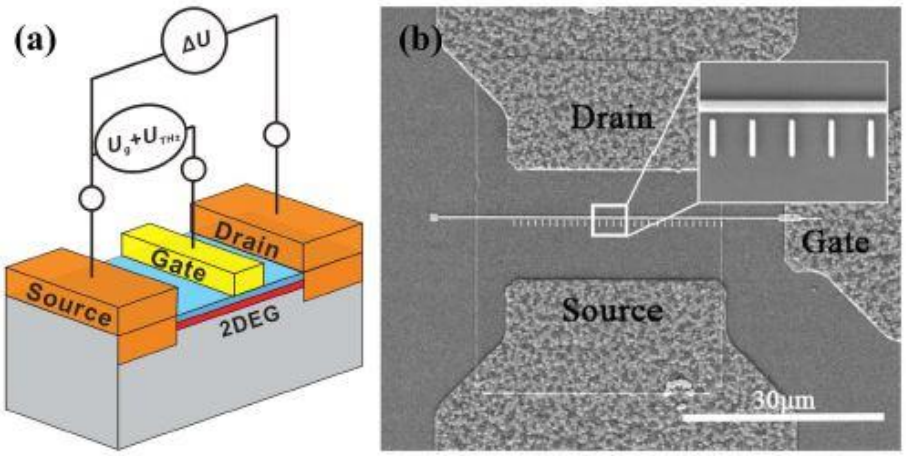

Figure 36 (a) Device schematic and (b) SEM image of the fabricated asymmetric nano antenna AlGaN/GaN HEMT for Terahertz detection [167].

which eventually leads to the decrease in responsivity as the temperature is increased. Figure 37 (a) depicts transfer characteristics with increasing temperature which shows a decrease in current and a linear shift in threshold voltage as shown in Figure 37 (b). Figure 37 (c) renders the responsivity of the device and a high responsivity and low noise equivalent power is obtained, depicting a decrease in responsivity as the temperature increases as shown in Figure 37 (d). The thermal noise from the GaN channel is a dominant source of noise in GaN THz detection. Noise equivalent power (NEP) is an important figure of merit in THz detection which can be estimated by:

$$NEP = \frac{(4KTR_{ds})^{0.5}}{R_v} \tag{1}$$

The NEP increases (from of 0.58 to 10 pW/Hz$^{0.5}$) with the increase in temperature due to the increase in thermal noise.

The THz spectrum is located in between infrared and microwave of electromagnetic spectrum. THz waves have a potential to penetrate most common materials and thus can be used in product quality control, non-destructive

inspection and security screening. THz waves also have low photon energy (1Million times less than X-rays) and are therefore non-ionizing and thus harmless for living beings. A hidden object image is successfully demonstrated by using the commercial GaN HEMT single pixel detector at 0.3 THz in room temperature ambience [168].

However, THz systems suffer from low resolution and low photon intensity drawbacks which hinder it to emerge as a mature technology. The transistor channel acts as a resonance cavity for these plasmon waves, where the Eigen modes correspond to the fundamental frequency and its odd harmonics. The fundamental plasma frequency is given by $\omega_o = \pi s/2L_g$ which can be tuned by changing gate voltage. In order to operate the device in plasma mode, channel length needs to satisfy the following condition: $L << L_{cr} = s\mu m/r$; where s is speed of propagation, μ is low field mobility and m is effective mass of electron. The operation in resonant or non-resonant mode depends on the relevant quality factor $Q = \omega T$, where ω is angular frequency and T is relaxation time. When $Q >> 1$, plasma waves form standing waves so that channel acts as a resonator of the

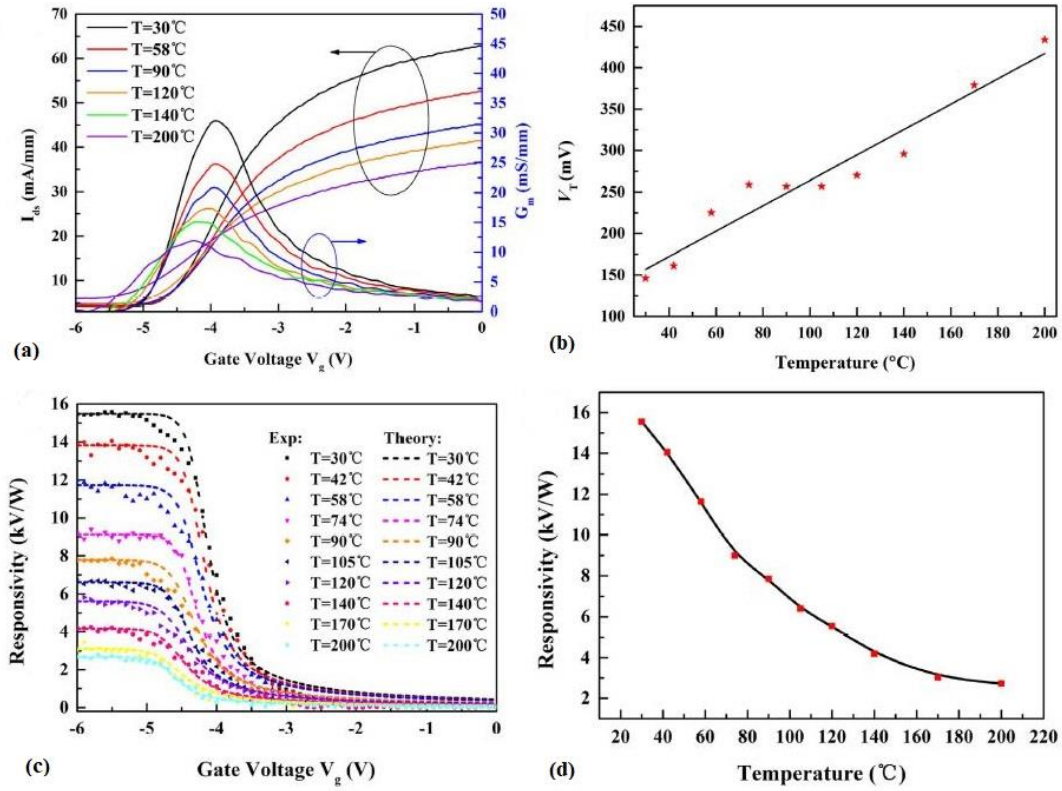

Figure 37 (a) Transfer characteristics of AlGaN/GaN HEMT at different temperatures (b) Modified thermal voltage due to temperature variation (c) Temperature dependent responsivity as a function of gate voltage and (d) Responsivity as a function of temperature at gate bias of -5.5V [167].

plasma oscillations. Whereas, if $Q << 1$ plasma wave will decay and not be able to reach drain side forming a non-resonant mode [169].

In order to suffice the requirements of the microelectronics to be used in satellite-based communication, radar technology and nuclear energy production the radiation hard devices which are radiation resistant are quintessential. Since, the primary cosmic rays emanating out of earth's atmosphere are mainly 90 % protons and 9 % alpha particles which will affect the associated microelectronic circuitry, therefore impact of such radiations is of paramount concern to develop radiation resistant systems such that the lifetime and device reliability is enhanced [170]. In this work the investigation of 18 MeV alpha particle irradiation dose on the electrical characteristics of silicon nitride in-situ passivated AlGaN/GaN HEMT is reported and it is observed that the output drain current decreases 32% and 41% for an alpha particle irradiation dose of $1x10^{12}$ and $1x10^{13}$ cm^{-2},

respectively. The degradation of device response can be attributed to the charged trap generation in GaN and AlGaN besides nuclear and electronic stopping transferring energy from radiation to the target atom which then causes lattice disorder and defects. These defects become the scattering centres causing reduction in mobility and carrier concentration. The degradation of 13.6% and 24.3% in mobility and 6.7% and 9.8% corresponding degradation of transconductance were observed when the irradiation of alpha particle dose was $1x10^{12}$ and $1x10^{13}$ cm^{-2} respectively. Similarly, a decrease in I_{ON}/I_{OFF} ratio and degradation of sub threshold slope was also observed.

An ALD based Al_2O_3 gate dielectric AlGaN/GaN HEMT is investigated for its dc performance characteristics when irradiated with different energy levels (5, 10 and 15 MeV) protons for a fixed proton dose of $5*10^{15}$ cm^2 [171]. The energetic protons relinquish their energy to the lattice site atoms of Ga and N which get displaced to form defects or create vacancies in GaN and AlGaN, however the band bending and carrier concentration were more sensitive to the concentration of traps in GaN. The energy for defect formation is lesser for Ga than N and thus forms acceptor like defect and N vacancy forms a donor type defect. These defects lead to the increase in sheet, transfer and specific contact resistance where the higher increase is for the lower irradiation energy level dose. The degradation in saturation current was 95.3%, 68.3% and 59.8% which is attributed to the decrease in carrier concentration due to trapping at defect centres and decrease in saturated carrier velocity along with positive shift in threshold voltage. Besides it also leads to mobility degradation due to scattering from defect centre close to the channel. The transconductance degradation was 88%, 54.4% and 40.7% for an irradiation dose of 5, 10 and 15 MeV, respectively. Also, the degradation of AlGaN/GaN interface is more pronounced when a lower irradiation energy dose was used, because it has shallower penetration depth and hence causes more damage at AlGaN/GaN interface. Some of the earlier reports of AlGaN/GaN HEMT harnessed as radiation sensor are given in Table VII.

Table VII Earlier reports on the AlGaN/GaN HEMT used for radiation sensing purpose

Author, Year, Reference	Details	Type of work	Sensitivity	Remarks
S Ahn, 2015 [171]	Effect of proton irradiation on AlGaN/GaN HEMT	Experimental	95.3%, 68.5% and 59.8% decrease in drain current was observed for 5, 10, 15 MeV proton irradiation, respectively.	In this paper an ALD based Al_2O_3 gate dielectric AlGaN/GaN HEMT is investigated for its dc performance characteristics when irradiated with different energy levels (5, 10 and 15 MeV) protons for a fixed proton dose of $5x10^{15}$ cm^2. It is observed that a maximum degradation of the device dc performance was observed when the lower irradiation energy dose was used. This is attributed to the energy loss of nonionizing irradiation in the active region of the device. Also, the degradation of AlGaN/GaN interface is more pronounced when a lower irradiation energy dose was used, because it has shallower penetration depth and hence causes more damage at AlGaN/GaN interface.
D Verheij, 2017 [166]	Radiation effects on GaN microwires	Experimental/ Thesis		GaN exhibits desirable material properties for radiation applications. When a GaN based material system is placed under energetic irradiation environment the properties of the material get changed due to the creation of defects such as frenkel pairs in Ga and N sublattice in the band gap.
H W Hou, 2017 [167]	High temperature THZ detector	Experimental	15.5 and 2.7 kV/W and low noise equivalent power of 0.58 and 10 $pW/Hz^{0.5}$	A fabricated GaN HEMT with nano antenna structure is proposed for THz detection capable of operating upto 200 ^oC at 0.14 THz. The dominant source of noise in GaN THz detection is the thermal noise from the GaN channel.
K Ahi, 2017 [169]	Review on GaN based devices on	Review		THz time domain spectroscopy can emerge as an alternate technology for imaging of packaged objects, material analysis, non-destructive inspection of composite materials,

	THz operation			industrial output quality control, 3D imaging, concealed weapon detection, thickness measurement, bio medical applications and holography. However, THz systems suffer from low resolution and low photon intensity drawbacks which hinder it to emerge as a mature technology.
C Fares, 2018 [170]	Effect of alpha particle irradiation dose on MISHEMT	Experimental	It is observed that the output drain current decreases 32% and 41% for an alpha particle irradiation dose of $1x10^{12}$ and $1x10^{13}$ cm^{-2}, respectively.	In this paper the investigation of 18 MeV alpha particle irradiation dose on the electrical characteristics of silicon nitride in-situ passivated AlGaN/GaN HEMT is reported. The degradation of device response can be attributed to the charged trap generation in GaN and AlGaN besides nuclear and electronic stopping transferring energy from radiation to the target atom which then causes lattice disorder and defects. These defects become the scattering centres causing reduction in mobility and carrier concentration.
E. Javadi, 2018 [168]	Continuous wave THz sensing using GaN HEMT	Experimental	Enhanced responsivity upto 1 KV/W was obtained for drain to source current of 10 µA while a low NEP of 11 $pw/Hz^{0.5}$ at 0.15 THz was observed.	The THz spectrum is located in between infrared and microwave of electromagnetic spectrum. THz waves have a potential to penetrate most common materials and thus can be used in product quality control, non-destructive inspection and security screening. THz waves also have low photon energy (1Million times less than X-rays) and are therefore non-ionizing and thus harmless for living beings. A hidden object image is successfully demonstrated by using the commercial GaN HEMT single pixel detector at 0.3 THz in room temperature ambience.

4 Future Outlook and Conclusion

The challenges in sensing arise from the constituents of the sensor itself such as the device used, sensing species or analyte to be sensed and the post detection circuit level signal processing. The complexity from the device perspective arises from the quality of device fabricated especially the defect free layer growth and good quality interfaces are desired, while the complexities associated from analyte perspective could be diffusivity of gas or the Debye screening effects in biosensors which renders the biomolecules above Debye length ineffective or as if they are not present and depends on ionic concentration of the solution among others. The most important aspects related to the sensors are the figure of merits such as sensitivity, selectivity, linearity, limit of detection, reproducibility, repeatability and signal to noise ratio have been discussed. The optimization of these FOMs is a great challenge as the sensor development involves the inter disciplinary combination from material, chemical, nanotechnology and medical research sciences, as every domain has its own constraints, besides the post detection signal processing and display involving analogue to digital conversion is associated with circuit level problems. Therefore, a good quality device is required for which a lot of research is going on to grow defect free material layers and interfaces while a lot needs to be done to understand the sensing kinetics in order to develop a robust sensor.

In summary, the basic material properties, modelling, simulation perspectives, fabrication process, various device structure designs for different sensing applications are discussed. The GaN and AlGaN/GaN HEMT material systems exhibit excellent properties which are highlighted and compared to Silicon, Gallium Arsenide, Silicon carbide, emerging Diamond and Gallium oxide material counterparts. Some fabrication insights regarding each layer of epitaxial system and further sensor development processes are also discussed where gas sensors depend on gate material, biosensors and heavy metal ion sensors rely on sensing region or gate functionalization. The sensing applications of AlGaN/GaN HEMT in terms of detecting gases, biomarkers for diseases, metal ions for water quality monitoring and ionizing radiation are reviewed and discussed in this work collectively. The sensing mechanisms for various applications are elucidated and different device structure

designs with their advantages are also discussed. This review will help in understanding the basics of AlGaN/GaN HEMT device structure, operation and mechanism of sensing for various applications in a single study.

Funding

This research did not receive any specific grant from funding agencies in the public, commercial, or not-for-profit sectors

Declaration of Competing Interest

The authors declare that they have no known competing financial interests or personal relationships that could have appeared to influence the work reported in this paper.

References

[1] X. Li and X. Liu, “Group III nitride nanomaterials for biosensing,” *Nanoscale*, vol. 9, no. 22, pp. 7320–7341, 2017, doi: 10.1039/c7nr01577a.

[2] J. Howgate, “GaN Heterostructures for Biosensing and Radiation Detection,” *D-Nb.Info*, 2012, [Online]. Available: http://d-nb.info/1031550933/34

[3] B. A. Prabowo, P. D. Cabral, P. Freitas, and E. Fernandes, “The challenges of developing biosensors for clinical assessment: A review,” *Chemosensors*, vol. 9, no. 11, 2021, doi: 10.3390/chemosensors9110299.

[4] P. Bergveld, R. van Hal, and J. Eijkel, “‘The remarkable similarity between the acid-base properties of ISFETs and proteins and the consequences for the design of ISFET biosensors’ Biosensors and bioelectronics, vol. 10, no. 5, pp. 405-414,” 1995.

[5] R. Bhardwaj, S. Sinha, N. Sahu, S. Majumder, P. Narang, and R. Mukhiya, “Modeling and simulation of temperature drift for ISFET-based pH sensor and its compensation through machine learning techniques,” *International Journal of Circuit Theory and Applications*, vol. 47, no. 6, pp. 954–970, Jun. 2019, doi: 10.1002/cta.2618.

[6] S. Sanjay, M. Hossain, A. Rao, and N. Bhat, “Super-Nernstian ion sensitive field-effect transistor exploiting charge screening in WSe2/MoS2 heterostructure,” *NPJ 2D Mater Appl*, vol. 5, no. 1, 2021, doi: 10.1038/s41699-021-00273-6.

[7] O. Ambacher *et al.*, “Two-dimensional electron gases induced by spontaneous and piezoelectric polarization charges in N- And Ga-face AlGaN/GaN heterostructures,” *J Appl Phys*, vol. 85, no. 6, pp. 3222–3233, 1999, doi: 10.1063/1.369664.

[8] J. P. Ibbetson, P. T. Fini, K. D. Ness, S. P. DenBaars, J. S. Speck, and U. K. Mishra, “Polarization effects, surface states, and the source of electrons in AlGaN/GaN heterostructure field effect transistors,” *Appl Phys Lett*, vol. 77, no. 2, pp. 250–252, Jul. 2000, doi: 10.1063/1.126940.

[9] R. Thapa *et al.*, “Biofunctionalized AlGaN/GaN high electron mobility transistor for DNA hybridization detection,” *Appl Phys Lett*, vol. 100, no. 23, pp. 1–5, 2012, doi: 10.1063/1.4727895.

[10] B. S. Kang *et al.*, “Prostate specific antigen detection using AlGaNGaN high electron mobility transistors,” *Appl Phys Lett*, vol. 91, no. 11, pp. 89–92, 2007, doi: 10.1063/1.2772192.

[11] B. H. Chu *et al.*, “Wireless detection system for glucose and pH sensing in exhaled breath condensate using A1GaN/GaN high electron mobility transistors,” *IEEE Sens J*, vol. 10, no. 1, pp. 64–70, 2010, doi: 10.1109/JSEN.2009.2035213.

[12] Z. Gu *et al.*, “Highly sensitive AlGaN/GaN HEMT biosensors using an ethanolamine modification strategy for bioassay applications,” *RSC Adv*, vol. 9, no. 27, pp. 15341–15349, 2019, doi: 10.1039/c9ra02055a.

[13] Z. Gu *et al.*, “Ethanolamine Modified ZnO Nanorods-Based Disposable Gate-AlGaN/GaN High Electron Mobility Transistor for pH Sensing,” *IEEE Sens J*, vol. 21, no. 3, pp. 2552–2558, 2021, doi: 10.1109/JSEN.2020.3023034.

[14] A. Nigam, N. Sharma, D. Lobanov, A. Novikov, and M. Kumar, “Ultrasensitive Detection of Mercury Ions under UV Illumination of MoS2Functionalized AlGaN/GaN Transistor,” *IEEE Trans Electron Devices*, vol. 67, no. 12, pp. 5693–5700, 2020, doi: 10.1109/TED.2020.3030000.

[15] W. Luo *et al.*, “Growth and fabrication of AlGaN/GaN HEMT based on Si(1 1 1) substrates by MOCVD,” *Microelectronics J*, vol. 39, no. 9, pp. 1108–1111, 2008, doi: 10.1016/j.mejo.2008.01.083.

[16] F. Roccaforte and M. Leszczynski, “Introduction to Gallium Nitride Properties and Applications,” *Nitride Semiconductor Technology*, pp. 1–39, 2020, doi: 10.1002/9783527825264.ch1.

[17] MUHAMMED A. ACAR, “FABRICATION, MODELING AND CHARACTERIZATION OF GaN HEMTs, AND DESIGN OF HIGH POWER MMIC AMPLIFIERS,” *M.Sc. Dissertation*, no. November, 2009.

[18] S. v. Novikov, C. R. Staddon, R. W. Martin, A. J. Kent, and C. T. Foxon, “Molecular beam epitaxy of free-standing wurtzite AlxGa1-xN layers,” *J Cryst Growth*, vol. 425, no. December, pp. 125–128, 2015, doi: 10.1016/j.jcrysgro.2015.02.010.

[19] M. A. Khan, J. N. Kuznia, J. M. van Hove, N. Pan, and J. Carter, “Observation of a two-dimensional electron gas in low pressure metalorganic chemical vapor deposited GaN-AlxGa1-xN heterojunctions,” *Appl Phys Lett*, vol. 60, no. 24, pp. 3027–3029, 1992, doi: 10.1063/1.106798.

[20] Madhulika *et al.*, “Analytical model to evaluate threshold voltage of GaN based HEMT involving nanoscale material parameters,” *Superlattices Microstruct*, vol. 152, no. January, p. 106834, 2021, doi: 10.1016/j.spmi.2021.106834.

[21] P. Javorka, “Fabrication and Characterization of AlGaN/GaN High Electron Mobility Transistors,” 2004.

[22] S. A. Eliza, “Modeling of AlGaN / GaN High Electron Mobility Transistor for Sensors and High-Temperature Circuit Applications A Dissertation Presented for the Doctor of Philosophy Degree The University of Tennessee , Knoxville,” 2008.

[23] M. A. Mastro, A. Kuramata, J. Calkins, J. Kim, F. Ren, and S. J. Pearton, “ Perspective—Opportunities and Future Directions for Ga 2 O 3 ,” *ECS Journal of Solid State Science and Technology*, vol. 6, no. 5, pp. P356–P359, 2017, doi: 10.1149/2.0031707jss.

[24] A. M. Bhat, N. Shafi, C. Sahu, and C. Periasamy, “Analysis of AlGaN/GaN HEMT and Its Operational Improvement Using a Grated Gate Field Plate,” *J Electron Mater*, vol. 50, no. 11, pp. 6218–6227, 2021, doi: 10.1007/s11664-021-09151-9.

[25] A. M. Bhat, N. Shafi, R. Poonia, and C. Periasamy, “Design and Analysis of a Field Plate Engineered High Electron Mobility Transistor for Enhanced Performance,” *J Electron Mater*, vol. 51, no. 7, pp. 3773–3781, 2022, doi: 10.1007/s11664-022-09646-z.

[26] “Gallium Nitride (GaN):Physics, Devices, and Technology,” *Taylor & Francis Group, LLC*, 2014.

[27] J. L. Chiang, Y. G. Shang, B. K. Yadlapalli, F. P. Yu, and D. S. Wuu, “Ga2O3 nanorod-based extended-gate field-effect transistors for pH sensing,” *Mater Sci Eng B Solid State Mater Adv Technol*, vol. 276, Feb. 2022, doi: 10.1016/j.mseb.2021.115542.

[28] H. Y. Chou, J. L. Chiang, C. T. R. Yu, J. M. M. Chen, and D. S. Wuu, “Sensing property of Ga2O3-based extended-gate field-effect transistors for a living cell viability sensor,” *Sens Actuators A Phys*, vol. 349, Jan. 2023, doi: 10.1016/j.sna.2022.114071.

[29] D. Guo, Q. Guo, Z. Chen, Z. Wu, P. Li, and W. Tang, “Review of Ga2O3-based optoelectronic devices,” *Materials Today Physics*, vol. 11. Elsevier Ltd, Dec. 01, 2019. doi: 10.1016/j.mtphys.2019.100157.

[30] H. Zhai, Z. Wu, and Z. Fang, “Recent progress of Ga2O3-based gas sensors,” *Ceramics International*, vol. 48, no. 17. Elsevier Ltd, pp. 24213–24233, Sep. 01, 2022. doi: 10.1016/j.ceramint.2022.06.066.

[31] Z. Gu *et al.*, “Highly sensitive AlGaN/GaN HEMT biosensors using an ethanolamine modification strategy for bioassay applications,” *RSC Adv*, vol. 9, no. 27, pp. 15341–15349, 2019, doi: 10.1039/c9ra02055a.

[32] H. Guo *et al.*, “Applications of AlGaN/GaN high electron mobility transistor-based sensors in water quality monitoring,” *Semiconductor Science and Technology*, vol. 35, no. 12. IOP Publishing Ltd, Dec. 01, 2020. doi: 10.1088/1361-6641/abb8fb.

[33] J. Schalwig, G. Müller, M. Eickhoff, O. Ambacher, and M. Stutzmann, “Gas sensitive GaN/AlGaN-heterostructures,” 2002.

[34] J. Ajayan *et al.*, “A critical review of AlGaN/GaN-heterostructure based Schottky diode/HEMT hydrogen (H2) sensors for aerospace and industrial applications,” *Measurement (Lond)*, vol. 186, Dec. 2021, doi: 10.1016/j.measurement.2021.110100.

[35] X. Xu *et al.*, “Wafer-level MOCVD growth of AlGaN/GaN-on-Si HEMT structures with ultra-high room temperature 2DEG mobility,” *AIP Adv*, vol. 6, no. 11, 2016, doi: 10.1063/1.4967816.

[36] Y. Cordier *et al.*, “MBE growth of ALGaN/GaN HEMTS on resistive Si(1 1 1) substrate with RF small signal and power performances,” *J Cryst Growth*, vol. 251, no. 1–4, pp. 811–815, 2003, doi: 10.1016/S0022-0248(02)02149-8.

[37] H. Amano, N. Sawaki, I. Akasaki, and Y. Toyoda, “Metalorganic vapor phase epitaxial growth of a high quality GaN film using an AlN buffer layer,” *Appl Phys Lett*, vol. 48, no. 5, pp. 353–355, 1986, doi: 10.1063/1.96549.

[38] D. Korakakis, H. M. Ng, M. Misra, W. Grieshaber, and T. D. Moustakas, “Growth and doping of AlGaN alloys by ECR-assisted MBE,” *MRS Internet Journal of Nitride Semiconductor Research*, vol. 1, no. January, 1996, doi: 10.1557/S1092578300001824.

[39] H. Y. Liu *et al.*, “Investigation of AlGaN/GaN Ion-Sensitive Heterostructure Field-Effect Transistors-Based pH Sensors with Al2O3 Surface Passivation and Sensing Membrane,” *IEEE Sens J*, vol. 16, no. 10, pp. 3514–3522, 2016, doi: 10.1109/JSEN.2016.2531107.

[40] T. Kabemura, S. Ueda, Y. Kawada, and K. Horio, “Enhancement of Breakdown Voltage in AlGaN/GaN HEMTs: Field Plate Plus High-k Passivation Layer and High Acceptor Density in Buffer Layer,” *IEEE Trans Electron Devices*, vol. 65, no. 9, pp. 3848–3854, 2018, doi: 10.1109/TED.2018.2857774.

[41] B. S. Kang *et al.*, “PH sensor using AlGaNGaN high electron mobility transistors with Sc2 O3 in the gate region,” *Appl Phys Lett*, vol. 91, no. 1, pp. 16–19, 2007, doi: 10.1063/1.2754637.

[42] N. Sharma *et al.*, “High-Resolution AlGaN/GaN HEMT-Based Electrochemical Sensor for Biomedical Applications,” *IEEE Trans Electron Devices*, vol. 67, no. 1, pp. 289–295, 2020, doi: 10.1109/TED.2019.2949821.

[43] N. Sharma, S. K. Dhakad, C. Periasamy, and N. Chaturvedi, “Refined isolation techniques for GaN-based high electron mobility transistors,” *Mater Sci Semicond Process*, vol. 87, pp. 195–201, Nov. 2018, doi: 10.1016/j.mssp.2018.05.015.

[44] S. Arulkumaran *et al.*, “Thermally stable device isolation by inert gas heavy ion implantation in AlGaN/GaN HEMTs on Si,” *Journal of Vacuum Science & Technology B, Nanotechnology and Microelectronics: Materials, Processing, Measurement, and Phenomena*, vol. 34, no. 4, p. 042203, Jul. 2016, doi: 10.1116/1.4955152.

[45] V. Kumar, L. Zhou, D. Selvanathan, and I. Adesida, “Thermally-stable low-resistance Ti/Al/Mo/Au multilayer ohmic contacts on n-GaN,” *J Appl Phys*, vol. 92, no. 3, pp. 1712–1714, Aug. 2002, doi: 10.1063/1.1491584.

[46] S. S. Mahajan, A. Dhaul, R. Laishram, S. Kapoor, S. Vinayak, and B. K. Sehgal, “Micro-structural evaluation of Ti/Al/Ni/Au ohmic contacts with different Ti/Al thicknesses in AlGaN/GaN HEMTs,” *Mater Sci Eng B Solid State Mater Adv Technol*, vol. 183, no. 1, pp. 47–53, 2014, doi: 10.1016/j.mseb.2013.12.005.

[47] S. Niranjan, A. Rao, R. Muralidharan, P. Sen, and D. N. Nath, “Performance Comparison of Au-Based and Au-Free AlGaN/GaN HEMT on Silicon,” *IEEE Trans Electron Devices*, vol. 69, no. 3, pp. 1014–1019, 2022, doi: 10.1109/TED.2021.3140193.

[48] N. S, I. Guiney, C. J. Humphreys, P. Sen, R. Muralidharan, and D. N. Nath, “Au-free recessed Ohmic contacts to AlGaN/GaN high electron mobility transistor: Study of etch chemistry and metal scheme,” *Journal of Vacuum Science & Technology B*, vol. 38, no. 3, p. 032207, 2020, doi: 10.1116/1.5144509.

[49] Y. K. Yadav, B. B. Upadhyay, M. Meer, S. Ganguly, and D. Saha, “Reduced Contact Resistance and Improved Transistor Performance by Surface Plasma Treatment on Ohmic Regions in

AlGaN/GaN HEMT Heterostructures," *Physica Status Solidi (A) Applications and Materials Science*, vol. 215, no. 9, pp. 1–6, 2018, doi: 10.1002/pssa.201700656.

[50] Y. Zhu, W. Cao, Y. Fan, Y. Deng, and C. Xu, "Effects of rapid thermal annealing on ohmic contact of AlGaN/GaN HEMTs," *Journal of Semiconductors*, vol. 35, no. 2, 2014, doi: 10.1088/1674-4926/35/2/026004.

[51] X. Ding *et al.*, "Molecular gated-AlGaN/GaN high electron mobility transistor for pH detection," *Analyst*, vol. 143, no. 12, pp. 2784–2789, 2018, doi: 10.1039/c8an00032h.

[52] J. Y. Pyo *et al.*, "AlGaN/GaN high-electron-mobility transistor pH sensor with extended gate platform," *AIP Adv*, vol. 8, no. 8, pp. 1–6, 2018, doi: 10.1063/1.5041847.

[53] F. S. Tulip, "Development and Modeling of a Biosensor Platform using AlGaN / GaN HEMT Devices," 2014.

[54] L. C. Clark and C. Lyons, "ELECTRODE SYSTEMS FOR CONTINUOUS MONITORING IN CARDIOVASCULAR SURGERY," 1965. doi: https://doi.org/10.1111/j.1749-6632.1962.tb13623.x.

[55] A. Nigam, N. Sharma, D. Lobanov, A. Novikov, and M. Kumar, "Ultrasensitive Detection of Mercury Ions under UV Illumination of MoS2Functionalized AlGaN/GaN Transistor," *IEEE Trans Electron Devices*, vol. 67, no. 12, pp. 5693–5700, 2020, doi: 10.1109/TED.2020.3030000.

[56] N. Sharma, A. Nigam, D. Lobanov, A. Gupta, A. Novikov, and M. Kumar, "Mercury (II) Ion Detection Using AgNWs-MoS2Nanocomposite on GaN HEMT for IoT-Enabled Smart Water Quality Analysis," *IEEE Internet Things J*, vol. 9, no. 16, pp. 14317–14324, 2022, doi: 10.1109/JIOT.2021.3071382.

[57] M. Xu *et al.*, "The GaAs/AlGaAs-Based Extended Gate HEMT Cardiac Troponin-I Biosensor: Design, Mechanism and Clinical Detection," *IEEE Sens J*, vol. 21, no. 17, pp. 18410–18416, Sep. 2021, doi: 10.1109/JSEN.2021.3087716.

[58] S. A. Jewett, M. S. Makowski, B. Andrews, M. J. Manfra, and A. Ivanisevic, "Gallium nitride is biocompatible and non-toxic before and after functionalization with peptides," *Acta Biomater*, vol. 8, no. 2, pp. 728–733, 2012, doi: 10.1016/j.actbio.2011.09.038.

[59] C. M. Foster, R. Collazo, Z. Sitar, and A. Ivanisevic, "Cell behavior on gallium nitride surfaces: Peptide affinity attachment versus covalent functionalization," *Langmuir*, vol. 29, no. 26, pp. 8377–8384, Jul. 2013, doi: 10.1021/la401503b.

[60] A. Podolska *et al.*, "Biocompatibility of semiconducting AlGaN/GaN material with living cells," *Sens Actuators B Chem*, vol. 169, pp. 401–406, Jul. 2012, doi: 10.1016/j.snb.2012.04.015.

[61] M. Wusiman and F. Taghipour, "Methods and mechanisms of gas sensor selectivity," *Critical Reviews in Solid State and Materials Sciences*, vol. 47, no. 3. Taylor and Francis Ltd., pp. 416–435, 2022. doi: 10.1080/10408436.2021.1941752.

[62] H. Yu *et al.*, “Capacitive sensor based on GaN honeycomb nanonetwork for ultrafast and low temperature hydrogen gas detection,” *Sens Actuators B Chem*, vol. 346, no. April, p. 130488, 2021, doi: 10.1016/j.snb.2021.130488.

[63] W. C. Chen, J. S. Niu, I. P. Liu, B. Y. Ke, S. Y. Cheng, and W. C. Liu, “Hydrogen sensing properties of a GaN/AlGaN-based Schottky diode with a catalytic platinum (Pt) hybrid structure,” *Sens Actuators B Chem*, vol. 331, no. June 2020, p. 129320, 2021, doi: 10.1016/j.snb.2020.129320.

[64] J. Ajayan *et al.*, “A critical review of AlGaN/GaN-heterostructure based Schottky diode/HEMT hydrogen (H2) sensors for aerospace and industrial applications,” *Measurement (Lond)*, vol. 186, Dec. 2021, doi: 10.1016/j.measurement.2021.110100.

[65] H. I. Chen *et al.*, “Hydrogen sensing performance of a Pd/HfO2/GaN metal-oxide-semiconductor (MOS) Schottky diode,” *Sens Actuators B Chem*, vol. 262, pp. 852–859, 2018, doi: 10.1016/j.snb.2018.02.077.

[66] S. T. Hung *et al.*, “SnO 2 functionalized AlGaN/GaN high electron mobility transistor for hydrogen sensing applications,” in *International Journal of Hydrogen Energy*, Sep. 2012, vol. 37, no. 18, pp. 13783–13788. doi: 10.1016/j.ijhydene.2012.03.124.

[67] G. H. Chung, T. A. Vuong, and H. Kim, “Demonstration of hydrogen sensing operation of AlGaN/GaN HEMT gas sensors in extreme environment,” *Results Phys*, vol. 12, pp. 83–84, Mar. 2019, doi: 10.1016/j.rinp.2018.11.064.

[68] W. P. Layer, S. Jung, K. H. Baik, F. Ren, and S. J. Pearton, “Pt-AlGaN / GaN Hydrogen Sensor With,” vol. 38, no. 5, pp. 657–660, 2017.

[69] R. Sokolovskij *et al.*, “The Impact of Gate Recess on the H Detection Properties of Pt-AlGaN/GaN HEMT Sensors,” *IEEE Sens J*, vol. 20, no. 16, pp. 8947–8955, 2020, doi: 10.1109/JSEN.2020.2987061.

[70] J. Ahn, D. Kim, K. H. Park, G. Yoo, and J. Heo, “Pt-Decorated Graphene Gate AlGaN/GaN MIS-HEMT for Ultrahigh Sensitive Hydrogen Gas Detection,” *IEEE Trans Electron Devices*, vol. 68, no. 3, pp. 1255–1261, 2021, doi: 10.1109/TED.2021.3053515.

[71] A. Varghese, A. Eblabla, and K. Elgaid, “Modeling and Simulation of Ultrahigh Sensitive AlGaN/AlN/GaN HEMT-Based Hydrogen Gas Detector with Low Detection Limit,” *IEEE Sens J*, vol. 21, no. 13, pp. 15361–15368, 2021, doi: 10.1109/JSEN.2021.3072476.

[72] T. A. Vuong, H. Y. Cha, and H. Kim, “Response enhancement of pt–algan/gan hemt gas sensors by thin algan barrier with the source-connected gate configuration at high temperature,” *Micromachines (Basel)*, vol. 12, no. 5, 2021, doi: 10.3390/mi12050537.

[73] C. Bishop *et al.*, “Experimental Study and Device Design of NO, NO2, and NH3 Gas Detection for a Wide Dynamic and Large Temperature Range Using Pt/AlGaN/GaN HEMT,” *IEEE Sens J*, vol. 16, no. 18, pp. 6828–6838, 2016, doi: 10.1109/JSEN.2016.2593050.

[74] Y. Halfaya *et al.*, “Investigation of the performance of HEMT-based NO, NO2 and NH3exhaust gas sensors for automotive antipollution systems,” *Sensors (Switzerland)*, vol. 16, no. 3, pp. 1–12, 2016, doi: 10.3390/s16030273.

[75] P. C. Chou *et al.*, “Study of an electroless plating (EP)-based Pt/AlGaN/GaN Schottky diode-type ammonia sensor,” *Sens Actuators B Chem*, vol. 203, pp. 258–262, 2014, doi: 10.1016/j.snb.2014.06.113.

[76] B. Shen, F. Li, Y. Xie, J. Luo, P. Fan, and A. Zhong, “High performance ammonia gas sensor based on GaN honeycomb nanonetwork,” *Sens Actuators A Phys*, vol. 312, no. 2, 2020, doi: 10.1016/j.sna.2020.112172.

[77] S. W. Lee, W. Lee, Y. Hong, G. Lee, and D. S. Yoon, “Recent advances in carbon material-based NO2 gas sensors,” *Sensors and Actuators, B: Chemical*, vol. 255. Elsevier B.V., pp. 1788–1804, Feb. 01, 2018. doi: 10.1016/j.snb.2017.08.203.

[78] T. Pham, G. Li, E. Bekyarova, M. E. Itkis, and A. Mulchandani, “MoS 2 -Based Optoelectronic Gas Sensor with Sub-parts-per-billion Limit of NO 2 Gas Detection,” *ACS Nano*, vol. 13, no. 3, pp. 3196–3205, 2019, doi: 10.1021/acsnano.8b08778.

[79] R. Kumar, O. Al-Dossary, G. Kumar, and A. Umar, “Zinc oxide nanostructures for no2 gas–sensor applications: A review,” *Nanomicro Lett*, vol. 7, no. 2, pp. 97–120, 2015, doi: 10.1007/s40820-014-0023-3.

[80] J. Sun, R. Sokolovskij, E. Iervolino, Z. Liu, P. M. Sarro, and G. Zhang, “Suspended AlGaN/GaN HEMT NO2 Gas Sensor Integrated with Micro-heater,” *Journal of Microelectromechanical Systems*, vol. 28, no. 6, pp. 997–1004, 2019, doi: 10.1109/JMEMS.2019.2943403.

[81] V. C. Nguyen, K. Kim, and H. Kim, “Performance optimization of nitrogen dioxide gas sensor based on pd-algan/gan hemts by gate bias modulation,” *Micromachines (Basel)*, vol. 12, no. 4, pp. 1–9, 2021, doi: 10.3390/mi12040400.

[82] M. Hjiri, F. Bahanan, M. S. Aida, L. el Mir, and G. Neri, “High Performance CO Gas Sensor Based on ZnO Nanoparticles,” *J Inorg Organomet Polym Mater*, vol. 30, no. 10, pp. 4063–4071, 2020, doi: 10.1007/s10904-020-01553-2.

[83] C. F. Lo *et al.*, “Effect of temperature on CO sensing response in air ambient by using zno nanorod-gated AlGaN/GaN high electron mobility transistors,” *Sens Actuators B Chem*, vol. 176, pp. 708–712, 2013, doi: 10.1016/j.snb.2012.10.051.

[84] S. C. Hung, W. Y. Woon, S. M. Lan, F. Ren, and S. J. Pearton, “Characteristics of carbon monoxide sensors made by polar and nonpolar zinc oxide nanowires gated AlGaN/GaN high electron mobility transistor,” *Appl Phys Lett*, vol. 103, no. 8, 2013, doi: 10.1063/1.4818671.

[85] C.-F. Lo *et al.*, “Carbon monoxide detection sensitivity of ZnO nanorod-gated AlGaN/GaN high electron mobility transistors in different temperature environments,” *Journal of Vacuum Science & Technology B, Nanotechnology and Microelectronics: Materials, Processing, Measurement, and Phenomena*, vol. 30, no. 1, p. 010606, Jan. 2012, doi: 10.1116/1.3672010.

[86] I. Rýger *et al.*, "AlGaN/GaN HEMT based hydrogen sensors with gate absorption layers formed by high temperature oxidation," in *Procedia Engineering*, 2012, vol. 47, pp. 518–521. doi: 10.1016/j.proeng.2012.09.198.

[87] H. Kim and S. Jang, "AlGaN/GaN HEMT based hydrogen sensor with platinum nanonetwork gate electrode," *Current Applied Physics*, vol. 13, no. 8, pp. 1746–1750, 2013, doi: 10.1016/j.cap.2013.07.008.

[88] S. C. Hung, W. Y. Woon, S. M. Lan, F. Ren, and S. J. Pearton, "Characteristics of carbon monoxide sensors made by polar and nonpolar zinc oxide nanowires gated AlGaN/GaN high electron mobility transistor," *Appl Phys Lett*, vol. 103, no. 8, Aug. 2013, doi: 10.1063/1.4818671.

[89] S. Jung, K. H. Baik, F. Ren, S. J. Pearton, and S. Jang, "Pt-AlGaN/GaN Hydrogen Sensor with Water-Blocking PMMA Layer," *IEEE Electron Device Letters*, vol. 38, no. 5, pp. 657–660, May 2017, doi: 10.1109/LED.2017.2681114.

[90] R. Sokolovskij *et al.*, "Application of a gateless AlGaN/GaN HEMT sensor for diesel soot particulate detection," *Sens Actuators B Chem*, vol. 349, Dec. 2021, doi: 10.1016/j.snb.2021.130811.

[91] B. S. Kang *et al.*, "Enzymatic glucose detection using ZnO nanorods on the gate region of AlGaNGaN high electron mobility transistors," *Appl Phys Lett*, vol. 91, no. 25, pp. 1–4, 2007, doi: 10.1063/1.2825574.

[92] A. Varghese, C. Periasamy, and L. Bhargava, "Fabrication and charge deduction based sensitivity analysis of gan mos-hemt device for glucose, mig, c-erbb-2, kim-1, and psa detection," *IEEE Trans Nanotechnol*, vol. 18, pp. 747–755, 2019, doi: 10.1109/TNANO.2019.2928308.

[93] K. H. Chen *et al.*, "C-erbB-2 sensing using AlGaNGaN high electron mobility transistors for breast cancer detection," *Appl Phys Lett*, vol. 92, no. 19, 2008, doi: 10.1063/1.2926656.

[94] S. Yang *et al.*, "Disposable Gate AlGaN/GaN High-Electron-Mobility Sensor for Trace-Level Biological Detection," *IEEE Electron Device Letters*, vol. 39, no. 10, pp. 1592–1595, Oct. 2018, doi: 10.1109/LED.2018.2868433.

[95] J. Yang *et al.*, "Zika virus detection using antibody-immobilized disposable cover glass and AlGaN/GaN high electron mobility transistors," *Appl Phys Lett*, vol. 113, no. 3, 2018, doi: 10.1063/1.5029902.

[96] Y. W. Kang *et al.*, "Human immunodeficiency virus drug development assisted with AlGaN/GaN high electron mobility transistors and binding-site models," *Appl Phys Lett*, vol. 102, no. 17, 2013, doi: 10.1063/1.4803916.

[97] H. H. Lee *et al.*, "AlGaN/GaN high electron mobility transistor-based biosensor for the detection of C-reactive protein," *Sensors (Switzerland)*, vol. 15, no. 8, pp. 18416–18426, 2015, doi: 10.3390/s150818416.

[98] H. H. Lee *et al.*, “Differential-mode HEMT-based biosensor for real-time and label-free detection of C-reactive protein,” *Sens Actuators B Chem*, vol. 234, pp. 316–323, 2016, doi: 10.1016/j.snb.2016.04.117.

[99] A. K. Pulikkathodi, I. Sarangadharan, Y.-H. Chen, G.-B. Lee, and Y.-L. Wang, “Aptamer Functionalized AlGaN/GaN HEMT Biosensor Array for Electrical Enumeration of Circulating Tumor Cells,” *ECS Trans*, vol. 77, no. 7, pp. 17–20, Apr. 2017, doi: 10.1149/07707.0017ecst.

[100] I. Sarangadharan *et al.*, “High sensitivity cardiac troponin I detection in physiological environment using AlGaN/GaN High Electron Mobility Transistor (HEMT) Biosensors,” *Biosens Bioelectron*, vol. 100, pp. 282–289, Feb. 2018, doi: 10.1016/j.bios.2017.09.018.

[101] T. Y. Tai *et al.*, “Design and Demonstration of Tunable Amplified Sensitivity of AlGaN/GaN High Electron Mobility Transistor (HEMT)-Based Biosensors in Human Serum,” *Anal Chem*, vol. 91, no. 9, pp. 5953–5960, May 2019, doi: 10.1021/acs.analchem.9b00353.

[102] K. Woo *et al.*, “Enhancement of cortisol measurement sensitivity by laser illumination for AlGaN/GaN transistor biosensor,” *Biosens Bioelectron*, vol. 159, Jul. 2020, doi: 10.1016/j.bios.2020.112186.

[103] N. Chaturvedi *et al.*, “GaN HEMT based biosensor for the detection of breast cancer marker (C-erbB2),” *Semicond Sci Technol*, vol. 36, no. 4, Apr. 2021, doi: 10.1088/1361-6641/abe83e.

[104] P. Kachhawa *et al.*, “Antigen-Antibody Interaction-Based GaN HEMT Biosensor for C3G Detection,” *IEEE Sens J*, vol. 22, no. 7, pp. 6256–6262, Apr. 2022, doi: 10.1109/JSEN.2022.3150027.

[105] S. Mishra, P. Kachhawa, P. Mondal, S. Ghosh, C. Tripura, and N. Chaturvedi, “AlGaN/GaN HEMT Based Biosensor for Detection of the HER2 Antigen Spiked in Human Serum,” *IEEE Trans Electron Devices*, vol. 69, no. 8, pp. 4527–4533, Aug. 2022, doi: 10.1109/TED.2022.3184658.

[106] H. T. Wang *et al.*, “Electrical detection of kidney injury molecule-1 with [formula omitted] high electron mobility transistors,” *Appl Phys Lett*, vol. 91, no. 22, p. 1448, 2007, doi: 10.1063/1.2815931.

[107] Y. L. Wang *et al.*, “Botulinum toxin detection using AlGaNGaN high electron mobility transistors,” *Appl Phys Lett*, vol. 93, no. 26, pp. 91–94, 2008, doi: 10.1063/1.3056612.

[108] B. H. Chu *et al.*, “Enzyme-based lactic acid detection using AlGaNGaN high electron mobility transistors with ZnO nanorods grown on the gate region,” *Appl Phys Lett*, vol. 93, no. 4, pp. 91–94, 2008, doi: 10.1063/1.2966158.

[109] Y. Song, Y. Lei, X. Yan, Y. Zhang, and Y. Liu, “Biosensors of ZnO nanotetrapods and HEMT for detecting uric acid,” *2012 38th Annual Northeast Bioengineering Conference, NEBEC 2012*, pp. 345–346, 2012, doi: 10.1109/NEBC.2012.6207106.

[110] H. F. Huq, H. Trevino II, and J. Castillo, “Characteristics of AlGaN/GaN HEMTs for Detection of MIG,” *Journal of Modern Physics*, vol. 07, no. 13, pp. 1712–1724, 2016, doi: 10.4236/jmp.2016.713154.

[111] R. E. G. van Hal, J. C. T. Eijkel, and P. Bergveld, “A general model to describe the electrostatic at electrolyte oxide interfaces, Advances in colloid and interface science, vol. 69,” 1996.

[112] M. Esposito, E. Patrick, and M. E. Law, *Modeling of AlGaN/GaN pH Sensors*. 2020.

[113] E. Patrick, M. Choudhury, and M. E. Law, “Simulation of the pH Sensing Capability of an Open-Gate GaN-Based Transistor,” *ECS Trans*, vol. 69, no. 13, pp. 15–23, Sep. 2015, doi: 10.1149/06913.0015ecst.

[114] M. Sciullo, M. Choudhury, E. Patrick, and M. E. Law, “Optimization of GaN-Based HEMTs for Chemical Sensing: A Simulation Study,” *ECS Trans*, vol. 75, no. 16, pp. 259–264, Aug. 2016, doi: 10.1149/07516.0259ecst.

[115] A. M. Bhat, N. Shafi, C. Sahu, and C. Periasamy, “AlGaN/GaN HEMT pH Sensor Simulation Model and Its Maximum Transconductance Considerations for Improved Sensitivity,” *IEEE Sens J*, vol. 21, no. 18, pp. 19753–19761, 2021, doi: 10.1109/JSEN.2021.3100475.

[116] N. Shafi, A. M. Bhat, J. S. Parmar, C. Sahu, and C. Periasamy, “Analytical Modeling of Surface Potential and Figure of Merit Computation for Planar Junctionless pH Sensing BioFET,” *IEEE Trans Nanotechnol*, vol. 20, pp. 534–542, 2021, doi: 10.1109/TNANO.2021.3089717.

[117] P. Pal, Y. Pratap, M. Gupta, and S. Kabra, “Analytical Modeling and Simulation of AlGaN/GaN MOS-HEMT for High Sensitive pH Sensor,” *IEEE Sens J*, vol. 21, no. 12, pp. 12998–13005, 2021, doi: 10.1109/JSEN.2021.3069243.

[118] A. M. Bhat, A. Varghese, N. Shafi, and C. Periasamy, “A Dielectrically Modulated GaN/AlN/AlGaN MOSHEMT with a Nanogap Embedded Cavity for Biosensing Applications,” *IETE J Res*, 2021, doi: 10.1080/03772063.2020.1869593.

[119] R. Poonia, A. M. Bhat, C. Periasamy, and C. Sahu, “Performance Analysis of MOS-HEMT as a Biosensor: A Dielectric Modulation Approach,” *Silicon*, no. 0123456789, 2022, doi: 10.1007/s12633-022-01742-3.

[120] R. Poonia, A. M. Bhat, C. Periasamy, and C. Sahu, “A highly sensitive Nano Gap Embedded AlGaN/GaN HEMT sensor for Anti-IRIS antibody detection,” *Micro and Nanostructures*, vol. 169, no. July, p. 207342, 2022, doi: 10.1016/j.micrna.2022.207342.

[121] N. Shafi, A. M. Bhat, J. S. Parmar, C. Sahu, and C. Periasamy, “Biologically Sensitive FETs: Holistic Design Considerations from Simulation, Modeling and Fabrication Perspectives,” *Silicon*, no. 0123456789, 2022, doi: 10.1007/s12633-022-01709-4.

[122] A. Varghese, C. Periasamy, and L. Bhargava, “Fabrication and charge deduction based sensitivity analysis of gan mos-hemt device for glucose, mig, c-erbb-2, kim-1, and psa detection,” *IEEE Trans Nanotechnol*, vol. 18, pp. 747–755, 2019, doi: 10.1109/TNANO.2019.2928308.

[123] A. Varghese, C. Periasamy, and L. Bhargava, “Analytical modeling and simulation-based investigation of AlGaN/AlN/GaN bio-HEMT sensor for C-ErbB-2 detection,” *IEEE Sens J*, vol. 18, no. 23, pp. 9595–9603, Dec. 2018, doi: 10.1109/JSEN.2018.2871718.

[124] W. Healy, “Site-binding Model of the Electrical Double Layer at the Oxide / Wa t er Iiit er face,” *J Chem Soc*, vol. Faraday Tr, pp. 1807–1818, 1973.

[125] L. Bousse, L. Bousse, N. F. de Rood, and P. Bergveld, “Operation of Chemically Sensitive Field-Effect Sensors As a Function of the Insulator-Electrolyte Interface,” *IEEE Trans Electron Devices*, vol. 30, no. 10, pp. 1263–1270, 1983, doi: 10.1109/T-ED.1983.21284.

[126] P. Bergveld, R. van Hal, and J. Eijkel, “The remarkable similarity between the acid-base properties of ISFETs and proteins and the consequences for the design of ISFET biosensors,” 1995.

[127] D. Landheer, G. Aers, W. R. McKinnon, M. J. Deen, and J. C. Ranuarez, “Model for the field effect from layers of biological macromolecules on the gates of metal-oxide-semiconductor transistors,” *J Appl Phys*, vol. 98, no. 4, 2005, doi: 10.1063/1.2008354.

[128] M. Waleed Shinwari, M. Jamal Deen, and D. Landheer, “Study of the electrolyte-insulator-semiconductor field-effect transistor (EISFET) with applications in biosensor design,” *Microelectronics Reliability*, vol. 47, no. 12, pp. 2025–2057, 2007, doi: 10.1016/j.microrel.2006.10.003.

[129] M. Stutzmann *et al.*, “GaN-based heterostructures for sensor applications,” *Diam Relat Mater*, vol. 11, no. 3–6, pp. 886–891, 2002, doi: 10.1016/S0925-9635(02)00026-2.

[130] G. Steinhoff, M. Hermann, W. J. Schaff, L. F. Eastman, M. Stutzmann, and M. Eickhoff, “pH response of GaN surfaces and its application for pH-sensitive field-effect transistors,” *Appl Phys Lett*, vol. 83, no. 1, pp. 177–179, 2003, doi: 10.1063/1.1589188.

[131] T. Kokawa, T. Sato, H. Hasegawa, and T. Hashizume, “Liquid-phase sensors using open-gate AlGaN⁄GaN high electron mobility transistor structure,” *Journal of Vacuum Science & Technology B: Microelectronics and Nanometer Structures*, vol. 24, no. 4, p. 1972, 2006, doi: 10.1116/1.2214701.

[132] B. S. Kang *et al.*, “Role of gate oxide in AlGaN/GaN high-electron-mobility transistor pH sensors,” *J Electron Mater*, vol. 37, no. 5, pp. 550–553, 2008, doi: 10.1007/s11664-007-0298-y.

[133] M. S. Z. Abidin, A. M. Hashim, M. E. Sharifabad, S. F. Abd Rahman, and T. Sadoh, “Open-gated pH sensor fabricated on an undoped-AlGaN/GaN HEMT structure,” *Sensors*, vol. 11, no. 3, pp. 3067–3077, Mar. 2011, doi: 10.3390/s110303067.

[134] M. Dipalo *et al.*, “Combining diamond electrodes with GaN heterostructures for harsh environment ISFETs,” *Diam Relat Mater*, vol. 18, no. 5–8, pp. 884–889, 2009, doi: 10.1016/j.diamond.2009.01.011.

[135] A. Podolska *et al.*, “Method to Predict and Optimize Charge Sensitivity of Ungated AlGaN/GaN HEMT-Based Ion Sensor Without Use of Reference Electrode,” *IEEE Sens J*, vol. 15, no. 9, pp. 5320–5326, 2015, doi: 10.1109/JSEN.2015.2439692.

[136] D. Xue *et al.*, “Enhancing the sensitivity of the reference electrode free AlGaN/GaN HEMT based pH sensors by controlling the threshold voltage,” *Sens Actuators B Chem*, vol. 306, no. December 2019, p. 127609, 2020, doi: 10.1016/j.snb.2019.127609.

[137] H. Y. Liu, W. C. Hsu, C. S. Lee, B. Y. Chou, and W. F. Chen, “Enhanced performances of AlGaN/GaN ion-sensitive field-effect transistors using H2O2-grown Al2O3 for sensing membrane and surface passivation applications,” *IEEE Sens J*, vol. 15, no. 6, pp. 3359–3366, 2015, doi: 10.1109/JSEN.2015.2390641.

[138] L. Wang, L. Li, T. Zhang, X. Liu, and J. P. Ao, “Enhanced pH sensitivity of AlGaN/GaN ion-sensitive field effect transistor with Al 2 O 3 synthesized by atomic layer deposition,” *Appl Surf Sci*, vol. 427, pp. 1199–1202, 2018, doi: 10.1016/j.apsusc.2017.09.072.

[139] L. Wang, Y. Bu, L. Li, and J. P. Ao, “Effect of thermal oxidation treatment on pH sensitivity of AlGaN/GaN heterostructure ion-sensitive field-effect transistors,” *Appl Surf Sci*, vol. 411, pp. 144–148, 2017, doi: 10.1016/j.apsusc.2017.03.167.

[140] L. Li, X. Li, T. Pu, Y. Liu, and J. P. Ao, “Normally off AlGaN/GaN ion-sensitive field effect transistors realized by photoelectrochemical method for pH sensor application,” *Superlattices Microstruct*, vol. 128, no. September 2018, pp. 99–104, 2019, doi: 10.1016/j.spmi.2019.01.018.

[141] H. Zhang, J. Tu, S. Yang, K. Sheng, and P. Wang, “Optimization of gate geometry towards high-sensitivity AlGaN/GaN pH sensor,” *Talanta*, vol. 205, no. July, p. 120134, 2019, doi: 10.1016/j.talanta.2019.120134.

[142] Q. Cheng *et al.*, “Planar Dual Gate GaN HEMT Cascode Amplifier as a Voltage Readout pH Sensor with High and Tunable Sensitivities,” *IEEE Electron Device Letters*, vol. 41, no. 3, pp. 485–488, 2020, doi: 10.1109/LED.2020.2967631.

[143] Y. Dong *et al.*, “Enhanced Stability and Sensitivity of AlGaN/GaN-HEMTs pH Sensor by Reference Device,” *IEEE Sens J*, vol. 21, no. 8, pp. 9771–9776, Apr. 2021, doi: 10.1109/JSEN.2020.3047204.

[144] Z. Gu *et al.*, “Ethanolamine Modified ZnO Nanorods-Based Disposable Gate-AlGaN/GaN High Electron Mobility Transistor for pH Sensing,” *IEEE Sens J*, vol. 21, no. 3, pp. 2552–2558, 2021, doi: 10.1109/JSEN.2020.3023034.

[145] S.-K. Cho and W.-J. Cho, “High-Sensitivity pH Sensor Based on Coplanar Gate AlGaN/GaN Metal-Oxide-Semiconductor High Electron Mobility Transistor,” *Chemosensors*, vol. 9, no. 3, p. 42, 2021, doi: 10.3390/chemosensors9030042.

[146] Y. He *et al.*, “Enhanced pH Sensitivity of AlGaN/GaN Ion-Sensitive Field-Effect Transistor by Recess Process and Ammonium Hydroxide Treatment,” *IEEE Trans Electron Devices*, vol. 68, no. 3, pp. 1250–1254, 2021, doi: 10.1109/TED.2021.3053496.

[147] X. Yang *et al.*, “Enhancing the Sensitivity of GaN High Electron-Mobility Transistors-Based pH Sensor by Dual Function of Monolithic Integrated Planar Multi-Channel and Ultraviolet Light,” *IEEE Trans Electron Devices*, vol. 68, no. 12, pp. 6437–6443, 2021, doi: 10.1109/TED.2021.3123263.

[148] M. Bayer, C. Uhl, and P. Vogl, “Theoretical study of electrolyte gate AlGaN/GaN field effect transistors,” *J Appl Phys*, vol. 97, no. 3, Feb. 2005, doi: 10.1063/1.1847730.

[149] A. M. Bhat, N. shafi, and C. Periasamy, “Investigation of AlGaN/GaN HEMT for pH sensing applications and sensitivity optimization,” *Superlattices Microstruct*, vol. 160, no. October, p. 107067, 2021, doi: 10.1016/j.spmi.2021.107067.

[150] K. T. Upadhyay and M. K. Chattopadhyay, “A Composition-Dependent Unified Analytical Model for Quaternary InAlGaN/GaN HEMTs for pH Sensing,” *J Electron Mater*, vol. 50, no. 6, pp. 3392–3405, 2021, doi: 10.1007/s11664-021-08836-5.

[151] A. Jarndal, L. Arivazhagan, E. Almajali, S. Mahmoud, S. Majzoub, and T. Bonny, “Enhancement of Sensitivity in AlGaN/GaN HEMT Based Sensor Using Back-Barrier Technique,” *IEEE Sens J*, Aug. 2022, doi: 10.1109/JSEN.2022.3190296.

[152] T. Kokawa, T. Sato, H. Hasegawa, and T. Hashizume, “Liquid-phase sensors using open-gate AlGaN⁄GaN high electron mobility transistor structure,” *Journal of Vacuum Science & Technology B: Microelectronics and Nanometer Structures*, vol. 24, no. 4, p. 1972, 2006, doi: 10.1116/1.2214701.

[153] H. Guo, X. Jia, Y. Dong, J. Ye, D. Chen, and R. Zhang, “Applications of AlGaN / GaN high electron mobility transistor-based,” 2020.

[154] S. Mishra, P. Kachhawa, R. R. Thakur, A. K. Jain, K. Singh, and N. Chaturvedi, “Detection of heavy metal ions using meander gated GaN HEMT sensor,” *Sens Actuators A Phys*, vol. 332, p. 113119, 2021, doi: 10.1016/j.sna.2021.113119.

[155] H.-T. Wang *et al.*, “Fast electrical detection of Hg(II) ions with AlGaN⁄GaN high electron mobility transistors,” *Appl Phys Lett*, vol. 91, no. 4, p. 042114, 2007, doi: 10.1063/1.2764554.

[156] J. Cheng *et al.*, “Ultrasensitive detection of Hg2+ using oligonucleotide- functionalized AlGaN/GaN high electron mobility transistor,” *Appl Phys Lett*, vol. 105, no. 8, 2014, doi: 10.1063/1.4894277.

[157] A. Nigam *et al.*, “Real time detection of Hg2+ ions using MoS2 functionalized AlGaN/GaN high electron mobility transistor for water quality monitoring,” *Sens Actuators B Chem*, vol. 309, no. January, p. 127832, 2020, doi: 10.1016/j.snb.2020.127832.

[158] A. Nigam, T. N. Bhat, V. S. Bhati, S. bin Dolmanan, S. Tripathy, and M. Kumar, “MPA-GSH Functionalized AlGaN/GaN High-Electron Mobility Transistor-Based Sensor for Cadmium Ion Detection,” *IEEE Sens J*, vol. 19, no. 8, pp. 2863–2870, 2019, doi: 10.1109/JSEN.2019.2891511.

[159] L. Zhao *et al.*, “A differential extended gate-AlGaN/GaN HEMT sensor for real-time detection of ionic pollutants,” *Analytical Methods*, vol. 11, no. 31, pp. 3981–3986, 2019, doi: 10.1039/c9ay01019j.

[160] L. Gu *et al.*, “Electrical detection of trace zinc ions with an extended gate-AlGaN/GaN high electron mobility sensor,” *Analyst*, vol. 144, no. 2, pp. 663–668, 2019, doi: 10.1039/c8an01770k.

[161] X. Jiang *et al.*, “L-Cysteine Functionalized Al0.18Ga0.82N/GaN High Electron Mobility Transistor Sensor for Copper Ion Detection,” *IEEE Trans Electron Devices*, vol. 69, no. 6, pp. 3367–3372, 2022, doi: 10.1109/TED.2022.3169120.

[162] X. Jia, D. Chen, L. Bin, H. Lu, R. Zhang, and Y. Zheng, “Highly selective and sensitive phosphate anion sensors based on AlGaN/GaN high electron mobility transistors functionalized by ion imprinted polymer,” *Sci Rep*, vol. 6, no. May, pp. 1–7, 2016, doi: 10.1038/srep27728.

[163] M. Myers *et al.*, “Nitrate ion detection using AlGaN/GaN heterostructure-based devices without a reference electrode,” *Sens Actuators B Chem*, vol. 181, pp. 301–305, 2013, doi: 10.1016/j.snb.2013.02.006.

[164] X. Liu *et al.*, “Wearable Multiparameter Platform Based on AlGaN/GaN High-electron-mobility Transistors for Real-time Monitoring of pH and Potassium Ions in Sweat,” *Electroanalysis*, vol. 32, no. 2, pp. 422–428, 2020, doi: 10.1002/elan.201900405.

[165] S. Rabbaa and J. Stiens, “Validation of a triangular quantum well model for GaN-based HEMTs used in pH and dipole moment sensing,” *J Phys D Appl Phys*, vol. 45, no. 47, Nov. 2012, doi: 10.1088/0022-3727/45/47/475101.

[166] D. Verheij, “Radiation sensors based on GaN microwires Engineering Physics,” 2017.

[167] H. W. Hou, Z. Liu, J. H. Teng, T. Palacios, and S. J. Chua, “High temperature terahertz detectors realized by a GaN high electron mobility transistor,” *Sci Rep*, vol. 7, pp. 3–8, 2017, doi: 10.1038/srep46664.

[168] E. Javadi, J. A. Delgado-Notario, N. Masoumi, M. Shahabadi, J. E. Velázquez-Pérez, and Y. M. Meziani, “Continuous Wave Terahertz Sensing Using GaN HEMTs,” *Physica Status Solidi (A) Applications and Materials Science*, vol. 215, no. 11, pp. 1–6, 2018, doi: 10.1002/pssa.201700607.

[169] K. Ahi, “Review of GaN-based devices for terahertz operation,” *Optical Engineering*, vol. 56, no. 09, p. 1, 2017, doi: 10.1117/1.oe.56.9.090901.

[170] C. Fares *et al.*, “ Effect of alpha-particle irradiation dose on SiN x /AlGaN/GaN metal–insulator semiconductor high electron mobility transistors ,” *Journal of Vacuum Science & Technology B*, vol. 36, no. 4, p. 041203, 2018, doi: 10.1116/1.5042261.

[171] S. Ahn *et al.*, “Effect of proton irradiation energy on AlGaN/GaN metal-oxide semiconductor high electron mobility transistors,” *Journal of Vacuum Science & Technology B,*

Nanotechnology and Microelectronics: Materials, Processing, Measurement, and Phenomena, vol. 33, no. 5, p. 051208, 2015, doi: 10.1116/1.4928730.